Acoustic Emission Monitoring of Prestressed Bridge Girders with Premature Concrete Deterioration

by

Piya Chotickai, B.S.C.E

Thesis

Presented to the Faculty of the Graduate School of

The University of Texas at Austin

in Partial Fulfillment

of the Requirements

for the Degree of

Master of Science in Engineering

The University of Texas at Austin

May 2001

Acoustic Emission Monitoring of Prestressed Bridge Girders with Premature Concrete Deterioration

Approved by
Supervising Committee:

_____

_____

Dedication

To my parents, Chirapat and Paungporn Chotickai

Acknowledgements

First of all, I would like to thank the Texas Department of Transportation for the funding provided for Project 1857. In particular I would like to thank Brian D. Merrill. His support made the project possible. I also would like to thank John A. Roberts for his help with my use of the bridges for testing. The continuous monitoring in San Antonio would never have succeeded without the help of Jon H. Kilgore, who provided and set everything up for the test, and Gilbert B. Hernandez, who gave me such wonderful help during monitoring.

I wish to express my sincere gratitude to my supervisor, Dr. Timothy Fowler for his support and guidance throughout this project, and for his patience and advice, while I was writing my thesis. I also would like to thank Dr. Richard Klingner and Dr. Michael Kreger, who provided assistance and advice during this research. I am grateful to the staff at the Phil M. Ferguson Structural Engineering Laboratory and other research members in the project: Joe Roche, Brian Tinkey, Anna Boenig, Yong-Mook Kim, Larry Memberg, and Amy Eskridge.

I would like to express special thanks to Jaroon Rungamornrat and Chayawee Wangcharoenrung for their advice, while I was writing my analysis program, and to Nat Ativitavas and Kazuo Endo who gave me a hand with the

field testing. Nat Ativitavas also gave me a feeling for and vision about acoustic emission. He gave me sympathy when I went through difficult times and gave me rides home too.

These acknowledgements would not be complete, if I did not mention my parents. They have always given me encouragement and inspiration in every phase of my life. Without them, I could not have gotten this far.

May 2001

Abstract

Acoustic Emission Monitoring of Prestressed Bridge Girders with Premature Concrete Deterioration

Piya Chotickai, MSE

The University of Texas at Austin, 2001

Supervisors: Timothy Fowler

Richard Kligner

Acoustic emission monitoring on prestressed concrete bridge girders subjected to premature concrete deterioration due to alkali-silica reaction (ASR) and delayed ettringite formation (DEF) was carried out at the University of Texas at Austin. Results from tests performed in the laboratory and from background noise testing on in-service bridge girders were used to develop a field test procedure. The procedure is based on acoustic emission parameters and can be used as a tool to evaluate the structural condition of an in-service prestressed concrete girder subjected to premature deterioration.

Table of Contents

List of Tables

List of Figures

Appendix

Procedure for Acoustic Emission Monitoring of Prestressed Concrete Girders

CHAPTER 1 - SCOPE

1.1 General[1] - This procedure defines instrumentation requirements, test procedures, and evaluation criteria for acoustic emission (AE) monitoring of prestressed concrete girders for the purpose of evaluating structural integrity. This procedure applies to new and in-service girders. It is also applicable to girders that exhibit premature concrete deterioration due to alkali-silica reaction (ASR) or delayed ettringite formation (DEF). An authorized representative of the Texas Department of Transportation shall approve in writing any deviation from this procedure. The test method requires loading of the girder. Typically, such loads will be applied by traffic as part of normal operation.

1.2 Limitations - The test method described in this procedure is subject to the following specific limitations.

1.2.1 Loading - Acoustic emission will only detect defects and overloads in portions of the girder that are stressed during the course of the test.

1.2.2 Materials - This procedure is limited to prestressed concrete. Reinforced concrete beams without prestressing cannot be evaluated under this procedure.

1.2.3 Applicability - The AE test detailed in this procedure will detect structural deterioration or structural overloads in a prestressed concrete girder, and applies to flexure-dominated and shear-dominated regions of the girder. The test method will also detect strand slippage.

1.2.4 Portions not Covered - The monitoring procedure will normally be used to evaluate a local region of a girder. When used in this manner, the procedure will not provide a structural evaluation of other regions of the girder.

---

[1] Inquiries about this procedure should be addressed to Mr. Brian D. Merrill, P.E., Texas Department of Transportation, 125 E. 11th Street, Austin TX, 78701-2483

1.3 Table of Contents - This procedure includes the following chapters:

CHAPTER 2 – APPLICABLE DOCUMENTS

2.1 ASTM - American Society for Testing and Materials.

E 569 Standard Practice for Acoustic Emission Monitoring of Structures During Controlled Stimulation.

E 650 Standard Guide for Mounting Piezoelectric Acoustic Emission Sensors.

E 750 Standard Practice for Measuring Operating Characteristic of Acoustic Emission Instrumentation.

E 976 Standard Guide for Determining the Reproducibility of Acoustic Emission Sensor Response.

E 1316 Standard Terminology for Nondestructive Examinations.

E 2075 Standard Practice for Verifying the Consistency of AE-Sensor Response Using an Acrylic Rod.

2.2 ASNT – American Society for Nondestructive Testing.

Recommended Practice No. SNT-TC-1A, “Personnel Qualification and Certification in Nondestructive Testing”.

CHAPTER 3 – DEFINITIONS

3.1 Definitions - The following definitions shall apply to this Procedure.

3.1.1 Amplitude – See signal amplitude, acoustic emission.

3.1.2 Channel, Acoustic Emission - An assembly of sensor(s), preamplifier or impedance matching transformer, filters, secondary amplifier or other instrumentation as needed, connecting cables, and detector or processor (ASTM E 1316). Each channel shall be analyzed independently.

3.1.3 Electronic Calibrator - A device that can repeatably induce a transient signal into an acoustic emission processor for the purpose of checking, verifying, and calibrating the test instrument.

3.1.4 Event, Acoustic Emission (Emission Event) - A local material change giving rise to acoustic emission (ASTM E 1316).

3.1.5 Felicity Effect - The presence of detectable acoustic emission at a fixed predetermined sensitivity level at stress levels below those previously applied (ASTM E 1316). The fixed sensitivity level will be the same as was used for the previous loading or test.

3.1.6 Felicity Ratio - The ratio of the stress at which the Felicity effect occurs to the previously applied maximum stress (ASTM E 1316). As used in this procedure, the Felicity ratio is determined from the ratio of the load (Section 3.2.1) at the onset of significant emission to the previously applied maximum load.

3.1.7 Filter – A hardware or software tool that is used to identify a data set based on specified characteristics. Filters are normally used to identify and eliminate unwanted data, such as emission caused by mechanical sliding or non-relevant sources.

3.1.8 First Hit – If stress waves from an event cause signals to exceed the threshold on more than one sensor, the signal with the earliest time of arrival is termed the first hit.

3.1.9 Historic Index - A measure of the change in signal strength throughout a test.

3.1.10 Hit – Any signal that exceeds the threshold and causes a system channel to accumulate data (ASTM E 1316).

3.1.11 Hit Definition Time - A specified time interval defining the end of a hit during which no additional threshold crossings occur. The hit definition time is measured from the last threshold crossing of the hit. The first threshold crossing following the hit definition time is part of the next hit.

3.1.12 Hit Duration (Duration) - The time from the first threshold crossing to the last threshold crossing of the signal or envelope of the linear voltage time signal. Hit duration does not include the hit definition time at the end of a hit.

3.1.13 MARSE - Measured area of the rectified signal envelope (ASME Code, Section V, Article 12). A measurement of the area under the envelope of the rectified linear voltage time signal from the sensor.

3.1.14 Non-relevant Indication – An NDT indication that is caused by a condition or type of discontinuity that is not rejectable. False indications are non-relevant (ASTM 1316).

3.1.15 Processor - A circuit that analyzes the AE waveform as required in Section 7.4.

3.1.16 Rearm Time - An interval following acquisition of a hit during which a channel is unable to accept additional data.

3.1.17 Signal Amplitude, Acoustic Emission - The peak voltage of the largest excursion attained by the signal waveform from an emission event (ASTM E 1316). For purposes of this procedure signal amplitude shall be measured in decibels.

3.1.18 Signal Strength - Area under the envelope of the linear voltage time signal from the sensor. The signal strength will normally include the absolute area of both the positive and negative envelopes. For purposes of this procedure, MARSE is used as a relative measure of signal strength.

3.1.19 Simulated Acoustic Emission Source - A device that can repeatably induce a transient elastic stress wave into the structure.

3.1.20 Time of Arrival – The time of a specified point on an AE signal. The specified point may differ for different instruments and different source location analysis methods. Example specifications are the first threshold crossing and the time at peak amplitude.

3.1.21 Voltage Threshold (Threshold) - A voltage level on an electronic comparator such that signals with amplitudes larger than this level will be recognized (ASTM E 1316).

3.1.21.1 Test Threshold - The threshold setting for monitoring conducted according to this procedure.

3.1.22 Zone - The area surrounding a sensor from which AE can be detected and from which AE will strike the sensor before striking any other sensors.

CHAPTER 4 - SUMMARY OF METHOD

4.1 General - The method consists of subjecting prestressed concrete girders to normal traffic loads and monitoring with sensors capable of detecting acoustic emission (transient stress waves) caused by overstressed regions of the girder. Acoustic emission is generated by microcracking, crack initiation and or growth, closing of cracks, strand slippage, and yielding and breakage of strands.

4.2 Structural Integrity Evaluation - This procedure provides guidelines to determine the location and significance of structural flaws. Evaluation criteria provide a basis to assess the structural integrity of the equipment.

4.3 Data Evaluation - Data evaluation is on a per channel basis and is based on Felicity ratio and large amplitude hits. For Felicity ratio calculations, onset of significant emission is based on historic index. Data are recorded continuously. Specific evaluation criteria and analysis methods are given in Chapter 12.

CHAPTER 5 - PERSONNEL QUALIFICATION

5.1 Personnel - Personnel performing acoustic emission testing of prestressed concrete girders (inspector) are required to attend a dedicated training course, pass a written examination, and have the recommended experience level. The training course shall be appropriate for specific NDT Level II qualification according to Recommended Practice No. SNT-TC-1A of the American Society for Nondestructive Testing, and should include as a minimum the following general topics:

1. Basic technology and terminology of acoustic emission.
2. Acoustic emission instrumentation.
3. Instrument checkout.
4. Characteristics of background noise and non-relevant emission.
5. Data collection and interpretation.
6. Data analysis including historic index calculations.

The inspector shall be familiar with the construction of prestressed concrete beams, failure mechanisms, and the provisions of this procedure. The experience level shall be that recommended by SNT-TC-1A for Level II certification in acoustic emission.

CHAPTER 6 - SIGNIFICANCE

General – This procedure detects overstressed regions in prestressed concrete girders. The overstress can occur because the structure is overloaded, or because the structure has degraded and can no longer carry the traffic and other loads with an adequate margin of safety. Common types of degradation are distributed cracking caused by alkali-silica reaction or delayed ettringite formation. Among the mechanisms that generate emissions are: cracking of the cement matrix and aggregates; crushing of the cement matrix and aggregates; breakage of the bond between the aggregate and cement matrix; failure of the bond between the prestressing strand and the concrete; yielding of the prestressing strand; and failure of the prestressing strand.

Applicability - Experimental and theoretical studies have been performed on prestressed concrete girders as part of a six year research project that led to development of this procedure[2,3,4]. AASHTO Type I girders with a 6.5 inch thick cast-in-place concrete slab were tested in shear and flexure. The compressive strength of the concrete slabs varied from 5,000 psi to 15,000 psi. Shear and flexure tests were performed on I-shaped Type C girders and on hollow box girders that showed distributed cracking due to alkali-silica reaction and delayed ettringite formation.

Continuous Monitoring – This procedure is suitable for continuous monitoring of in-service girders under normal traffic loads. Usually, application of the procedure will not result in traffic disruption.

Follow-up – Overstressed regions of the girder detected by AE should be examined on the basis of the significance of emission. Other

---

[2] Yepez Roca, Luis Octavio, "Acoustic Emission Examination of High Strength Prestressed Concrete Girders", Thesis, Master of Science in Engineering, The University of Texas at Austin, August 1997.

[3] Tinkey, Brian Victor, "Nondestructive Testing of Prestressed Bridge Girders with Distributed Damage", Thesis, Master of Science in Engineering, The University of Texas at Austin, May 2000.

[4] Piya, Chotickai, "Acoustic Emission Monitoring of Prestressed Bridge Girders with Premature Concrete Deterioration", Thesis, Master of Science in Engineering, The University of Texas at Austin, May 2001.

nondestructive examination techniques, repair, and retest may be required. Recommendations for repair and examination by other nondestructive test methods are outside the scope of this procedure.

CHAPTER 7 - INSTRUMENTATION

7.1 General - The AE instrumentation consists of sensors, electronic signal processing and recording equipment, together with digital hardware and software for analyzing and displaying data in accordance with the provisions of this procedure.

7.2 Sensors – Sensors shall have a resonant response centered on 150 kHz. Each sensor shall utilize preamplifier circuitry that includes a band pass filter centered on the resonant peak and shielded against electromagnetic (EMI) and radio frequency interference (RFI). Integral sensors incorporate the sensor and preamplifier in the same shielded casing. As a result, they are very effective at rejecting EMI and RFI and are required for this application. Sensors shall be temperature-stable over the range of intended use, and shall not exhibit sensitivity changes greater than guaranteed by the manufacturer over this range. Sensors shall have omnidirectional response, with variations not exceeding 2 dB from the peak response. Minimum sensitivity shall be -80 dB referred to 1 volt per microbar, determined by face-to-face ultrasonic calibration. This method measures relative sensitivity of the sensor. AE sensors used in the same test shall not vary in peak sensitivity by more than 3 dB from the average. If the preamplifier is of differential design, a minimum of 40 dB of common-mode noise rejection shall be provided. The unfiltered frequency response shall not vary more than 3 dB over the operating frequency and temperature range of the sensors, filters, and preamplifiers.

7.2.1 Teed Sensors - Sensors shall not be teed (commoned) into a single channel.

7.2.2 Filters – Band pass filters shall be located in the preamplifier, or may be integrated into the component design of the sensor and preamplifier. Additional filters shall incorporated into the processor. Characteristics of these filters are specified in Paragraph 7.8.

7.3 Power Signal Cable - The cable providing power to the preamplifier and conducting the amplified signal to the main processor shall be shielded

against electromagnetic noise. Signal loss shall be less than 1 dB per 100 ft of cable length. The cable length shall not exceed five hundred feet.

7.4 Data Processor, Measurement, and Recording - The main processor(s) shall have processing circuits through which sensor data will be processed. If used, the main amplifier shall have signal response with variations not exceeding 3 dB over the frequency range of 100 to 200 kHz, and temperature range of 0 to 140^{o}F. The instrumentation shall measure and record data by channel number. The following parameters for each hit shall be measured and recorded within the specified frequency range:

- Hit arrival time.
- Hit duration.
- Peak amplitude.
- Signal strength or MARSE.
- Relative load.

Details and accuracy of data measurement shall be as specified in below. The instrument shall store the year, month, day, hour, and minute of the start of each data file as part of the test record. The maximum relative load for each of the past 30 days shall be recorded and stored.

7.4.1 Data Analysis Threshold – A fixed threshold shall be used and shall be set according to the procedure given in Paragraph A.2.1. For most instruments, the threshold will be 55 dB.

7.4.2 Number of Channels - The data acquisition system shall have the minimum number of channels necessary to provide coverage of the primary region(s) of interest, and sufficient guard channels to prevent background noise contaminating the relevant data. Separate instruments can be used to monitor different regions of interest on the same girder.

7.4.3 Arrival Time - Hit arrival time shall be recorded globally by channel to an accuracy of 500 nanoseconds and shall be based on the peak amplitude.

7.4.4 Hit Duration - Hit duration shall be accurate to +/-5 micro-seconds.

7.4.5 Peak Amplitude Detection - Amplitude shall be measured in decibels referenced to 0dB as 1 ΦV at the preamplifier input. Comparative calibration must be established per the requirements of Appendix A. Usable dynamic range shall be a minimum of 45 dB with 1 dB resolution over the frequency band of 100 to 200 kHz, and the temperature range of 0^o to 140^o F. Not more than 2 dB variation in peak detection accuracy shall be allowed over the stated temperature range. Amplitude values shall be stated in dB, and must be referenced to a fixed gain output of the system (sensor or preamplifier).

7.4.6 Signal Strength or MARSE - Signal strength or MARSE shall have a resolution of 1% of the value obtained from a one millisecond duration, 150 kHz pulse having an amplitude 15 dB above the data analysis threshold. Useable dynamic range shall be a minimum of 35 dB. Relative values of signal strength given in Table A.4 shall be accurate to !5%.

7.4.7 Data Acquisition Rate - The instrumentation shall be capable of measuring and recording data at a minimum rate of 200 hits per second. This rate shall apply to the entire instrument, regardless of the number of channels and the distribution of hits between channels.

7.4.8 Rearm Time - Individual channel rearm times are permitted under this procedure. If used, the rearm time shall commence immediately following the end of the hit definition time. The rearm time shall apply only to the channel that detected the hit, and shall not affect other channels. The rearm time shall be as small as possible, but not greater than 200 microseconds.

7.4.9 Hit Definition Time - The hit definition time shall be 400 microseconds.

7.5 Relative Load – A relative measure of the load applied to the structure must be continuously monitored during the monitoring period and recorded as part of the data record for each hit. The load will generally be the normal traffic load. In certain circumstances, such as during a follow-up test when AE has indicated an overstress condition, it may be desirable to apply a known load at a controlled rate. The relative load can be based on a measurement of strain, displacement, or acceleration in the region of interest. The load measurement shall be supplied to the instrument in the form of a DC current. As specified in Paragraph 7.4, the daily maximum relative load shall be recorded and stored for Felicity ratio calculations.

7.6 Front End Filters - Band pass filters of the type defined in Paragraph 7.8 shall be used. Guard sensors are also required. No other front end filters shall be used. Data from all hits having amplitude greater than the test threshold shall be recorded as defined in paragraph 7.4.

7.7 Guard Sensors – Guard sensors shall be used to eliminate background traffic noise from the data. Guard sensors shall be controlled by the instrument hardware with real time rejection of non-relevant emission. Arrangement and set-up of the guard sensors is detailed in Paragraph 9.3.

7.8 Filters - Additional filters shall be incorporated into the processor to limit frequency range and thereby EMI and RFI. The combination of sensor/preamplifier and processor filters shall be of the band pass type, and shall provide a minimum of 24dB/octave signal attenuation. Filters and/or integral design characteristics shall ensure that the principal processing frequency from the sensors is in the range of 100 to 200 kHz.

7.9 Power Supply – Provision must be made for a stable power supply. For remote monitoring, this may require internal batteries operating in combination with an external source. The instrument shall retain data records in the event of a power failure.

7.10 Real Time Data Analysis - The instrumentation shall be capable of providing the following real time or near real time analyses:

7.10.1 Previous Maximum Relative Load – The maximum relative load for each day of the past thirty days is required for Felicity ratio determination. This value shall be updated once per day.

7.10.2 Onset of Significant Acoustic Emission – The historic index shall be calculated for each hit according to the procedure given in Paragraph 12.4.1. As defined in Paragraph 12.4.1, the onset of significant emission occurs when the historic index exceeds 1.85. Once this value is exceeded, it shall be assumed that significant emission continues to occur until the historic index again falls to 1.85 or less.

7.10.3 Felicity Ratio – If significant emission is detected, the relative load corresponding to the onset of significant emission shall be divided by the maximum relative load during the previous thirty days to determine the Felicity ratio. The Felicity ratio shall be determined for each new onset of acoustic emission.

7.10.4 Analysis Records - The AE instrument shall record the value of Felicity ratio, global time, previous maximum relative load, and the relative load corresponding to each onset of significant emission. The global time shall be recorded to an accuracy of one second.

7.11 Post-test Data Analysis - Provision shall be included for downloading the data to an IBM format personal computer (PC) for playback, display, post-test filtering, analysis, and permanent storage. PC software to accomplishing these functions shall be available.

7.12 Performance Requirements, Calibration, and Verification - The AE instrumentation shall meet the performance requirements specified in Paragraph 7.4. Calibration shall be in accordance with these requirements and the calibration values defined in Mandatory Appendix A. Calibration and instrument verification shall be as follows:

- A complete calibration at intervals not exceeding one year.
- Instrument users shall develop and document an instrument and sensor verification technique that shall be performed at three month intervals.

- Permanent copies of the document certifying the date of the most recent calibration and instrument verification shall be provided to the Texas Department of Transportation.

CHAPTER 8 - TEST PREPARATION AND DATA ACQUISITION

8.1 Preliminary Information - Prior to setting up the test instruments, the inspector shall be furnished with the following information.

- Girder configuration. In most instances this information can be obtained by visually examining the girder or by reviewing the drawings.
- Date of manufacture, installation, and operation, together with any unique operating conditions.
- Test History**.** Previous visual inspection and acoustic emission examination results.

8.2 Safety - All safety requirements unique to the test location shall be met.

8.3 Environmental – It may be necessary to suspend monitoring if the ambient temperature falls below 32^{o}F (0^{o}C) and ice builds up on the structure. Ice will act as a source of emission.

8.4 Background Noise - It is important to capture real emissions during data monitoring periods. In order to accomplish this, background noise must be at a minimum. Prior to a test, the inspector shall review the test site to identify all potential sources of extraneous acoustic noise. The following paragraphs identify some frequently encountered sources of background noise.

8.4.1 EMI and RFI - Field experience has shown that care should be exercised in dealing with electrical background noise sources; for example, EMI is usually due to motors, switch gear, solenoids, and the like. It can also be caused by a bad power supply, particularly an inadequate ground. RFI can be distinguished from EMI with an oscilloscope and correlation plot. Design and shielding of sensors, and/or narrow band filters, can control both RFI and EMI. Power source EMI can be controlled with a constant voltage supply unit.

8.4.2 Wind and Vibration - Visually examine the sensors and other hardware to verify that the equipment is securely mounted and will not be subject to wind or vibration induced movement.

8.4.3 External Noise - Uncontrolled noise caused by rain, sleet, hail, snow, wind blown particles, air hoses, air horns, blasting, etc., shall be evaluated. Where practical, sensors shall be acoustically isolated from air borne noise sources. In some cases it may be necessary to suspend monitoring until weather conditions change. The United States Department of Transportation is sponsoring two Small Business Incentive Research projects on acoustic emission monitoring. The technology developed by these projects may be suitable for dealing with background noise from rain and other weather related sources.

8.5 Data Acquisition and Data Quality - Acquisition of genuine, valid, acoustic emission is essential to the success of the acoustic emission examination. In order to acquire consistent accurate data the following actions shall be carried out:

- Use the procedures given in Chapter 10 to thoroughly check the instrumentation performance immediately prior to the start of monitoring, after a long delay, and after completion of monitoring.
- Conduct a background noise monitoring check before each load application, as required by section 11.2, to ensure that a source of extraneous noise is not present during the test.
- Periodically monitor the performance of the instrumentation during the test.
- Periodically monitor the data during the test to note possible extraneous noise and to ensure that non-relevant emission, such as that generated by an internal instrument malfunction, or EMI, does not contaminate the data. Refer to Section 12.2 for techniques that can be used to evaluate data quality during the course of the test.

8.6 Test Log - The inspector shall maintain a test log recording data file names, test times, and other significant test occurrences.

CHAPTER 9 – SENSOR MOUNTING AND LOCATION

9.1 General – In order to obtain consistent AE data sensors must be securely mounted and coupled to the girder. Sensor mounting is discussed in Section 9.2. The sensors shall be placed with a couplant between the sensor face and the concrete surface. All signal cables must be constrained to prevent stressing the sensor or loss of coupling and to avoid extraneous noise from wind induced movement of the sensors and cables.

9.2 Mounting - ASTM E 650 provides guidance for mounting sensors. Acceptable types of couplant are given in Paragraph 9.2.2. Care must be exercised to assure that adequate couplant is applied. The preferred method of securing sensors in place is shown in Figure 9.2. The surface of concrete tends to be rough with dust and loose particles. Accordingly, it is difficult to attach sensors and hold-downs. Duct tape is unsatisfactory, and attaching the sensors directly to the concrete surface with glue does not work well. The spring steel hold-down shown in Figure 9.2 maintains a continuous pressure on the sensor. The hold-down is one inch wide and each attachment tab should be approximately 2" long. The large glued area with a thick glue line seems to work best. Hot melt glue has been found to provide a satisfactory long lasting bond. Couplant loss shall be checked per the procedures described in paragraph 10.2.

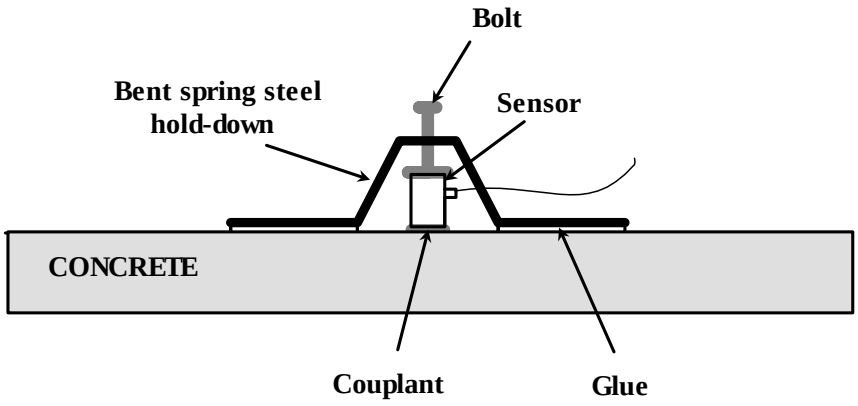

Figure 9.2 – Recommended Method for Attaching Sensors to Concrete.

9.2.1 Surface Contact - The sensor shall be mounted with the center of the sensor face directly coupled to the surface of the girder. Reliable coupling between the sensor and concrete surface must be assured and the surface in contact with the sensor face must be clean and free of particulate matter. Certain types of paint or coatings, geometric discontinuities, and surface roughness can cause signal loss. The magnitude of this type of signal loss shall be checked using the procedure defined in Paragraph 10.2. In certain cases, it may be necessary to reduce signal loss by locally removing paint from the surface of the girder.

9.2.2 Couplant - Commercially available couplants for ultrasonic flaw detection may be used. Silicone based stopcock grease has been found to be particularly suitable. Couplant selection should minimize changes in coupling sensitivity during a test. Consideration should be given to the length of the monitoring period and to the expected ambient temperature at the site.

9.3 Sensor Locations – The primary consideration in choosing sensor locations is the need to detect structural defects in regions of the girder that exhibit premature concrete deterioration, or in regions of concern identified by an authorized representative of the Texas Department of Transportation. Figure 9.3 illustrates the basic scheme for monitoring the designated regions. The hatched area is the surface representation of the region to be monitored. This is termed the area of interest. The primary sensors acquire data from this region. The guard sensors are arranged around the area of interest to detect nonrelevant emission originating outside the monitoring zone. The perpendicular bisectors of the lines between the primary sensors and the adjacent guard sensors define the boundary of the area of interest. If a guard sensor detects a "first hit", the hardware shall suspend data acquisition of the primary sensors for sufficient time to allow the stress wave to pass the primary sensor. The guard sensors are used to reject data and do not participate in the measurement function. The lockout time for the guard sensors shall be the time for a pencil break induced stress wave to travel from the guard sensor to the primary sensor plus 50%. As discussed in Paragraph 10.4, the efficacy of the guard sensors shall be checked during the system performance check.

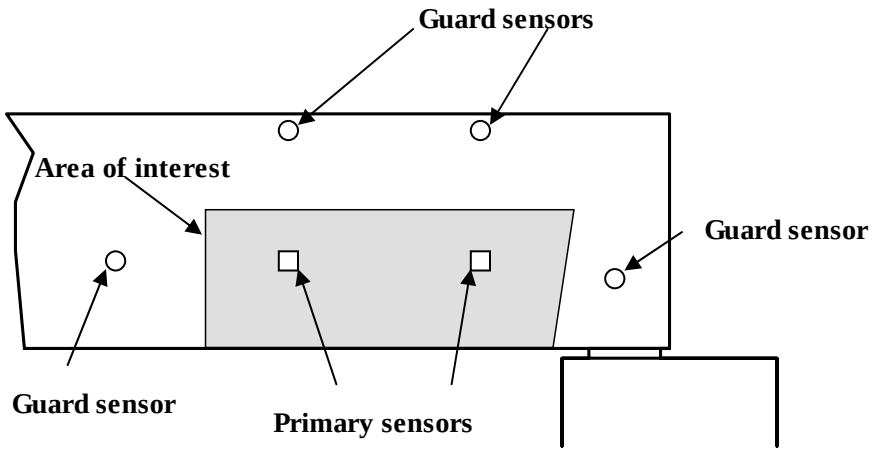

Figure 9.4 – Primary and Guard Sensors

9.4 **Sensor Spacing** - Sensors shall be spaced such that a 0.5 mm mechanical pencil (2H) leads broken on the surface of the concrete within the area of interest is detected by one of the primary sensors. All lead breaks shall be done at an angle of approximately 30 degrees to the concrete surface with a 2.5 mm lead extension. The maximum distance between primary sensors shall be 24 inches.

CHAPTER 10 – INSTRUMENTATION SETTINGS AND PERFORMANCE CHECK

10.1 Channel Sensitivity – Hsu pencil lead breaks are used as the primary technique for assuring channel sensitivity (ASTM E 976). With this technique, 0.5 mm (2H) pencil leads are broken at an angle of approximately 30° to the test surface with a 0.1 inch (2.5 mm) extension. Prior to testing three breaks shall be made at the same distance from each sensor. The average peak amplitude shall meet the provisions of paragraph 10.2 and shall not vary more than 4 dB from the average of all sensors. Any channel failing this check shall be investigated and replaced or repaired as necessary. The channel shall be rechecked with three more lead breaks and the new data used in place of the data from the defective channel. The average peak amplitude of the entire data set shall be recalculated to check that all channels meet the !4 dB criterion. These data shall be recorded and retained with the examination record.

10.2 Coupling Loss - Signal loss between the sensor and concrete surface shall be determined by comparing data obtained from pencil breaks with the data shown in Table 10.2. Amplitude values shall be not less than those shown in the table.

Table 10.2 – Minimum Average Amplitude of Pencil Breaks

Distance of Break from Sensor	MINIMUM AMPLITUDE, DB
Next to sensor	70
6 inches	58

10.3 Primary and Guard Sensors – The efficacy of the guard sensor arrangement and the ability of the primary sensors to detect emission from the area of interest shall be checked with random pencil breaks in the area bounded by the guard sensors. At least five breaks shall be within the area of interest, and at least five shall be outside.

10.4 Circuit Continuity Verification - All sensor/channel combinations shall be checked at intervals not exceeding one month and at the end of the

monitoring period using the pencil lead break technique. The purpose of this verification is to check that all sensors are functioning and in contact with the concrete. Channels that do not respond to the pencil break or have low sensitivity during the monitoring period shall be repaired or replaced. Channels that do not respond to the lead break or have low sensitivity after the monitoring period shall be noted in the test report.

CHAPTER 11 – LOADING AND BACKGROUND NOISE

11.1 General – As defined in Paragraph 7.5, the loading shall be by traffic and the relative value recorded with each AE hit.

11.2 Background Noise Monitoring – A monitoring period for background noise is required before each acoustic emission inspection. This period shall be one hour. Sources of background or extraneous noise must be identified and minimized. Types of background noise are discussed in Section 8.4. If the inspector judges background noise to be excessive, either before or during the monitoring period, the AE test shall be terminated. "Excessive" background noise either before or during the test is a matter of judgement based on experience.

CHAPTER 12 - INTERPRETATION OF RESULTS

12.1 General - Analysis of the test data shall be performed real time, or near real time by the monitoring instrument. A data quality analysis according to the procedures given in Paragraph 12.2 shall be conducted if an emission category of "warning" or "serious" is reported. This shall be followed by post-test analysis of the data to confirm these indications. If required, post-test filtering shall be performed as detailed in section 12.3. Structural evaluation procedures are given in section 12.4. Felicity ratio per channel is used to determine emission categories defining the structural significance of an indication.

12.2 Data Quality Analysis - ASTM E 1316 states that an indication is subject to interpretation as false, non-relevant, or relevant. In order to make this interpretation, the emission characteristics shall be examined to determine if data from non-relevant sources are included in the data set and that genuine AE hits have been recorded. This examination should include a review of data correlation plots, graphs, and data listing. Other sources shall be reviewed (weather bureau records, accident records, etc.) to determine if any unusual occurrences or background noise were present at any time during the test. In the analysis of the test data, background noise shall be properly discounted. Post-test filtering shall be used to eliminate non-relevant data.

12.3 Post-test Filters - Post-test filters are used to remove non-genuine data that may give a false or non-relevant indication (ASTM E 1316), or extraneous noise.

12.3.1 Time Filters – A time filter is used to eliminate bursts of extraneous noise such as caused by wind gusts, rain and impacts.

12.3.2 Channel Filter - Many noise sources, such as faulty instrumentation, will affect only one or two channels. All hits on the channel(s) showing a response to an external noise source must be removed from the data set for the period of the noise.

12.4 Structural Evaluation – The acoustic emission categories given in Table 12.4a define evaluation criteria that shall be used to determine the

significance of the indication. The criteria are based on Felicity ratio for each channel and shall be applied in turn to the data recorded by each channel. The emission must satisfy both criteria in order to be classified in a particular category. The evaluation shall be based on the minimum Felicity ratio recorded during the monitoring period. If no emission is recorded, no category is assigned.

Table 12.4a – Acoustic Emission Categories and Evaluation Criteria

Evaluation Criteria	**Emission Category**					
	All Regions of the Girder		**Flexure-Dominated Region**		**Shear-Dominated Region**	
	Not Significant	**Minor**	**Warning**	**Serious**	**Warning**	**Serious**
Felicity ratio	Not Measurable	Measur-able	≤0.95	≤0.60	≤0.90	≤0.60
Maximum amplitude during loading	≥Threshold	≥75	≥75	≥75	≥75	≥75

12.4.1 Onset of Significant Emission – The Felicity ratio is defined as the ratio of the load at onset of significant emission to the previously applied maximum load. Under this procedure, onset of significant emission is defined by a historic index greater than 1.85. Historic index calculations shall be limited to the last 2000 hits recorded on a channel. The historic index is defined by the following equation.

$$H(t) = \frac{N}{N-K} \frac{\sum_{i=K+1}^{i=N} S_{Oi}}{\sum_{i=1}^{i=N} S_{Oi}}$$

Where:

H(t) is the historic index at time *t*.
N is the number of hits (ordered by time) up to and including time *t*.
S_{Oi} is the signal strength of the i*th* hit.
K is an empirically derived factor that varies with the number of hits. Values for K are given in Table 12.4b.

Table 12.4b – K Values to be used for Historic Index Analysis

Number of Hits	K
<50	Not Applicable
50-200	N-30
201-500	0.85N
500-2000	N-35

12.4.2 Significance of Indication – The significance of the emission categories defined in Table 12.4a are given in Table 12.4c.

Table 12.4c – Structural Significance of AE Categories

CATEGORY	**Structural Significance**
None	None
Minor	Minor indication, note for future tests. No further action required.
Warning	Follow-up inspection and evaluation required. Repair may be necessary.
Serious	Indication of significant structural deterioration. Inspection and repair shall be performed. It may be necessary to remove the girder from service.

CHAPTER 13 – TEST REPORT

13.1 Requirement - A test report shall be issued for each concrete girder tested.

13.2 Content - A test report shall include but not be limited to the following:

1. Complete identification and description of the girder tested. This is to include the location of the test site, the designation of the girder, and the girder type.

2. Sketch showing sensor locations and numbers.

3. Structural evaluation based on the acoustic emission data and analysis method specified in Chapter 12. Defect areas can be marked on the sensor location sketch.

4. Recommendations for follow-up action.

5. Emission categories, Felicity ratio, and maximum amplitudes for each occurrence of significant emission from the monitored region(s).

6. Data recorded during the instrumentation settings and performance check specified in Chapter 10

7. Any unusual effects or observations during or prior to monitoring.

8. Period of monitoring.

9. A description of the AE instrumentation, including manufacturer's name, model number, and sensor type.

10. Dates of most the recent calibration and instrument verification.

11. Test organization and name(s) of inspector(s).

MANDATORY APPENDIX A - INSTRUMENT CALIBRATION

A.1 General - The performance and threshold definitions vary for different types of acoustic emission instrumentation. Parameters such as signal strength and amplitude vary from manufacturer to manufacturer and from model to model by the same manufacturer. This appendix describes techniques for generating common baseline levels for the different types of instrumentation. The amplitude decibel values are for a typical piezoelectric crystal using the measurement scale specified in Paragraph 7.7.4. Signal strength values are typical MARSE values measured in Volt-seconds multiplied by 10^5. The procedures defined in this appendix are intended for baseline instrument calibration at 60 to 80^o F. Instrument manufactures are permitted to use other procedures consistent with ASTM Standards, industry practice, and written in-house practices. Procedures used by instrument manufacturers must be shown to provide threshold, amplitude, and signal strength values that can be directly related to the values obtained by use of this appendix. It is recommended that instrument users develop approximate calibration techniques, along the lines outlined in this appendix. For field use, a portable acrylic rod can be carried with the equipment and used for periodic checking of sensor, preamplifier, and channel sensitivity.

A.2 Data Analysis Threshold - The data analysis threshold shall be determined using a 1 foot x 10 foot x 1/2 inch, 99% pure lead sheet suspended clear of the floor with the long side parallel to the floor. The data analysis threshold is defined as the average measured amplitude of 10 hits generated by a 0.3 mm pencil lead (2H) break at a distance of 27 inches from the sensor. Each break shall be done at an angle of approximately 30 degrees to the test surface with a 0.1 in lead extension. The sensor shall be mounted 12 inches from the end of the sheet and mid-distance between the 10 foot sides of the sheet. The sensor may be mounted using duct tape tightly wrapped around the backside of the sheet to firmly hold the sensor against the lead sheet. Silicone based stopcock grease shall be applied between the face of the sensor and the lead sheet. Based on the calibration procedure given in this paragraph the test threshold for most instruments is 55 dB.

A.3 Decibel Calibration - Instruments shall be calibrated using the 1 foot x 10 feet x 2 inches, 99% pure lead sheet. Decibel values shall be determined as the average measured amplitude of ten hits generated by a 0.3 mm (2H) pencil lead break at the distances shown in the table below. Each pencil lead break shall be done at an angle of approximately 30 degrees to the lead sheet surface with a 0.1 in lead extension from the pencil. Typical decibel values are given in Table A.3.

TABLE A.3 – DECIBEL CALIBRATION VALUES

Distance of Pencil Break from Sensor	Typical Decibel Value
6’ – 0”	40
5’ – 0”	44
4’ – 0”	48
3’ – 0”	52
2’ – 0”	56
1’ – 0”	61
6”	66
4”	70

A.4 Signal Strength Calibration (MARSE) - The signal strength calibration values given in Table A.4 shall be confirmed electronically with a constant amplitude 150 kHz pulse of 1 millisecond duration input to each channel. The evaluation criteria given in Section 12.4 are based on these values. Signal strength calibration values may vary between instruments, but should maintain the same relative values as listed in the table.

TABLE A.4 - SIGNAL STRENGTH CALIBRATION VALUES

Amplitude of Input Signal [1,2], dB	Typical Signal Strength[3] Calibration Value, V-sec x 10 [5]	Relative Value [4]
45	25	1.0
55	79	3.2
65	251	10
75	791	31.6

Notes:

1. See Appendix A.3 for explanation of decibel values.
2. Input signal is a constant amplitude 150 kHz pulse of 1 millisecond duration.
3. Signal strength values are typical MARSE values measured in Volt-seconds multiplied by 10^5.
4. The "Relative Value" is the ratio of the signal strength calibration value of a constant amplitude 150 kHz pulse of 1 millisecond duration with a given amplitude (dB) to the signal strength calibration value of a constant amplitude 150 kHz pulse of 1 millisecond duration with an amplitude 5dB above the data analysis threshold.

A.5 Hit Duration - The accuracy of the hit duration measurement shall be confirmed electronically with a constant amplitude 150 kHz pulse, varied from 50 to 500 microseconds duration, input to each channel. A calibrated transient waveform recorder shall be used to confirm the time duration of the input pulse.

Chapter 1 - Introduction

1.1 BACKGROUND OF PROJECT

In late 1995, the Texas Department of Transportation (TxDOT) became aware of premature concrete deterioration in several prestressed concrete girders and in-service structures throughout the state. Based upon investigation by scanning electron microscopy and petrographic analysis, this premature concrete deterioration problem has been attributed to a combination of alkali-silica reaction (ASR) and delayed ettringite formation (DEF) (Lawrence et al. 1997). As statewide inspection of in-service concrete structures progresses, more structures with this problem are being identified. The cost for replacing and repairing these structures is already significant and will continue to increase.

In order to determine the structural significance of the concrete deterioration, TxDOT sponsored research Project 1857, "Structural Assessment of In-Service Bridges with Premature Concrete Deterioration." This project focuses on seven specific tasks (Klingner and Fowler 1998):

Task 1 – Conduct field investigations to confirm and monitor existing premature concrete deterioration, the rate of increase of such deterioration, and the effect of different remedial measures on that rate of increase.

Task 2 – Conduct laboratory investigations of local effects of premature concrete deterioration.

Task 3 – Develop nondestructive evaluation techniques for determining degree and type of concrete deterioration.

Task 4 – Develop petrographic techniques for assessing severity of deterioration from samples taken from field investigations.

Task 5 – Develop engineering models for evaluating the global reduction in capacity of a structural element due to local premature concrete deterioration.

Task 6 – Develop an overall methodology for predicting the probable loss in capacity over time of a deteriorated structural element, based on external evidence, NDE, and engineering models.

Task 7 – Develop recommended actions by TxDOT for handling any given case of premature concrete deterioration.

1.2 SCOPE OF THIS THESIS

The scope of this thesis is related to Tasks 3 and 6 of the tasks outlined in Section 1.1. This thesis concentrates on acoustic emission, a non-destructive test method. Acoustic emission monitoring of shear-dominated fatigue tests and pull-out tests is reported. Background noise tests were carried out on in-service bridges. These tests monitored noise in the frequency range used to detect acoustic emission from concrete. This information is needed in order to develop field applications of the technology.

In this thesis, a procedure is proposed for acoustic emission field monitoring of prestressed concrete bridge girders. The procedure is based on

field data from shear-dominated fatigue tests, the pull-out tests, previous research reported by Yepez (1997) and by Tinkey (2000), and the field background noise tests.

1.3 OTHER RESEARCHERS ON THE PROJECT

Dr. Timothy J. Fowler, Dr. Richard E. Klingner, and Dr. Michael E. Kreger are supervising professors on the project. Other student researchers include:

- Anna Boenig conducted tests in the laboratory and undertook field observations in order to correlate the damage in prestressed concrete girders with their structural capacities (Boenig 2000) (Tasks 1 and 2).
- Brian Tinkey conducted the following nondestructive tests in the laboratory in order to quantify distributed damage in prestressed concrete girders (Task 3): visual inspection, acoustic emission, impact echo, and short pulse radar (Tinkey 2000).
- Joe Roche conducted full-scale fatigue tests on a prestressed box concrete girder in order to determine the effects of premature concrete deterioration on shear-fatigue strength of pre-cracked prestressed concrete girders (Roche 2001) (Task 2).
- Larry Memberg is performing strand pull-out tests on slices removed from the full-scale box girders (Task 2).

- Luz Funez completed a preliminary report on the field observations, and monitored crack patterns and crack widths in specimens in the laboratory (Task 1).
- Yong-Mook Kim has performed tests on Type C prestressed girders and pull-out tests on slices removed from these girders. He is developing strut-and-tie models to predict structural capacities of the girders subjected to different levels of premature deterioration (Task 5).
- Amy Eskridge is working on the related study 4069, "Mitigation Techniques for In-Service Structures with Premature Concrete Deterioration." She will also conduct field observations of ASR/DEF damaged structures.

Chapter 2 - Literature Review

2.1 INTRODUCTION TO ACOUSTIC EMISSION

Acoustic emission (AE) is a passive inspection technique that has been widely used to assess structural integrity. In several industries, the practical application of acoustic emission technology to field inspection has advanced steadily over the past 25 years. Standard test procedures have been developed by number of organizations including the American Society for Nondestructive Testing, the Association of American Railroads, the American Society of Mechanical Engineers, and the American Society for Testing and Materials. Titles of some of the more important of these procedures are given in the reference list (ASNT, AAR, ASME, ASTM).

Acoustic Emission is defined as "The class of phenomenon whereby transient elastic waves are generated by the rapid release of energy from localized sources within a material, or the transient waves so generated" (ASTM E1316). For most nondestructive test applications, emission is monitored in the range of 10 kHz to 1MHz. Emission can be from many different mechanisms including deformation and fracture. In metals, acoustic emission sources include yielding, corrosion, and crack growth (Heiple and Carpenter 1987a, 1987b). In composites, matrix cracking, fiber breakage, and fiber debonding are common sources of emission (Fowler 1979).

In addition to internal acoustic emission sources, external noise such as mechanical rubbing, wind, air hoses, and filling can create elastic waves, which interfere with genuine data. These extraneous noises need to be prevented in the test or filtered out before the data are analyzed.

Acoustic emission is generated by the material itself. In contrast, other types of stress-wave nondestructive testing methods, such as impact echo and ultrasonics, need an external input source. An additional advantage of acoustic emission compared to these other methods is that it is a global test. A global test covers a large area with one test, whereas the other methods cover a very limited area and are referred to as local tests. Acoustic emission can also be used for continuous monitoring, which is important for many in-service structures. A drawback of acoustic emission is that it depends on the applied load. As a result, some discontinuities may not emit detectable acoustic emission under a particular load.

2.1.1 Acoustic Emission Signals

In the acoustic emission technique, transient elastic stress waves in the material are detected by piezoelectric sensors attached to the surface of the structure. These sensors convert pressure on the face of the sensor into an electrical output. The sensors are designed to operate in a specific frequency range of interest. This is usually accomplished with a piezoelectric crystal that is resonant in the specific frequency range. The signal from the sensor is amplified

and passed through a band-pass filter before being transmitted to the acoustic emission instrument.

The acoustic emission signal contains the characteristics of the stress wave. As a stress wave travels through the material, its high-frequency components are attenuated more rapidly than the low-frequency components. Sensors located away from the source of a stress wave will detect only low frequency. As noted above, acoustic emission transducers typically operate in the range of 10 kHz to 1 MHz. Therefore, selecting different types of acoustic emission sensors will lead to different acoustic emission signals. Important parameters also include amplitude, duration, and signal strength. Figure 2.1 shows a schematic of acoustic emission signal.

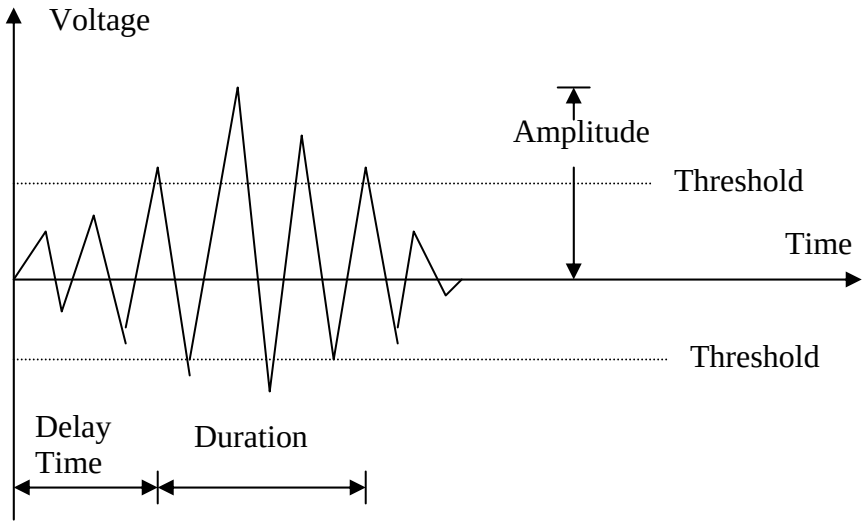

Figure 2.1 – Typical Acoustic Emission Signal

The following definitions are used in this thesis:

- **Signal Amplitude, Acoustic Emission**: The peak voltage of the largest excursion attained by the signal waveform from an emission event (ASTM E 1316). For the purposes of this thesis signal amplitude is measured in decibels.

- **Hit Duration (Duration)**: The time from the first threshold crossing to the last threshold crossing of the signal or envelope of the linear voltage time signal (AAR IM-101).

- **Felicity Effect**: The presence of detectable acoustic emission at a fixed predetermined sensitivity level at stress levels below those previously applied (ASTM E 1316). The fixed sensitivity level will be the same as was used for the previous loading or test.

- **Felicity Ratio:** The ratio of the stress at which the Felicity effect occurs to the previously applied maximum stress (ASTM E 1316).

- **Hit Arrival Time:** The time of the first threshold crossing of a sensor hit, measured against a time reference that is common to all sensors (global clock). For time-of-arrival source location, a hit arrival time corresponding to the global clock time of the peak amplitude, or other predefined point on the signal waveform, may be used (CARP).

- **Hit Definition Time:** A specified time interval defining the end of a hit during which no additional threshold crossings occur. The hit definition time is measured from the last threshold crossing of the hit. The first threshold crossing following the hit definition time is part of the next hit (CARP).

- **Kaiser Effect:** The absence of detectable acoustic emission at a fixed sensitivity level (threshold), until previously applied stress levels are exceeded (ASTM E 1316).

- **MARSE:** Measured area of the rectified signal envelope (ASME Section V, article 12). A measurement of the area under the envelope of the rectified linear voltage time signal from the sensor (AAR IM-101).

- **Signal Strength**: Area under the envelope of the linear voltage time signal from the sensor. The signal strength normally includes the absolute area of both the positive and negative envelopes (AAR IM-101). For the purposes of this thesis, MARSE is used as a relative measure of signal strength.

- **Voltage Threshold (Threshold):** A voltage level on an electronic comparator such that signals with amplitudes larger than this level will be recognized (ASTM E1316).

2.1.2 Intensity Analysis

Intensity analysis is a method for evaluating structural integrity. It is used as a tool to evaluate the condition of a structure. Intensity analysis can be used to determine whether a structural member has a rejectable flaw. A rejectable flaw is referred to as a defect. If the structure contains a defect, a range of actions can result:

(i) It can be noted for reference;

(ii) It can be tested more often;

(iii) It can be scheduled for repair; or

(iv) It can be immediately removed from service.

Intensity analysis is carried out on a per-channel basis. The method uses historic index and severity, both of which are based on the signal strength parameter.

Historic index compares the signal strength of the most recent hits to the signal strength of all hits. It is sensitive to changes in slope in the curve of cumulative signal strength versus time. Rapid increase in historic index represents significant change in the slope of the cumulative signal strength curve. The occurrence of a change in slope is often referred to as the "knee" in the curve. This knee in the curve represents the onset of a new damage mechanism. Historic index is defined by Equation (2.1).

$$H(t) = \frac{N}{N-K}\left(\frac{\sum_{i=K+1}^{i=N} S_{Oi}}{\sum_{i=1}^{i=N} S_{Oi}}\right) \quad \text{.....(2.1)}$$

Where:

H(t) is the historic index at time t.

N is the number of hits up to and including time t.

S_{Oi} is the signal strength or MARSE of the *i*th hit.

K is an empirically derived factor that varies with the number of hits.

Values of K are given in Table 2.1 for fiber reinforced plastic (FRP) tanks and pressure vessels (CARP). K values for metal tanks and vessels are given in Table 2.2 (MONPAC). As can be seen, the values of K are different for different materials.

Table 2.1 - K Factor for FRP Tanks and Vessels (CARP)

Number of Hits, N	**K**
<20	Not applicable
20 to 100	0
101 to 500	0.8N
> 500	N-100

Table 2.2 - K Factor for Metal Tanks and Vessels (MONPAC)

Number of Hits, N	K
<10	Not applicable
10-15	0
16-75	N-15
76-1000	0.8N
>1000	N-200

The second factor is severity. It is the average of the largest signal strength hits striking a sensor. The use of signal strength to define severity reduces the effect of distance from the sensor, and allows the intensity analysis to be used on the full range of field geometries. Severity is defined by Equation 2.2 (CARP).

$$S_r = \frac{1}{J}\sum_{m=1}^{m=J} S_{Om} \quad \text{.....(2.2)}$$

Where:

S_{Om} is the signal strength of the *m*th hit. *m* is ordered on the magnitude of the signal strength with m=1 being the hit having the largest signal strength.

J is an empirically derived constant that depends on the material of construction. Table 2.3 and 2.4 show values of J for FRP and metal tanks and pressure vessels.

Table 2.3 - J Factor for FRP Tanks and Vessels (CARP)

Total Number of Hits	**J**
<20	Not applicable
>20	20

Table 2.4 - J Factor for Metal Tanks and Vessels (MONPAC)

Total Number of Hits	**J**
<10	Not applicable
>10	10

The results of historic index and severity for each channel are plotted on an intensity chart which uses a log scale for both historic index and severity. Figure 2.2 shows the intensity chart for FRP vessels monitored with 150 kHz sensors. The chart is divided into zones of defect intensity marked as: “Insignificant”, “Minor”, “Intermediate”, “Follow-up” and “Major”.

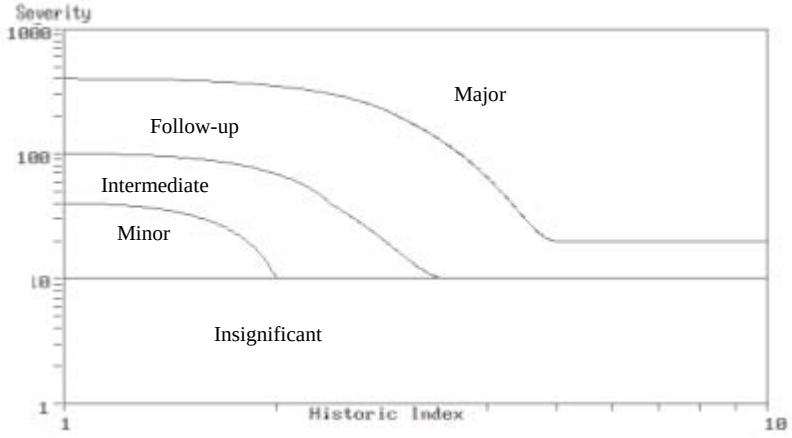

Figure 2.2 – Intensity Chart for FRP Vessels Monitored with 150 kHz Sensors (CARP)

2.1.3 Signature Analysis

An amplitude distribution function has been used for processing acoustic emission signals. It provides a method to quantify acoustic emission data and a means of discriminating between various source mechanisms (Pollock 1978).

One of the most useful tools of amplitude distribution analysis is the power law model. It was first developed from an observation that amplitude

distributions often appear as straight lines, when plotted on logarithmic axes. The mathematical model can be expressed as Equation 2.3 (Pollock 1981).

$$\Phi(V) = (V/V_t)^{-b} \quad \text{.....(2.3)}$$

Where:

$\Phi(V)$ is the normalization of the cumulative distribution function. It represents the probability that an emission's amplitude exceeds the amplitude V. $\Phi(V_t)$ is equal 1.

V is the detected hit's amplitude (Voltage).

V_t is the lowest amplitude considered in the model (Voltage).

b is a constant that depends on mechanism and material.

The slope of a plot between log of the cumulative distribution function ($\Phi(V)$) and log amplitude (V) is the "b" value in Equation 2.3. It characterizes the mechanism of the deformation in a material. The deformation mechanism in a material changes as the stress increases. Accordingly, the b-value is also a function of stress and changes as stress increases. The b-value does not depend on the distance from a source to a sensor. It normally decreases when a material is subjected to higher stress and tends to decrease for the propagation of a crack in a brittle material. Table 2.5 shows the b-values in various materials.

Table 2.5 - b-Values in Various Materials (Pollock 1981)

Material	*Deformation Mechanism*	*b-value*
Steels		
A516	Plastic zone growth	4.0
A537	Plastic zone growth	1.5-2.0
Other metals		
7075-T6 Al	Growth of crack and plastic zone	1.0
Ti-13Al-22Nb	Tensile test	1.1
Non-metals		
Fiber glass	Inter-layer crack propagation	1.7
Graphite epoxy composite	Surface damage by thermal stress	2.0
Other processes		
Cadmium-plated steel	Debonding of plating	1.0
Steel pipeline	Rainfall	1.2

In some cases, the power law model does not fit with experimental data. In these situations, other models such as the log normal and the Weibull model are used. The power law model, however, is the most widely used model for characterizing amplitude distribution.

2.2 ACOUSTIC EMISSION FROM CONCRETE

Compared with other types of materials, for instance steel and fiber-reinforce plastics, concrete attenuates an acoustic emission signal more rapidly. This is because of microcracks and the nonhomogeneous property of the concrete. The tests done by Uomoto (1987) on concrete beam specimens (10 x 10 x 120 cm) and cylinders (10 cm diameter; 20 cm height) show that amplitude detected by 140 kHz sensors reduces approximately 100 dB/m. This value is quite large compared to the attenuation in steel. Considering the background noise of about 30 dB, the effective range of acoustic emission monitoring using this type of sensor is limited to 20 to 30 cm. Attenuation of the acoustic emission signal in prestressed concrete is less than in reinforced concrete because prestressed concrete remains uncracked, or the cracks are closed and in compression, until it reaches a high percentage of its ultimate load (Yepez 1997).

The sources of acoustic emission in plain concrete depend on the type of loading. For pure compression load, the emission is generated from crushing of matrix and aggregate, while for pure tension, it is induced from cracking of the matrix and bond breaking between matrix and aggregate. The sources of acoustic emission also include friction and crushing when cracks are opening or closing during unloading and early compression.

A number of tests have been performed on reinforced concrete members in order to comprehend the mechanism of acoustic emission in these types of structures and to try to apply acoustic emission as a tool for evaluating the structural integrity of reinforced concrete beams (Karabinis and Fowler 1983).

2.2.1 Yuyama et al.

A series of tests was carried out by Yayama et al. (1999). These included cyclic loadings applied to reinforced concrete beams with a single reinforcing bar, large repaired beams, beams deteriorated due to corrosion of reinforcement, and two beams with different damage levels. The test results show that the Kaiser effect starts to break down when shear cracking starts to play an important role. In a damaged specimen, the Felicity ratio, or concrete beam integrity (CBI) will reduce and it can be used as a criterion to measure the severity of damage in a specimen. These results also agree with cyclic loading on a reinforced concrete rigid frame (Yuyama 1995). The Kaiser effect existed when the tensile crack width was smaller than 0.15-0.20 mm. This effect broke down when the crack width exceeded this value, or when transverse shear cracks started to play a primary role at the interface between the reinforcement and the concrete matrix.

Yuyama et al. also showed that amplitude and AE activity during unloading are a good representation of the damage mechanism in a reinforced concrete beam. Table 2.6 shows an example of evaluation criterion for damage induced in reinforced concrete beams.

Table 2.6 - An Example of Evaluation Criteria for Damage Induced in Reinforced Concrete Beams (Yuyama et al. 1999)

Fracture Stage		Damage Level (Crack width)	Amplitude (dB)	CBI Ratio	AE Activity During Unloading
I	Early microcracks	Low	40 – 60	Larger	Low
	Main tensile cracks	(W < 0.12-0.20 mm)	80 – 100	than 1	
II	Secondary tensile cracks	Medium	40 – 80	0.8 - 0.9	Medium
	Internal shear cracks	(0.12-0.20 mm < W)			
III	Slips between reinforcement And concrete Or Slips between repaired part And original concrete	High (0.5 mm < W)	40 – 60	Smaller than 0.8	High

2.2.2 Barnes and Fowler

As described before, acoustic emission works by detecting a stress wave in a material. Accordingly, it is difficult to apply acoustic emission to a reinforced concrete structure (Barnes and Fowler 1998). Tension cracks start forming at low load and provide a barrier to transmission of the wave through the structure. Stress waves generated from these cracks also mask the waves from significant damage.

2.3 ACOUSTIC EMISSION FROM PRESTRESSED CONCRETE

The prestressing force in a prestressed concrete structure prevents formation of new tension cracks at low load and closes any that may be present. Therefore, a prestressed concrete structure provides a good environment for the transmission of acoustic emission stress waves.

2.3.1 Luis Yepez

There were many tests done by Luis Yepez (1997) at the University of Texas at Austin. His tests introduced the application of acoustic emission to full scale prestressed concrete girders. Acoustic emission monitoring was done on AASHTO Type I prestressed girders with a 6.5-inch thick concrete slab cast on top. The ability of acoustic emission to predict and locate crack before their appearance at the surface was indicated from the results. Cumulative energy increased significantly shortly before both shear and flexure cracks were observed on the surface of the girder. This increase corresponded to the formation of the microcrack network within the concrete. Another parameter that changed considerably before cracking was historic index (HI). This parameter was used to define the onset of emission because it could define the load corresponding to the change in energy release clearer than a cumulative energy versus time plot. The results showed that the acoustic emission signal started to be significant at 40-50% of ultimate load when the specimens failed by flexure. A similar change was observed at 30-40% of ultimate load when the specimens failed by shear. These results are shown in Figure 2.3.

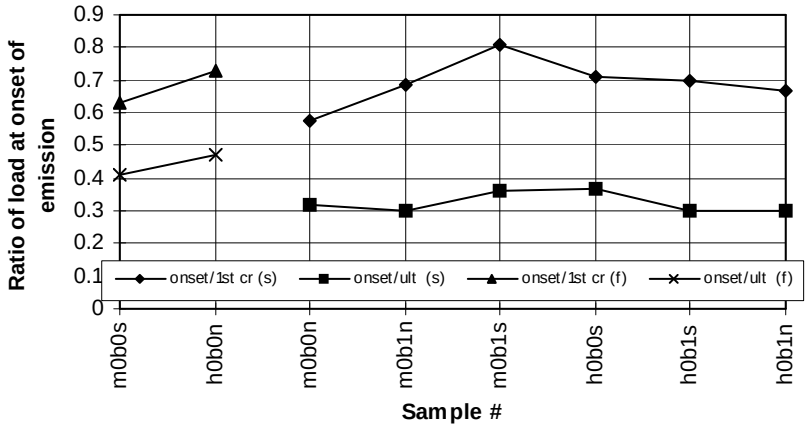

Figure 2.3 – Ratio of Load at Onset of Emission to First Cracking Load and to Ultimate Load as a Function of Test Sample (Yepez 1997)

Moment tensor analysis (Ohtsu 1988) was applied by Yepez to the test results using the Sigma program from Physical Acoustic Corporation. The analysis was used to obtain information about the location and type of a crack. The results from the moment tensor analysis agreed well with the actual crack type and visible pattern on the surface of the beams. Many sensors, however, were needed in order to compensate for the attenuation of the signal and to obtain three-dimensional source location.

2.3.2 Tinkey

Another researcher studying the application of acoustic emission to prestressed concrete girders was Tinkey (2000). Several tests were conducted on full scale prestressed box girders and full scale Type C prestressed girders with ASR/DEF damage. The beams had different levels of premature deterioration.

The author reported that acoustic emission showed considerable promise for evaluating distributed damage in prestressed concrete. The Felicity ratio provided a good indication of the structural significant of the damage. The more severe the damage in the specimen, the lower the value of the Felicity ratio. The cumulative signal strength criterion was used to determine the onset of significant emission. Figure 2.4 shows representative results from the tests performed on the box girders.

Other potential indicators were the amount of emission during loading, amount of emission during load hold, and high amplitude hits. Preliminary evaluation criteria using the Felicity ratio and the number of high amplitude hits during loading were proposed. Tinkey's work contributed to a better understanding of acoustic emission on prestressed concrete girders with premature cracking. Other nondestructive evaluation techniques were evaluated by Tinkey including: visual inspection, short-pulse radar, and impact-echo. It was concluded that visual inspection is suitable for preliminary evaluation but it is subjective. Short-pulse radar and impact-echo needed more research before they could be to be used to quantify the amount of distributed damage in concrete.

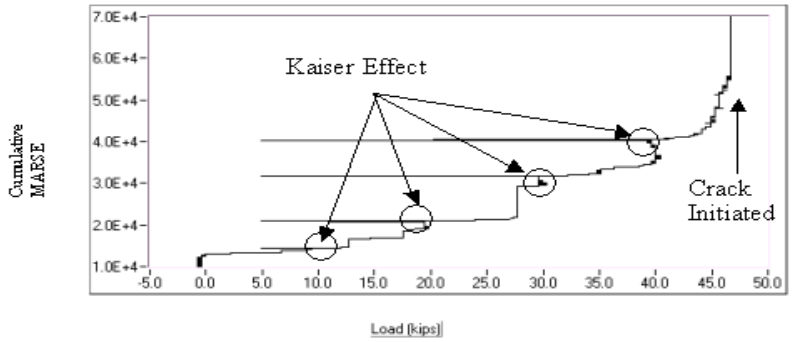

a) Initial Loading of Flexure-Dominated Box Girder Test Prior to Cracking (BG1)

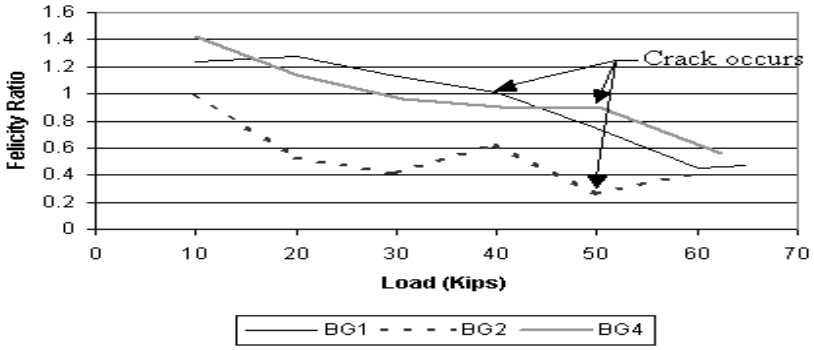

Failure Loads: BG1 = 118.6 kips, BG2 = 116.3 kips, BG4 = 118.9 kips

b) Effect of Load on Felicity Ratio for Flexure-Dominated Box Girders

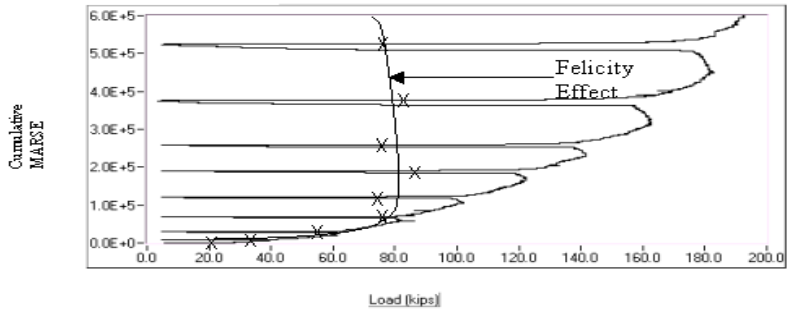

c) Shear-Dominated Box Girder Test (BG1S)

Figure 2.4 – Felicity Effect of Tests on Box Girder (Tinkey 2000)

2.3.3 CARP Procedure

As mentioned previously, the Felicity ratio is a good indicator of the damage level in a specimen. It is obtained directly from the ratio of the load at the onset of significant emission to the previously applied maximum load. The onset of significant emission used to determine the Felicity ratio is sometimes based on operator experience. This is a subjective measurement and efforts have been made to define onset of emission. For composite tanks and pressure vessels, the following guidelines are recommended by CARP for determining the onset of significant emission on an individual channel.

- More than 5 bursts of emission during a 10% increase in load. One or more hits constitute a burst, and all hits for the five seconds following the initial hit are considered part of the same burst.
- Cumulative duration more than $N_D/20$ during a 10% increase in load. N_D is a duration criteria defined in the CARP Recommended Practice.
- Emission continues at a load hold. Continuing emission is defined as a rate of more than 3 hits per minute.

The characteristics of emission from concrete are different from the characteristics observed in other materials. Specific criteria to define the onset of significant emission in concrete will be proposed in this thesis.

2.4 ULTRASONIC INSPECTION ON CONCRETE

Ultrasonic testing is defined as “a nondestructive method of examining materials by introducing ultrasonic waves into, through or onto the surface of the

article being examined and determining various attributes of the material from effects on the ultrasonic waves" (ASTM E 1316). In the context of this definition, ultrasonic means "Pertaining to mechanical vibrations having a frequency greater than approximately 20 kHz." Typically, ultrasonic inspection of materials uses a wave frequency in the range of 500 kHz to 25 MHz. Ultrasonic wave propagation is governed by the Equation 2.4.

$$\lambda = V/f \quad \text{.....(2.4)}$$

Where:

λ is the wavelength.

V is the wave velocity.

f is the wave frequency.

As frequency is increased, the wavelength decreases, providing less penetration, but greater resolution and sensitivity. High attenuation is a major problem in applying ultrasonic techniques to concrete. To overcome the high attenuation and thick sections typical in concrete construction, a lower-frequency wave is required. This in turn results in a loss of sensitivity.

Concrete is a non-homogeneous material. The variation in aggregate sizes depends on the composition. The heterogeneity requires low testing frequencies in order to ensure that the ultrasonic wavelength is greater than the maximum particle size of the aggregate. Otherwise, the ultrasonic wave cannot pass through the concrete matrix, and reflects at the surface of aggregate. The maximum detectable flaw size with ultrasonic testing is $\lambda/2$. Wavelengths used for

ultrasonic testing of concrete are 20 to 100 mm, corresponding to frequencies between 200 and 40 kHz (Popovics et al. 1990).

Tests by Bungey (1990) show that the rates of attenuation of an ultrasonic wave in concrete increase significantly when alkali-silica reaction (ASR) is presented. 54 kHz and 82 kHz transducers were used and the tests were performed on small specimens. Attenuation measurements showed a 50% increase in attenuation at 0.3% expansion and an 80% increase at about 0.5% expansion. It is believed that the increase in attenuation reflects the increase in internal cracking.

2.4.1 Compressive Strength

If the path length is known, and the travel time is measured, the wave velocity can be determined. Through the relationships betweens pulse velocity and dynamic modulus of elasticity and between compressive strength and dynamic modulus of elasticity, the strength of concrete can be correlated to the pulse velocity. The relationship between strength and pulse velocity is affected by factors such as moisture content, aggregate content, and aggregate types. The relationship is expressed as an exponential function, as shown in Equation 2.5 (Swamy and Al-Hamed 1982).

$f_c = a \cdot e^{(b \cdot v)}$…….(2.5)

where:

f is the compressive strength;

V is the pulse velocity; and

a and b are empirical constants.

2.4.2 Thickness Measurement

Another application of the ultrasonic technique in concrete is measurement of the thickness. Knowing the velocity of the wave in concrete, the thickness can be calculated by measuring the travel time of a wave through the structural component. For this application, there are number of problems. One of the major problems is the fault signals that come from the reflections between surface waves and large aggregate particles on the surface of concrete. These reflections usually arrive earlier at the receiver than the signal reflected from the backside of the concrete, therefore and cover the reflected signal. For this reason, the through-transmission technique is preferred. With this method, the transmitter and receiver probes are placed on opposite sides of the specimen (Hillger 1994). Unfortunately, access to both sides is not always possible.

2.4.3 Defect Detection

Ultrasonic inspection is used extensively to detect flaws in metal components. The principle is similar to that used to measure thickness. For defect detection, the travel time of a wave that reflects off a flaw is measured.

Knowing the directions of the incident and reflected waves, the position of the flaw can be determined. Unfortunately, ultrasonic defect detection has not been successful in concrete because of high attenuation, thick sections, and reflections from aggregate particles and other internal flaws. The impact-echo method has been developed in order to overcome some of these problems.

2.4.4 Assessment of Concrete with Internal Cracking

The ultrasonic technique has been used to evaluate the condition of concrete. Pulse velocity and peak signal amplitude are used as indicators of concrete condition. For sound concrete, the pulse travel path is uninterrupted, while for cracked concrete, the pulse is reflected and/or diffracted at the cracks. Only a small portion of the wave, if any, takes the direct route and most of the wave takes longer routes. Consequently, the velocity of the wave in sound concrete appears to be faster than in concrete with even minor cracks. Likewise, the peak signal amplitude through sound concrete is higher than though cracked concrete because of energy reflection at cracks (Olson 1990). Figure 2.5 shows the wave detected from tests done on a precast concrete segment that was severely cracked during the erection of a post-tensioned segmental highway bridge. The monitored thickness ranged from 36 to 66 mm.

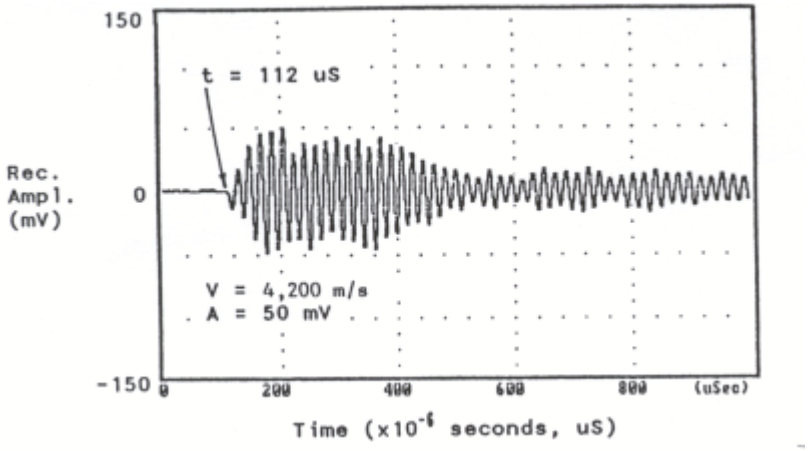

a) Sound Concrete

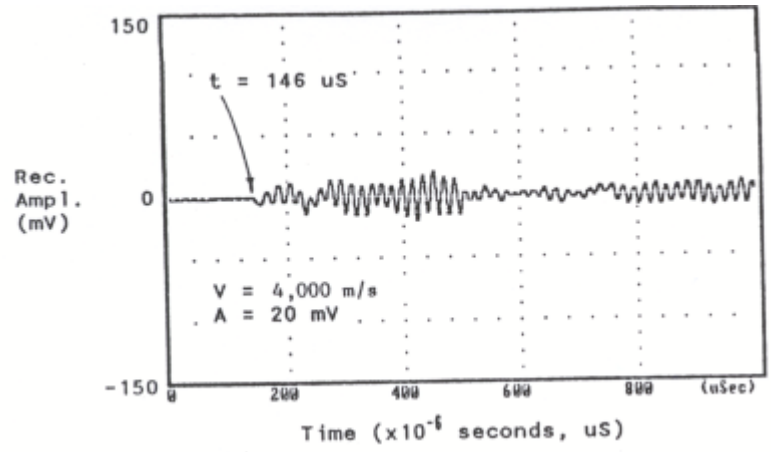

b) Partial Crack

Figure 2.5 – Ultrasonic Pulse Velocity Record (Olson 1992)

Application of the ultrasonic technique to concrete is still limited. A long wavelength with high pulse energy is required to order to overcome the high attenuation in concrete. Ultrasonic techniques have been used to evaluate the condition of structural concrete by measuring compression wave velocity and

attenuation. Based on a literature review and conversations with ultrasonic equipment vendors, the ultrasonic technique is not readily applicable to the full-scale box girders discussed in this thesis. Accordingly, the technique is not pursued further here.

Chapter 3 – Acoustic Emission Monitoring of Shear-Dominated Fatigue Tests

Two phases of acoustic emission monitoring were performed in the Ferguson Structural Engineering Laboratory of the University of Texas at Austin. In the first phase, shear-dominated fatigue tests were carried out on a full-scale prestressed box girder. In the second phase, strand pull-out tests were carried out and the test results will be reported in Chapter 4. A laboratory experiment is performed under controlled conditions, to allow the researcher to understand the behavior of material and to provide a foundation for field monitoring. In this thesis, results from both test phases are combined with the results from field background noise monitoring and previous researchers' studies to propose an acoustic emission field monitoring procedure for prestressed concrete bridge girders.

3.1 SPECIMEN DESCRIPTION

In the spring of 1999, four prestressed concrete box girders were sent to the Ferguson Structural Engineering Laboratory at the University of Texas at Austin. These girders were fabricated at Heldenfels Brothers, Inc. plant in San Marcos, TX and never put into service. The girders had premature deterioration due to the combination of delayed ettringite formation (DEF) and alkali-silica reaction (ASR). The four girders had the same dimensions but showed different

levels of premature deterioration. The surface condition of the girders was documented in another thesis by Tinkey (2000). Flexure-dominated tests and shear-dominated tests were performed on three of the box girders by other researchers, Boenig (2000) and Tinkey (2000). The remaining one, designated BG3 in both researchers' reports, was used to investigate structural performance under shear-dominated fatigue loading.

The prestressed concrete box girders were 69.83 ft nominal length and the wall thickness was 5 inches. Expanded polystyrene was used to fill the interior voids and to serve as interior formwork. 2.17 ft long solid end blocks were cast on both ends and 1 ft long intermediate stiffeners were cast at 23.33 ft from each end. Thirty ½ inch diameter 270 ksi, low relaxation prestressing strands were spaced at 2 inch intervals in the bottom of the girder (Figure 3.1). The concrete design strength was 6000 psi.

Fatigue tests were performed on the shear span of a full scale prestressed box beam girder. This girder had damage along the length due to premature deterioration. The level of damage was classified as "intermediate" on a scale of good, intermediate, and severe (Boenig 2000). The magnitude of the maximum applied loads was much higher than those imposed by normal traffic conditions.

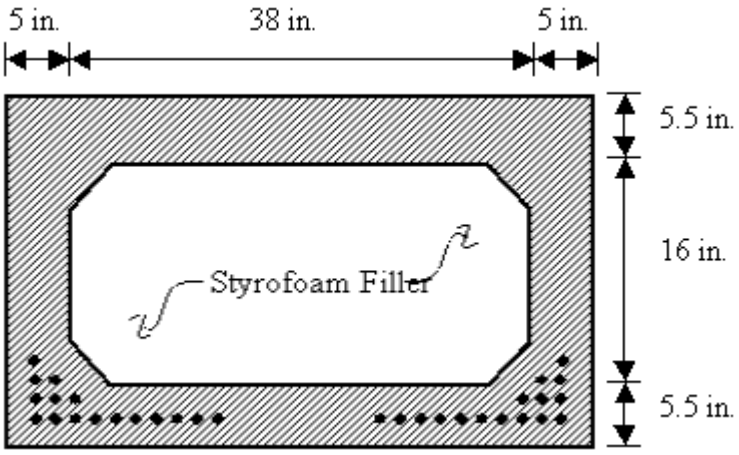

Figure 3.1 – Cross-Section of Box Girder Specimen

3.2 TEST SETUP

The prestressed concrete box girder, BG3, was sawn in half because of the space limitations of the testing area. Each end was tested under cyclic loading with different load ranges. An MTS 458.10 controller was used to control the system. An electronic signal representing the level of load was fed to the acoustic emission instrument.

Specimens were supported on Grade 70 neoprene pads in order to duplicate the support conditions in the field and to isolate the beams from external background noise. Cement paste and Hydrostone (gypsum plaster) were used to level the specimens and to provide a smooth surface. The Hydrostone was cast on the supports and on the top surface of the specimens. Two hydraulic rams were used to load the girder. Two transverse steel beams were placed underneath the rams to transfer the load to the specimens. The beams were placed on rollers that

were oriented in the longitudinal direction and placed above the beam webs in order to prevent a punching shear failure of the top flange. The same grade of 1/8 inch thick neoprene pad was placed between the rollers and the girder in order to prevent background noise from the rams contaminating the acoustic emission data during cyclic loading. The test setup is shown in Figure 3.2.

Figure 3.2 – Test Setup of Shear-Dominated Fatigue Test

Acoustic emission instruments were used to monitor the tests. Physical Acoustic Corporation (PAC) R6I and R15I resonant sensors were mounted on both sides of girders. The R6I sensor has a resonant frequency of 60 kHz and incorporates an integral 40 dB preamplifier. The R15I sensor is similar, but has a 150 kHz resonant frequency. The arrangement of sensors was chosen so as to

cover the expected failure area (Tinkey 2000). The sensor arrangement is shown in Figure 3.3. Before recording acoustic emission data, pencil lead breaks were used to verify that sensors were properly coupled to the specimens and functioning properly (AAR). Three 0.3 mm Pentel 2H leads were broken at 1 in. from each sensor. The leads were extended approximately 2.5 mm for each break, and were oriented at 30 degrees to the surface of the concrete. The average amplitude recorded by each sensor was not permitted to vary more than 4 dB from the average of all sensors.

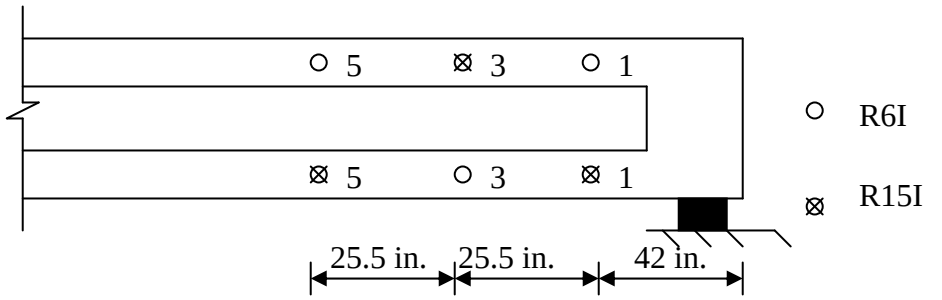

a) West Side

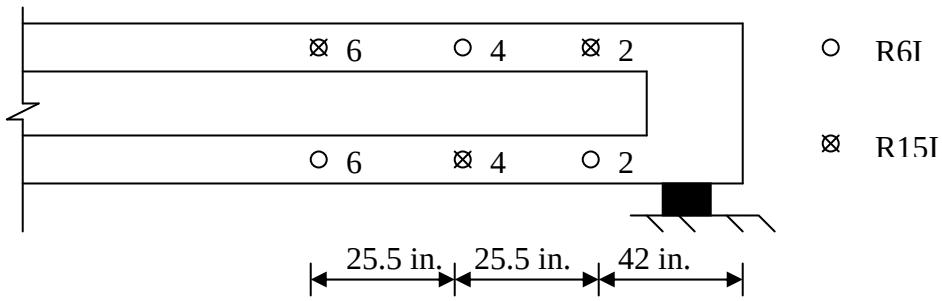

b) East Side

Figure 3.3 – Sensor Locations on Fatigue Specimen

3.3 LOADING SCHEDULE

Specimens were loaded cyclically in a shear-dominated region. Figure 3.4 shows the positions of the loads and supports. The specimens were subjected to the monotonic cyclic load that induced tensile strain on the bottom flange and compressive strain on the top flange.

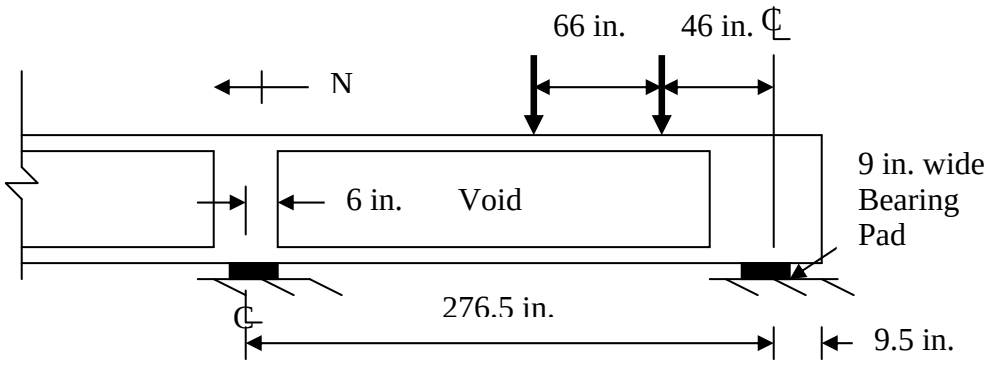

Figure 3.4 – Loading Positions in Shear-Dominated Fatigue Test

In the first test, named Fatigue Test A, a 315 kip static load was applied to the specimen. During the first static load, the loading was held at intermediate levels of 136, 260,and 300 kips so that cracks could be marked. Following the first static loading, the pre-cracked section was subjected to cyclic loading that varied from 20 kips to 300 kips. The frequency of sinusoidal loading varied between 0.25 Hz and 1.3 Hz. The maximum applied cyclic load was approximately 75% of the experimentally determined shear capacity of similar specimens tested under statically. The non-zero minimum load was necessary to prevent complete unloading of the girder and to prevent movement of the

specimen during cyclic loading. Static overload tests were performed after 100, 1000, and 10,000 cycles. During these static tests, load was increased from 5 kips to 300 kips, held at this load level until acoustic emission had died out, and then increased to 315 kips. This load was also held until acoustic emission ceased. After that, the load was decreased to 5 kips and again held until emission died out. Figure 3.5 shows the loading schedule for Fatigue Test A. The load schedule was designed to measure the Felicity ratio and to acquire acoustic emission data during loading, load hold, and unloading. During static loading, linear potentiometers and acoustic emission instruments were used to monitor strains and stress-wave signals. After static loading to 1,000 and 10,000 cycles, acoustic emission data were recorded for 10 minutes during cyclic loading. The specimen failed at 28,133 cycles during cyclic loading.

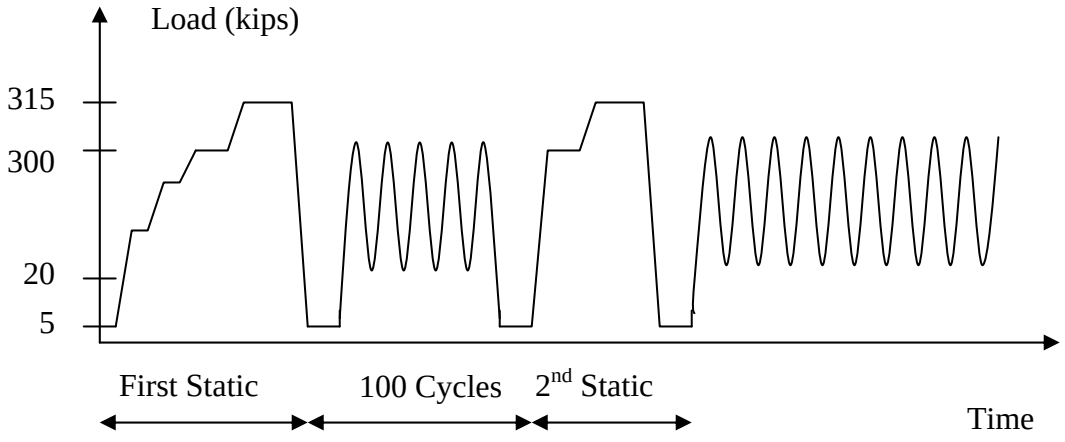

Figure 3.5 – Loading Schedule of Fatigue A

The loading schedule for the second test, called Fatigue Test B, was similar to that used for Fatigue Test A, except for the maximum static load and cyclic load range. In Fatigue Test B, a 250 kip static load was initially applied to the specimen in order to pre-crack it. The pre-cracked specimen was subjected to a sinusoidal cyclic load that ranged from 20 kips to 200 kips. Intermediate static overloads were performed after 10, 100, 1000, 10,000, 100,000, 200,000, 438,000, 500,000, 763,000, 1 million, 1.25 million, 1.50 million, 1.78 million, 2.02 million, 2.32 million, 2.56 million, 2.78 million, 3.07 million, and 3.33 million load cycles. During these static tests, the load was increased slowly from 5 kips to 200 kips, and held at this load until acoustic emission died out. The load was then increased to 210 kips and again held until emission subsided. After that, load was decreased to 5 kips. Following each static load test, acoustic emission data were recorded for 10 minutes of cyclic loading. The specimen did not fail during fatigue cycling. After 3.33 million cycles, cyclic loading was stopped and the specimen was loaded statically to failure. Failure occurred at 365 kips.

3.4 INSTRUMENTATION

Two acoustic emission instruments were used to record data during the shear-dominated fatigue tests. A six-channel MISTRAS 2001 instrument manufactured by Physical Acoustic Corporation (PAC) was used with the 60 kHz resonant sensors. This instrument has the ability to record waveforms, use guard sensors, and acquire a parametric signal from an external source. The electric signal from the MTS controller allowed the load to be recorded as part of the data

set. In addition, the MISTRAS records the following parameters for each hit: channel number, time of arrival to an accuracy of 250 nanoseconds, amplitude, signal strength (MARSE), duration, and rise time. A 24 channel instrument, known as a Transportation Instrument, also manufactured by PAC, was also used to acquire acoustic emission data. This instrument was used with the 150 kHz resonant sensors. The Transportation Instrument records the following parameters for each hit: channel number, time of arrival to an accuracy of 1 ms, amplitude, signal strength (MARSE), and duration. The instrument does not record waveforms or the applied load. Table 3.1 shows the instrument settings used for the shear-dominated fatigue tests.

Table 3.1 - Test Parameters for Shear-Dominated Fatigue Test

Quantity	*Values*
Hit Definition time (HDT)	400 μs
Voltage Threshold	40 dB for R15I and 55 dB for R6I
Sensor Preamplifier	40 dB
Peak Definition Time	200 μs
Hit Lock out time	200 μs

3.5 ONSET-OF-EMISSION CRITERIA

If significant damage occurs in a specimen, the nature of the damage can be determined from the acoustic emission parameters. The Felicity Ratio is one

such parameter. The lower the Felicity ratio, the more structurally significant the damage in the specimen. By definition, the Felicity ratio is the ratio between the load at the onset of significant emission and the previous maximum load. The load at the onset of significant emission is sometimes determined by the inspector, based on experience. Recent work has attempted to replace this subjective measure of the onset of significant emission with a quantitative measure based on the pattern and type of acoustic emission data (Tinkey 2000, MONPAC PLUS, CARP). The criteria to determine the onset of significant emission are also different for each type of material.

Signal strength is the most effective parameter to describe the trend of acoustic emission data because it takes both amplitude and duration into account. Acoustic emission data must be considered in its entirety and emphasizing an individual hit may lead to misinterpretation of the data. High signal strength is normally associated with damage in a specimen. Therefore, a graph of cumulative signal strength versus load is particularly important to describe what is going on in the specimen. A graph of cumulative signal strength versus time is sometimes used to describe damage in a specimen tested in a controlled environment. The rate of emission is dependent on the rate of applied load, and a graph of cumulative signal strength versus time can be used only when the load is being applied at a constant rate. A high slope in the curve of cumulative signal strength versus load corresponds with significant damage in a specimen. Normally, this curve will not show a significant change in slope when only emission from insignificant damage is detected. Three criteria listed below are

proposed to determine the onset of significant emission or the "knee" in the curve of an individual channel. The effectiveness of each of these criteria will be examined against the observed behavior of the girders under fatigue loading.

1) The slope of a cumulative signal strength versus time curve for a 20 hit window is greater than 50. For the purposed of analysis, consecutive 20 hit windows are considered.
2) The curvature or rate of change in slope of a cumulative signal strength versus time curve for a 40 hit increment is larger than 12.

$$\text{Curvature} = \frac{S_{i+1} - S_i}{\left[\left(\frac{t_3 - t_2}{2}\right) - \left(\frac{t_2 - t_1}{2}\right)\right]} = \frac{2(S_{i+1} - S_i)}{(t_3 - 2t_2 + t_1)} \quad \text{.....(3.1)}$$

Where:

S_i is the slope of a cumulative signal strength versus time curve for the i^{th} 20 hit increment;

S_{i+1} is the slope of a cumulative signal strength versus time curve for the $(i+1)^{th}$ 20 hit increment;

t_1 is the time in seconds at the beginning of the i^{th} 20 hit increment;

t_2 is the time in seconds at the end of the i^{th} 20 hit increment and at the beginning of the $(i+1)^{th}$ 20 hit increment; and

t_3 is the time in seconds at the end of the $(i+1)^{th}$ 20 hit increment.

It is important to note that the increments are for constant numbers of hits and not constant time intervals. Accordingly, $(t_3 - t_2)$ is not necessarily equal to $(t_2 - t_1)$.

3) The historic index, calculated from the criteria in Table 3.2 is larger than 1.5 for R6I sensors and 1.85 for R15I sensors. The proposed K values are based on trial-and-error analysis of the fatigue test data.

Table 3.2 – K-Values Used in Historic Index for Concrete

Number of Hits	*K*
<50	Not Applicable
50-200	N-30
201-500	0.85N
>500	N-75

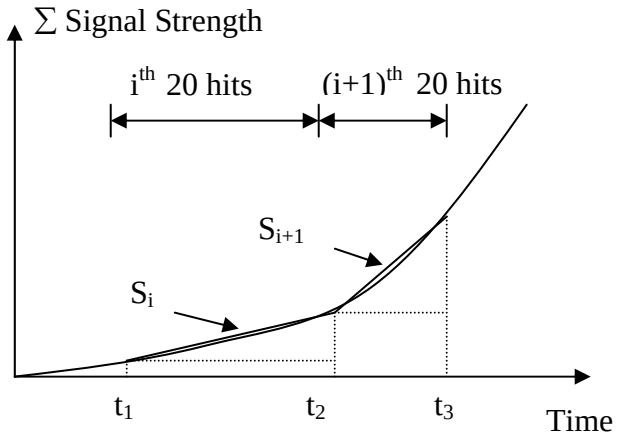

Figure 3.6 – Variables for the Onset-of-Significant-Emission Criteria

3.6 RESULTS OF SHEAR-DOMINATED FATIGUE TESTS ON BOX GIRDERS

Acoustic emission data from two fatigue tests is analyzed and separated in two groups; emission during quasi-static loading and during cyclic load. For the quasi-static load, emission during unloading, the Felicity ratio, and amplitude of emission during loading are considered. When specimens were subjected to cyclic loading, the amount of signal strength for specific numbers of cycles is considered.

3.6.1 Cyclic Loading of Fatigue Test A

The first shear-dominated fatigue test was performed on the northern part of BG3. The Felicity ratios are determined for each quasi-static static test. The onset of significant emission used to calculate the Felicity Ratio is determined by using each criterion described in the previous section. Table 3.3 and Table 3.4 show the results from the analyses. During unloading, only emission with an amplitude equal to 55 dB or higher is considered

During all loading cases, high amplitude hits (>85 for R6I and >75 for R15I) were detected.

Table 3.3 – Lowest Felicity Ratios of Fatigue A for R6I Sensors

# Cycles	Slope		Curvature		HI		Emission during	Max Amp during
	Load (kips)	FR	Load (kips)	FR	Load (kips)	FR	Unloading, Hits	Loading (dB)
1	-	-	-	-	-	-	2861	100
100	268.49	0.89	264.76	0.88	270.30	0.90	760	87
1,000	246.64	0.82	262.47	0.87	267.50	0.89	550	95
10,000	81.82	0.27	121.47	0.40	113.74	0.38	724	92

Table 3.4 – Lowest Felicity Ratios of Fatigue A for R15I Sensors

# Cycles	Slope		Curvature		HI		Emission during	Max Amp during
	Load (kips)	FR	Load (kips)	FR	Load (kips)	FR	Unloading, Hits	Loading (dB)
1	-	-	-	-	-	-	538	98
100	257.88	0.86	260.29	0.87	267.71	0.89	43	89
1,000	257.35	0.86	246.09	0.82	268.16	0.89	35	85
10,000	122.53	0.41	145.57	0.49	140.72	0.47	52	83

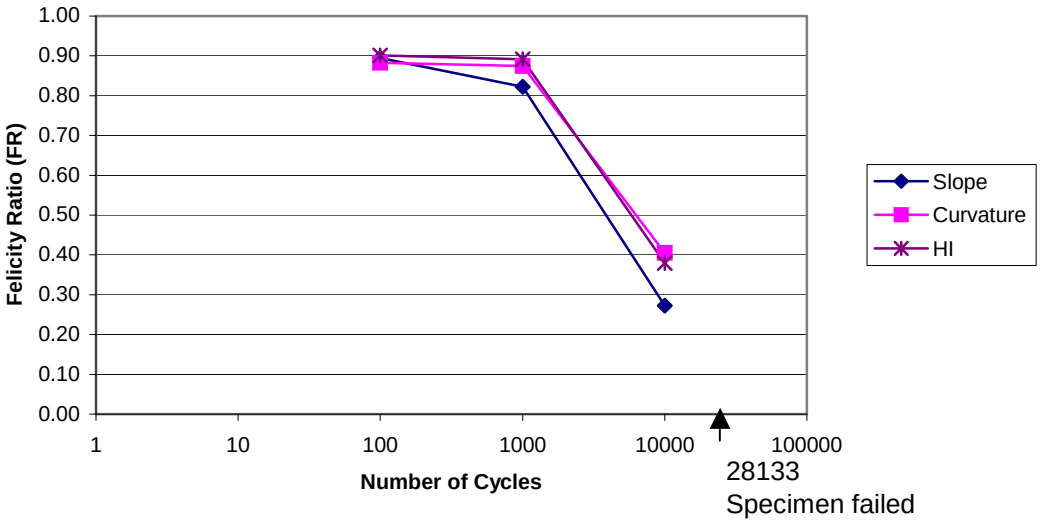

a) R6I

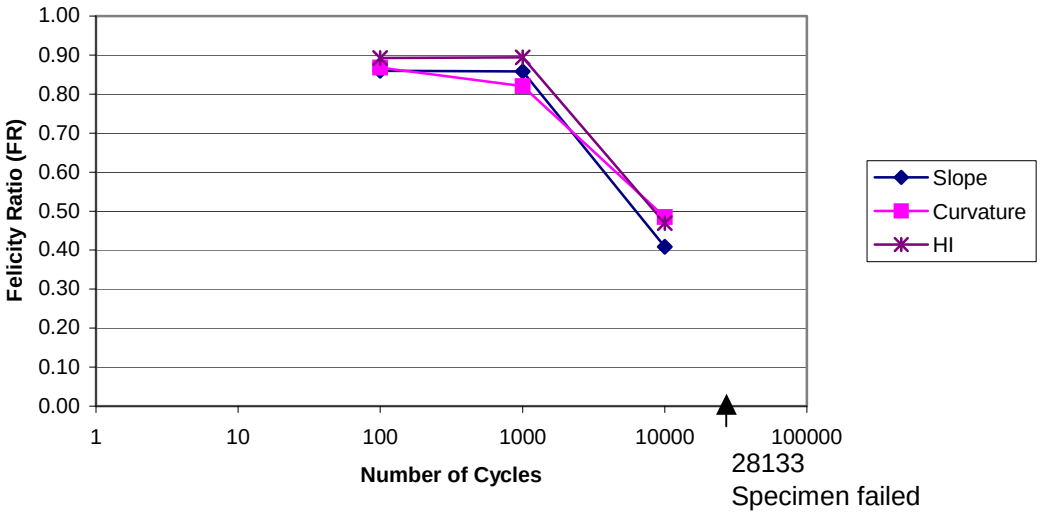

b) R15I

Figure 3.7 – The Felicity Ratios for Fatigue Test A

The Kaiser effect broke down at a small number of cycles because shear cracks started to play an important role. The Felicity ratios calculated from curvature, slope and HI are very similar. At 100 and 1,000 cycles, the lowest Felicity ratios are approximately 0.88 for the R6I sensors and 0.87 for the R15I sensors. Felicity ratios reduced dramatically at 10,000 cycles, with a value of 0.35 for the R6I sensors and 0.46 for the R15I sensors. The specimen failed at 28,133 cycles.

The number of hits during unloading is not a good index of damage in a specimen subjected to cyclic loading. The emission during unloading did not change much as the number of cycles increased. This is probably because opening of cracks and rubbing between aggregates during cyclic loading reduced emission during the quasi-static load.

The acoustic emission data recorded during 10 minutes of cyclic loading were also analyzed. The Fatigue Test A specimen failed at a small number of cycles. Even though this is not really representative of the behavior of an in-service prestressed concrete girder that is expected to be subjected to many million cycles, the data are instructive. The relationship between cumulative signal strength for 200 cycles after a quasi-static overload versus number of cycles is shown in Figure 3.8. The energy released after 10,000 cycles decreased significantly, especially the data recorded by the R6I sensors.

Figures 3.9 through 3.17 show details of the acoustic emission data for the quasi-static loads following 100, 1,00, and 10,000 cycles. Data are shown for

both the R6I and R15I sensors. Cumulative signal strength (MARSE), slope, curvature and historic index are shown on a per-channel basis.

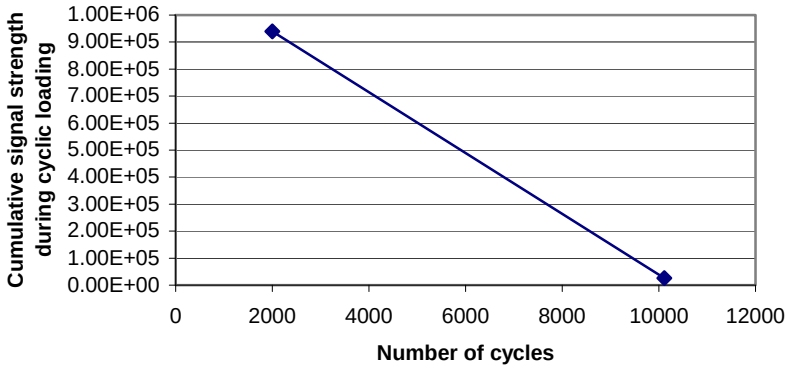

a) R6I

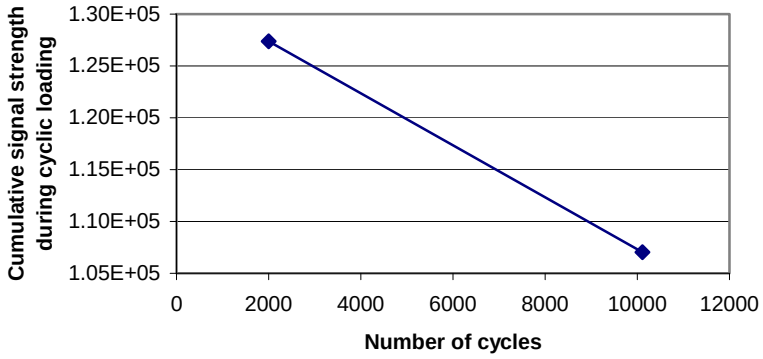

b) R15I

Figure 3.8 – Cumulative Signal Strength during Cyclic Loading for 200 Cycles Following a Quasi-Static Overload

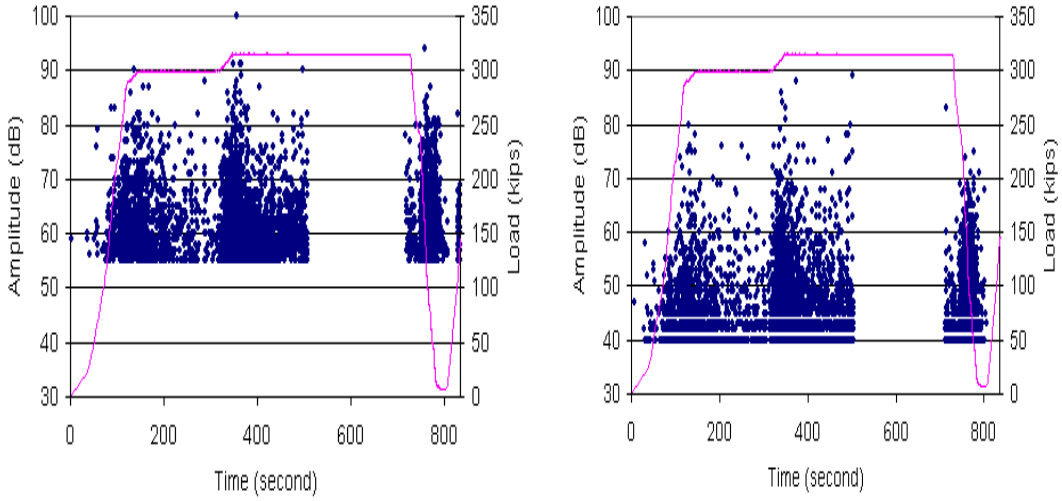

R6I R15I

a) Amplitude vs Time

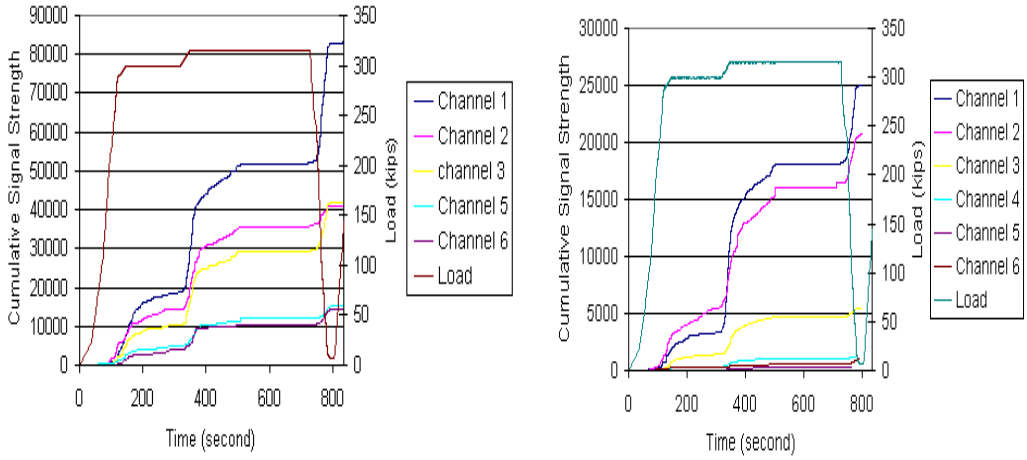

R6I R15I

b) Cumulative Signal Strength vs Time

Figure 3.9 – Time-Based Graphs at 100th Cycle

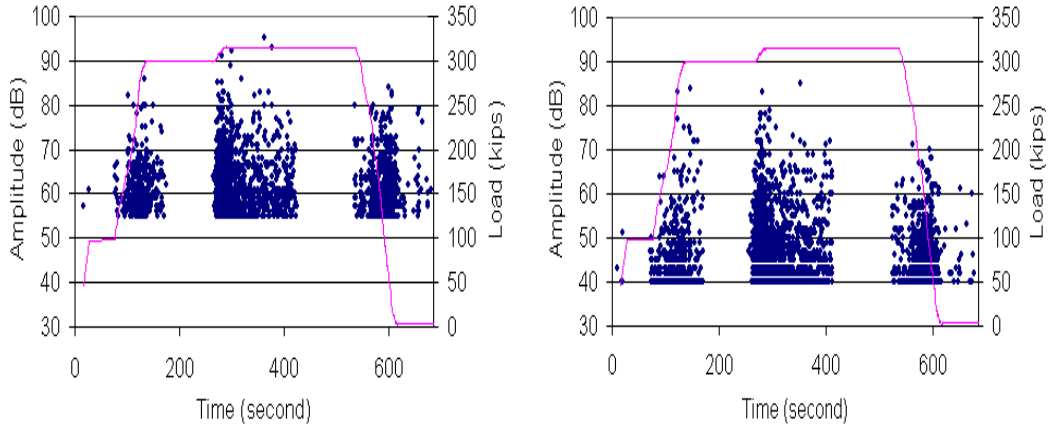

R6I R15I

a) Amplitude vs Time

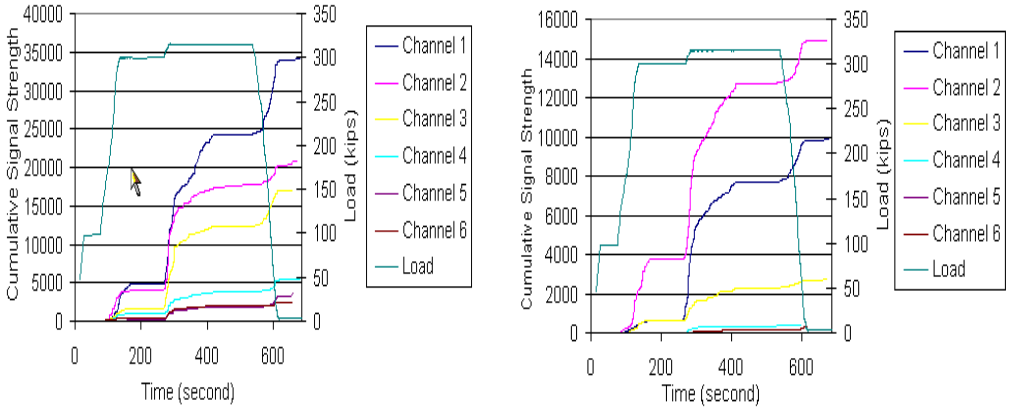

R6I R15I

b) Cumulative Signal Strength vs Time

Figure 3.10 – Time-Based Graphs at 1,000th Cycle

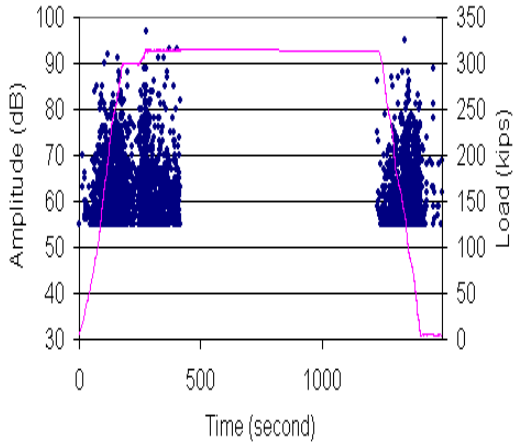

R6I

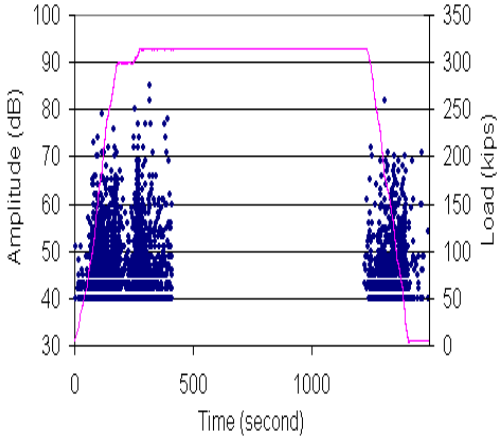

R15I

a) Amplitude vs Time

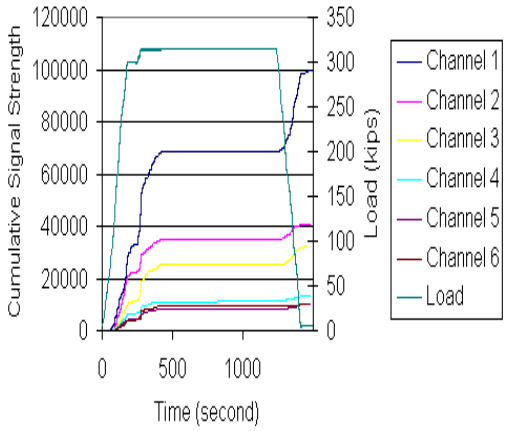

R6I

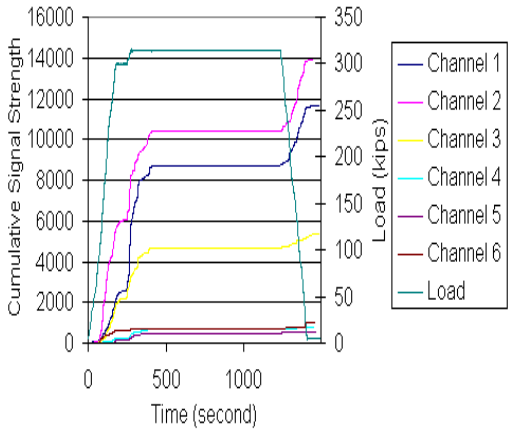

R15I

b) Cumulative Signal Strength vs Time

Figure 3.11 – Time-Based Graphs at 10,000th Cycle

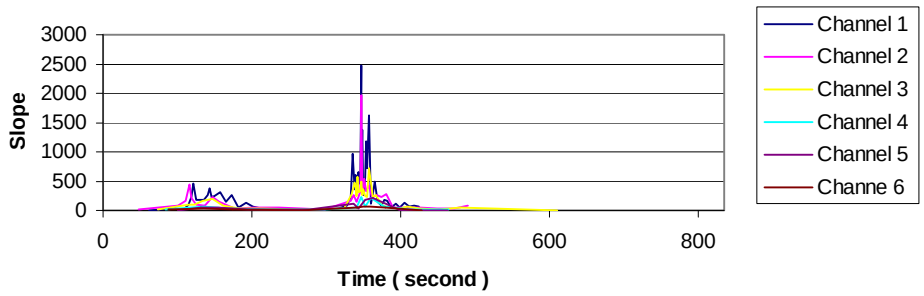

a) At 100th Cycle

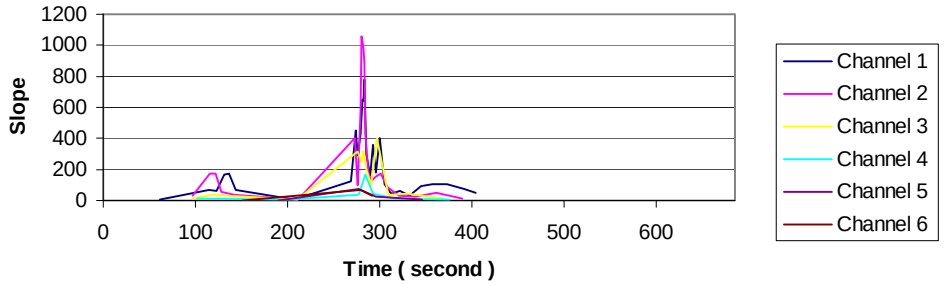

b) At 1,000th Cycle

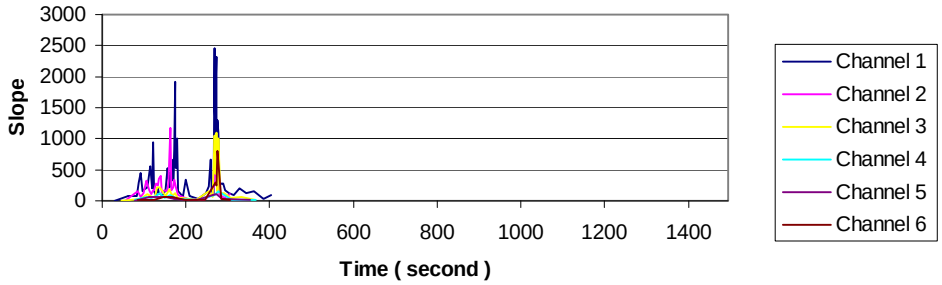

c) At 10,000th Cycle

Figure 3.12 – Slope of Cumulative Signal Strength vs Time Curve for R6I Sensors (Fatigue Test A)

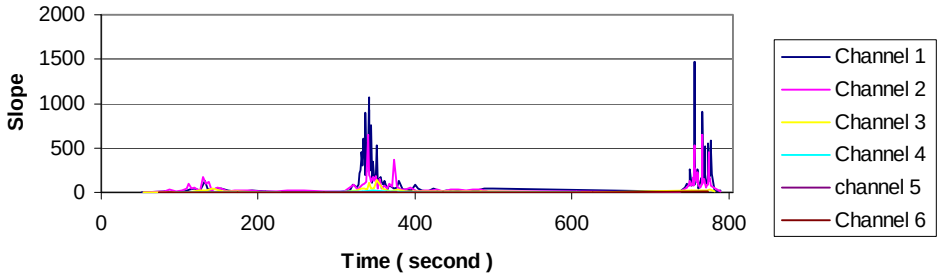

a) At 100th Cycle

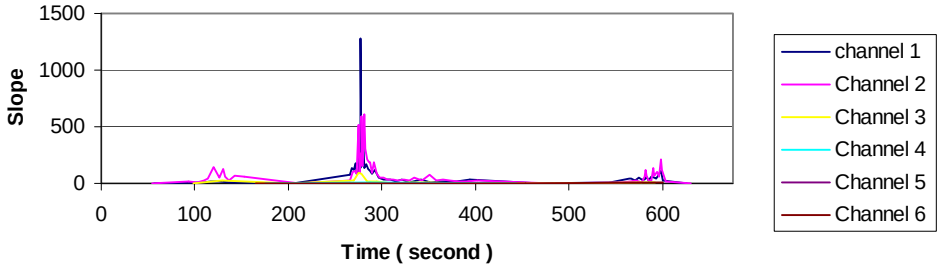

b) At 1,000th Cycle

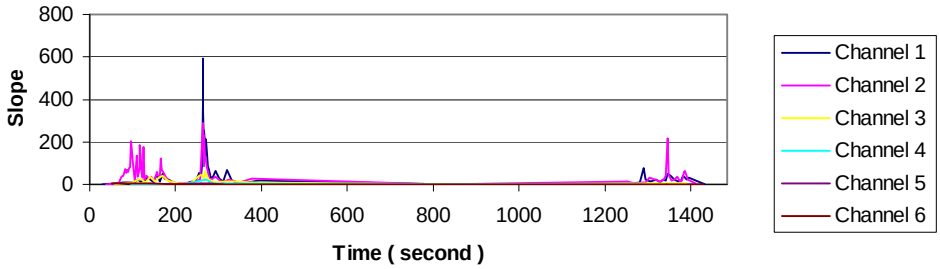

c) At 10,000th Cycle

Figure 3.13 – Slope of Cumulative Signal Strength vs Time Curve for R15I Sensors (Fatigue Test A)

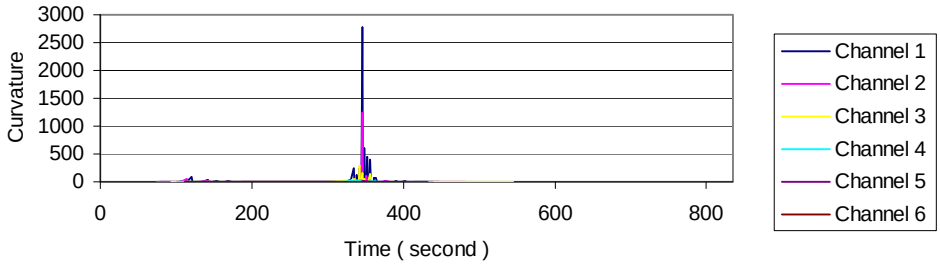

a) At 100th Cycle

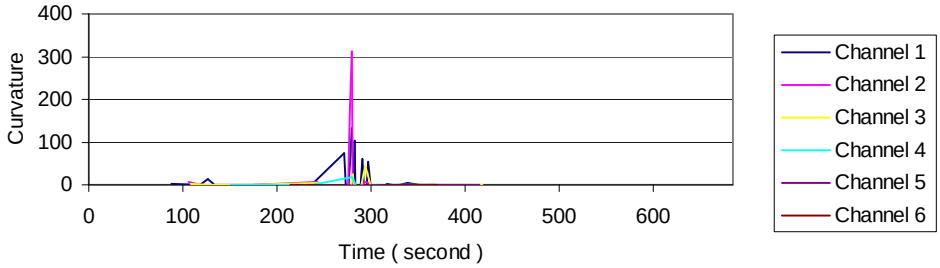

b) At 1,000th Cycle

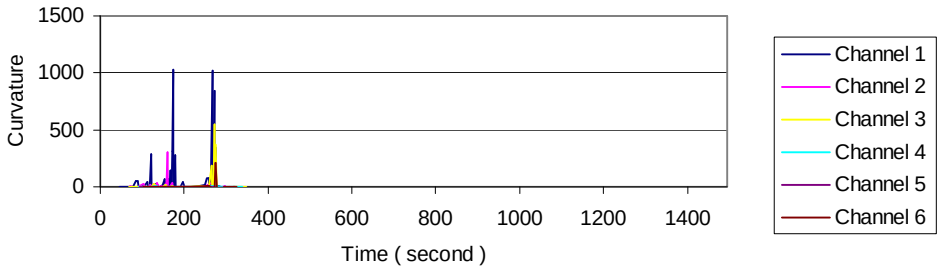

c) At 10,000th Cycle

Figure 3.14 – Curvature of Cumulative Signal Strength vs Time Curve for R6I Sensors (Fatigue Test A)

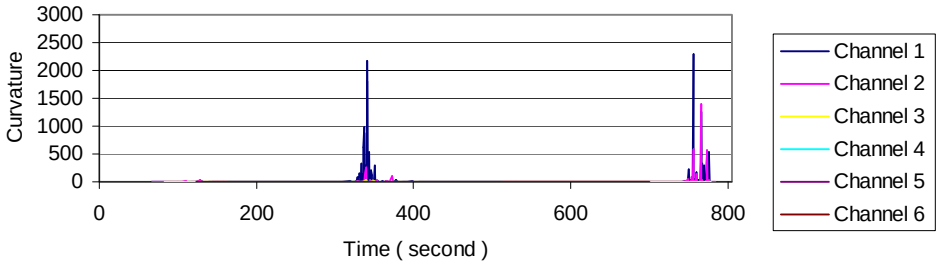

a) At 100th Cycle

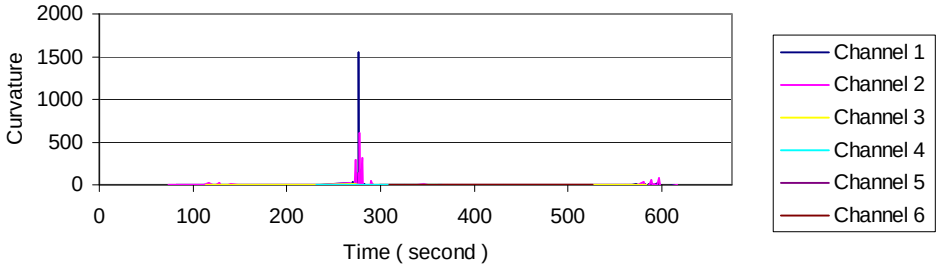

b) At 1,000th Cycle

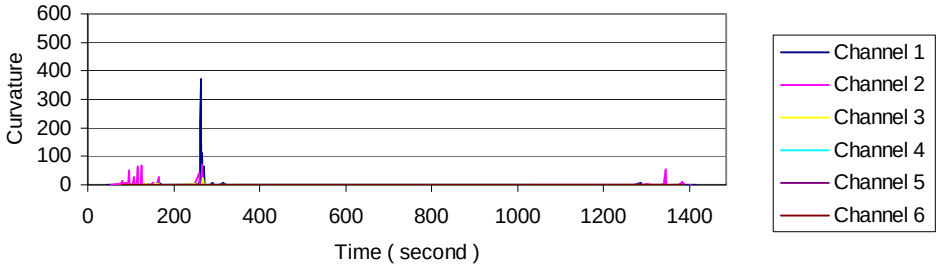

c) At 10,000th Cycle

Figure 3. 15 – Curvature of Cumulative Signal Strength vs Time Curve for R15I Sensors (Fatigue Test A)

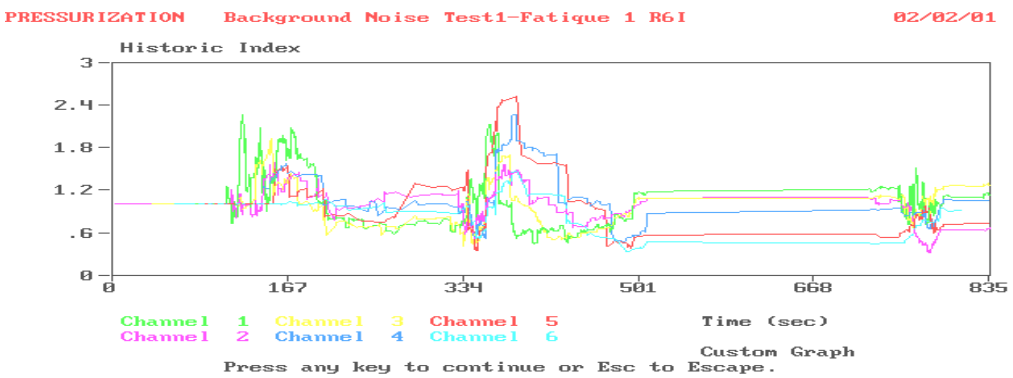

a) At 100th Cycle

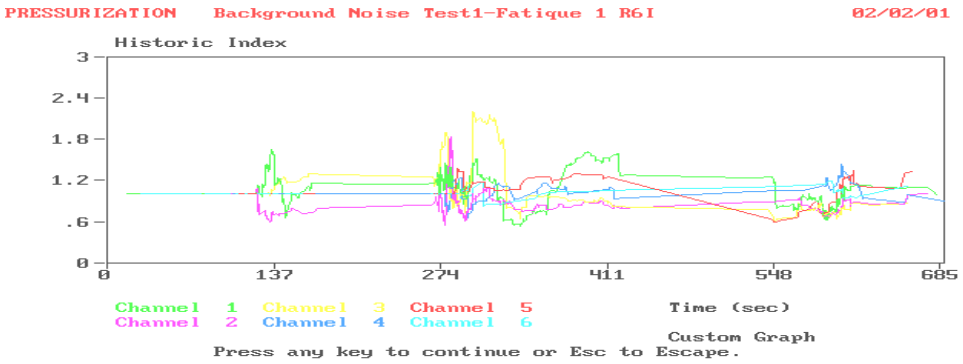

b) At 1,000th Cycle

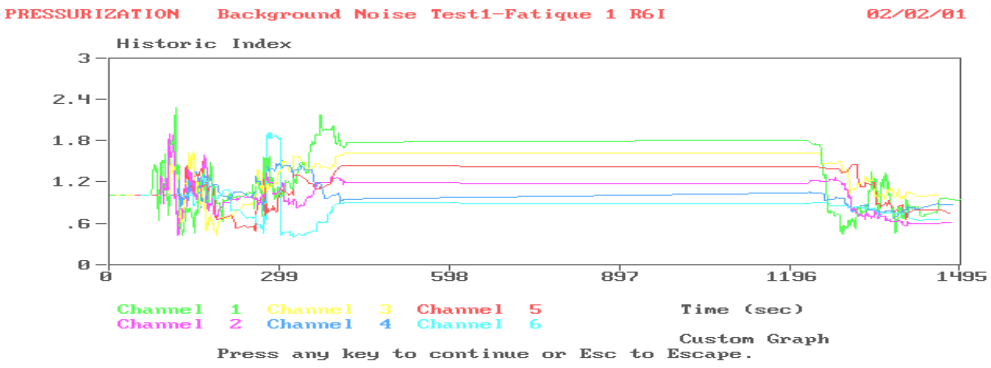

c) At 10,000 Cycles

Figure 3.16 – Historic Index vs Time Curve for R6I Sensors (Fatigue Test A)

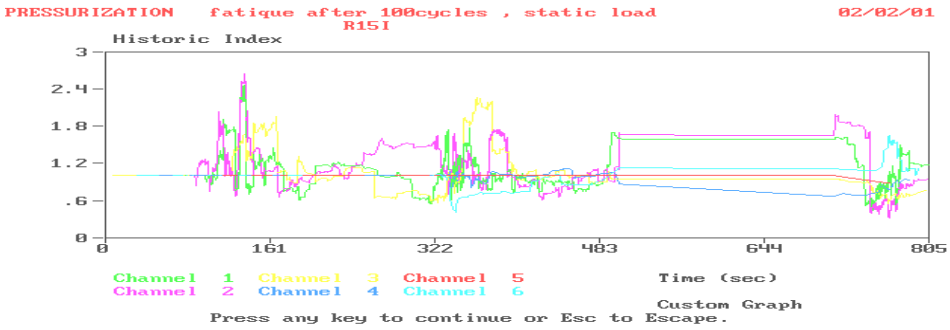

a) At 100th Cycle

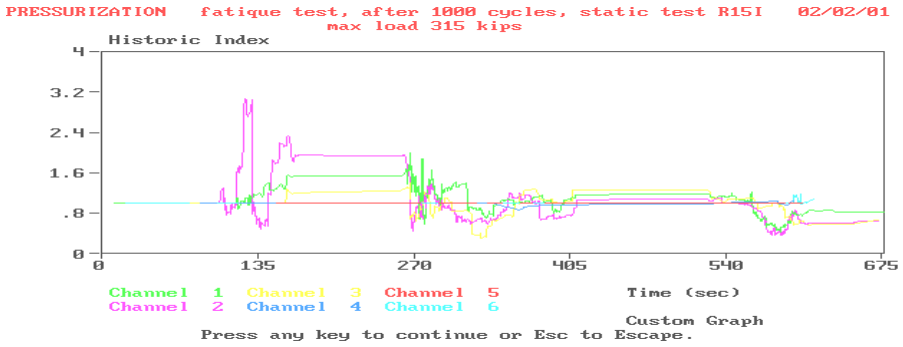

b) At 1,000th Cycle

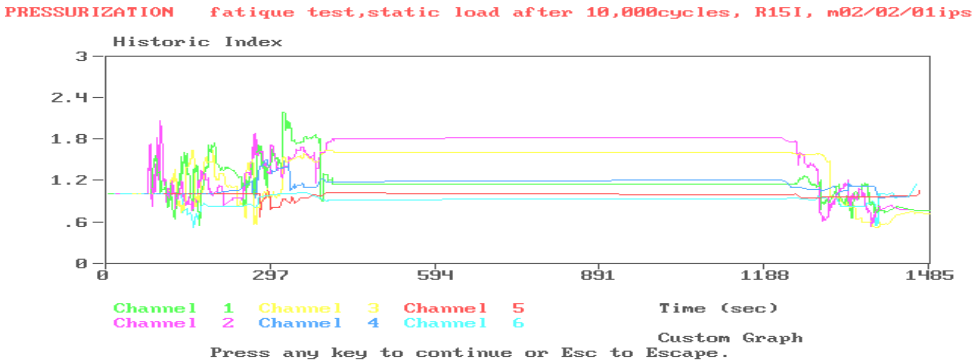

c) At 10,000th Cycle

Figure 3.17 – Historic Index vs Time Curve for

R15I Sensors (Fatigue Test A)

3.6.2 Cyclic Loading of Fatigue Test B

The second shear-dominated fatigue test was performed on the southern part of the prestressed concrete box girder, BG3. Felicity ratios were determined for each quasi-static test. The onset of significant emission used for calculating the Felicity ratio was determined from the three criteria listed in Section 3.5. Tables 3.5 and 3.6 and Figures 3.18 show the results from the analyses. Because of an instrument error, the R6I data recorded at 10, 100, 1,000 cycles are not available and are not shown.

In the Fatigue B Test, the specimen was subjected to a 250 kip initial static load. Sinusoidal cyclic loading varying from 20 to 200 kips was imposed on the specimen. No new major cracks occurred after 3.33 millions cycles. Pre-existing cracks were already open. Fewer than 120 hits were detected on each channel for all quasi-static load testing.

No significant emission occurred during each quasi-static load. Therefore, the load at the onset of significant emission was higher than 210 kips and the Felicity ratios were greater than 0.84 during cyclic load testing. Isolated hits with high signal strength, however, were detected at 200,000, 2,020,000, 2,320,000, and 2,780,000 cycles. The numbers of hits during unloading were fewer than 15 for both the R6I and R15I sensors. These numbers are much smaller than the numbers from Fatigue Test A.

Table 3.5 – Felicity Ratios of Fatigue B for R6I Sensors

	Slope		Curvature		HI		Emission during	Max Amp during
# Cycles	Load (kips)	FR	Load (kips)	FR	Load (kips)	FR	Unloading, Hits	Loading (dB)
10	-	-	-	-	-	-	-	-
100	-	-	-	-	-	-	-	-
1,000	-	-	-	-	-	-	-	-
10,000	NSE						10	66
100,000	NSE						11	81
2.00E+05	191.90	0.77	190.30	0.76	210.00	0.84	7	83
4.05E+05	196.75	0.79	NSE		NSE		4	82
5.00E+05	NSE		NSE		NSE		13	80
7.63E+05	NSE		NSE		NSE		4	72
1.00E+06	NSE		NSE		NSE		4	70
1.26E+06	NSE		NSE		NSE		3	68
1.50E+06	NSE		NSE		NSE		6	75
1.78E+06	NSE		NSE		NSE		2	80
2.02E+06	NSE		NSE		210.00	0.84	5	81
2.32E+06	NSE		NSE		210.00	0.84	8	74
2.56E+06	NSE		NSE		NSE		2	68
2.78E+06	NSE		NSE		210.00	0.84	5	83
3.07E+06	NSE		NSE		NSE		3	68

Table 3.6 – Felicity Ratios of Fatigue B for R15I Sensors

	Slope		Curvature		HI		Emission during	Max Amp during
# Cycles	Load (kips)	FR	Load (kips)	FR	Load (kips)	FR	Unloading, Hits	Loading (dB)
10	NSE		NSE		NSE		3	73
100	NSE		NSE		NSE		3	73
1,000	NSE		NSE		NSE		2	77
10,000	NSE		NSE		NSE		2	64
100,000	NSE		NSE		NSE		0	56
2.00E+05	NSE		NSE		NSE		1	60
4.05E+05	NSE		NSE		NSE		2	65
5.00E+05	NSE		NSE		NSE		1	60
7.63E+05	NSE		NSE		NSE		1	66
1.00E+06	NSE		NSE		NSE		1	59
1.26E+06	NSE		NSE		NSE		0	57
1.50E+06	NSE		NSE		NSE		2	60
1.78E+06	NSE		NSE		NSE		0	62
2.02E+06	NSE		NSE		210	0.84	0	80
2.32E+06	NSE		NSE		NSE		0	69
2.56E+06	NSE		NSE		NSE		0	75
2.78E+06	NSE		NSE		NSE		1	63
3.07E+06	NSE		NSE		NSE		0	67

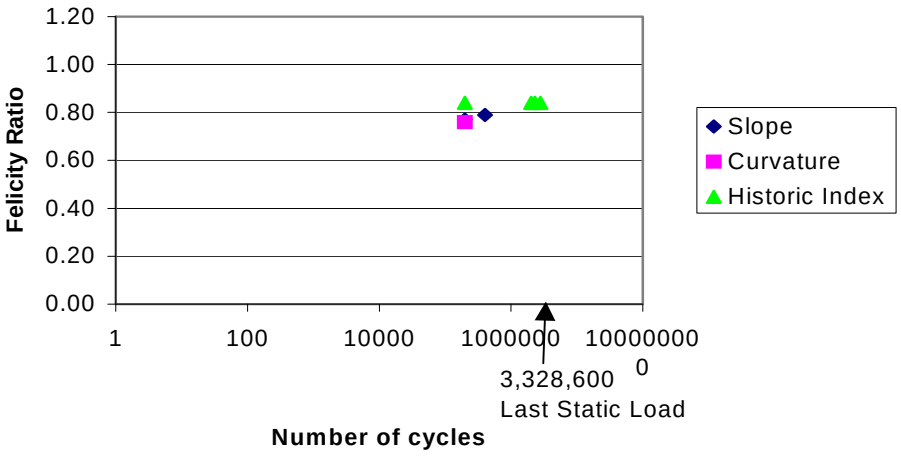

a) R6I

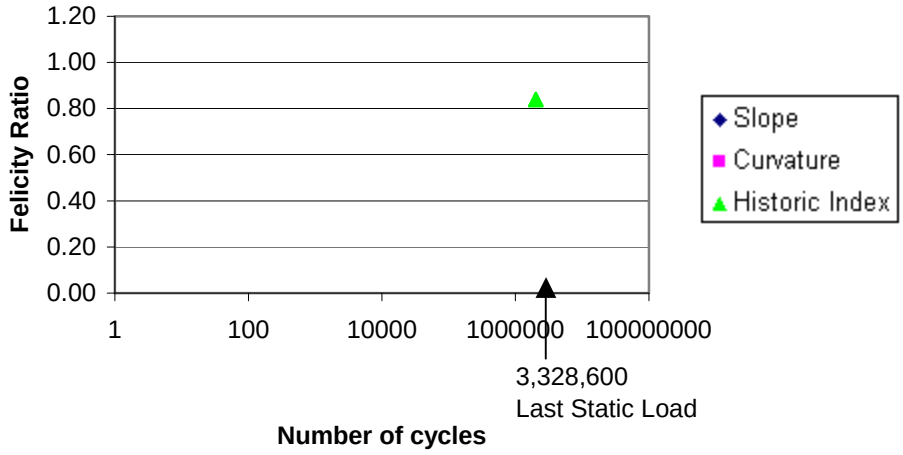

b) R15I

Figure 3.18 - Felicity Ratios for Fatigue Test B

The data recorded during cyclic loading were also analyzed, and are shown in Figure 3.19. In this case, data were analyzed for 700 cycles after each quasi-static load. For the R6I sensors, below 400,000 cycles the magnitude of cumulative signal strength was small and had no significant change. This was because the first static load was much higher than the maximum cyclic load. The cumulative signal strength tended to increase after 500,000 cycles and then decreased after reaching the peak at 1 million cycles. In the overall picture, the cumulative signal strength decreased substantially after the first static load but after a large number of cycles, acoustic emission activity increased. For the R15I sensors, the data recorded during 700 cycles was much less than for the R6I sensors and tended to increase with the number of cycles.

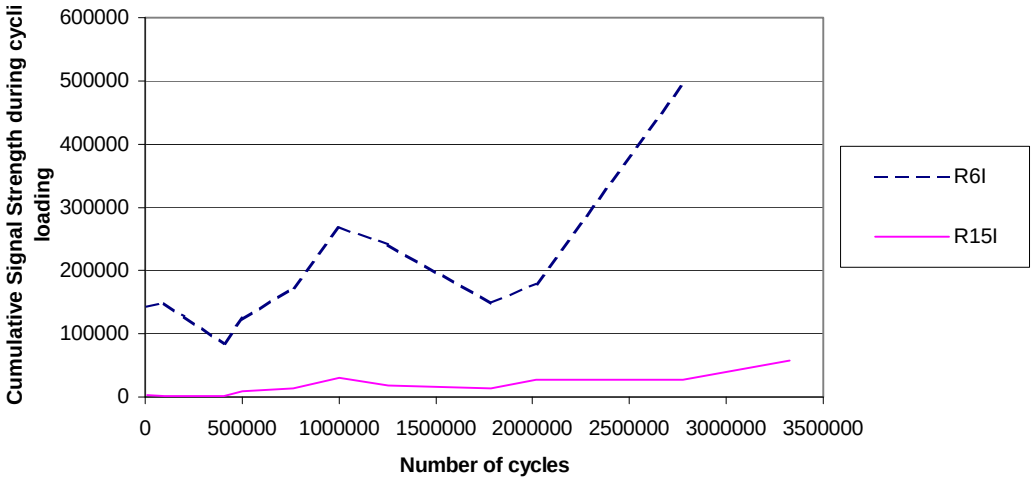

Figure 3.19 – Cumulative Signal Strength during Cyclic Load for 700 Cycles following a Quasi-Static Overload

3.6.3 Load to Failure of Fatigue B

After 3.33 million cycles, the specimen was loaded statically to failure, using a stepped loading procedure with intermediate unloading (Figure 3.20). This loading figure was used in order to determine the Felicity ratio and number of hits during load holds.

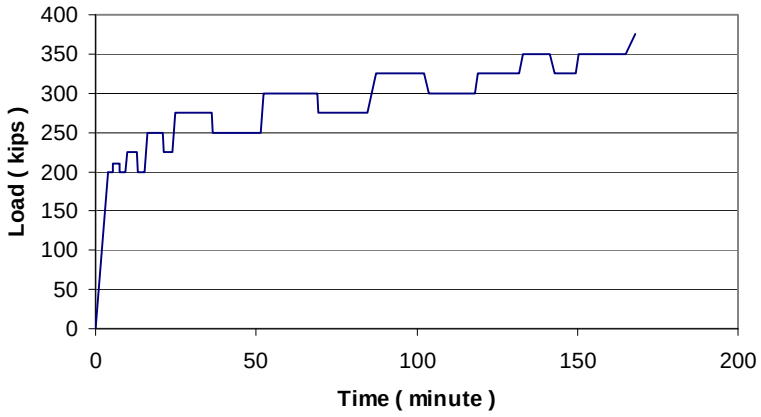

Figure 3.20 – Loading History of Static Load to Failure

Felicity ratios were determined according to criteria stated in Section 3.5. The results are shown in Table 3.7, Table 3.8 and Figure 3.21. With the selected loading sequence, it is impossible for the Felicity ratio after the first step to be less than 0.88 because the load held after unloading in each step was not lower than 88% of the previous maximum load. During static loading, the onset of significant emission was first detected at 238 kips, higher than the maximum load imposed on the specimen during cyclic loading but less than the initial static load. Visual inspection indicated no significant damage during cyclic load. This is constant with the onset of emission being above the maximum cyclic load.

The Felicity ratios decreased as the load on the specimen increased and more damage was observed. The Felicity ratios determined from each criterion were close to each other. It is probable that the Felicity ratios would have been much lower, if magnitude of the unloading had been greater. Emission during load holds started to increase considerably after 275 kips. The number of hits

increased significantly when the load was increased. Higher numbers of high-amplitude emissions (> 85 for R6I and >75 for R15I) were also detected when the stepped static load was higher than 275 kips. The specimen failed at 365 kips. Figures 3.22 through 3.25 show details of the acoustic emission data for the static load to failure. Results for analysis of the slope, curvature, and historic index are shown on a per-channel basis.

Table 3.7 - Felicity Ratios of Static Load to Failure for R6I Sensors

Previous Max Load	Slope		Curvature		HI	
(kips)	Load (kips)	FR	Load (kips)	FR	Load (kips)	FR
250	NSE		NSE		NSE	
250	NSE		NSE		NSE	
250	237.80	0.95	239.87	0.96	242.69	0.97
250	258.15	1.03	262.80	1.05	252.80	1.01
275	276.25	1.00	278.67	1.01	279.53	1.02
300	293.54	0.98	297.54	0.99	305.82	1.02
325	310.85	0.96	313.12	0.96	312.50	0.96
350	327.14	0.93	328.33	0.94	333.60	0.95

Note: NSE = No Significant Emission

Table 3.8 - Felicity Ratios of Static Load to Failure for R15I Sensors

Previous Max Load	Curvature		Slope		HI	
(kips)	Load (kips)	FR	Load (kips)	FR	Load (kips)	FR
250	NSE		NSE		NSE	
250	NSE		NSE		NSE	
250	234.18	0.94	233.91	0.94	239.40	0.96
250	252.86	1.01	250.13	1.00	257.12	1.03
275	273.16	0.99	279.16	1.02	284.12	1.03
300	301.96	1.01	303.40	1.01	305.43	1.02
325	313.70	0.97	311.20	0.96	315.56	0.97
350	327.50	0.94	329.43	0.94	334.56	0.96

Note: NSE = No Significant Emission

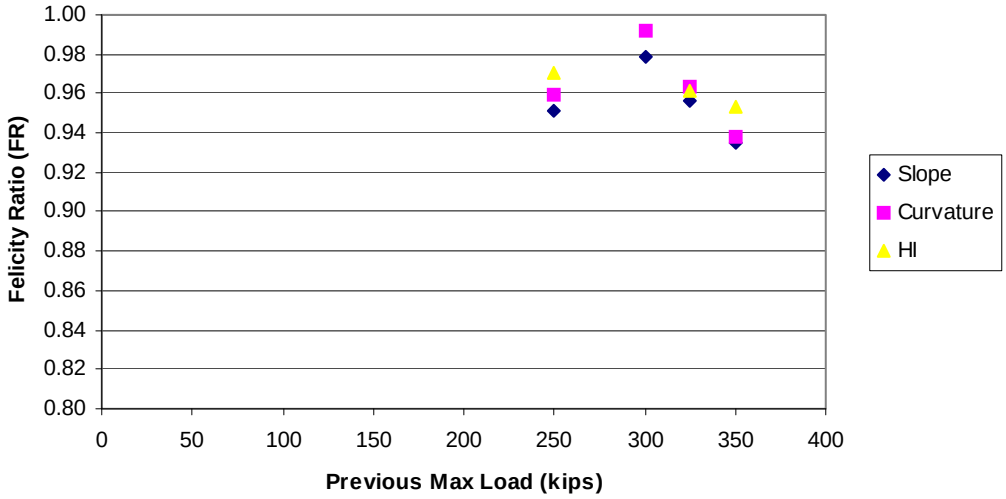

a) R6I

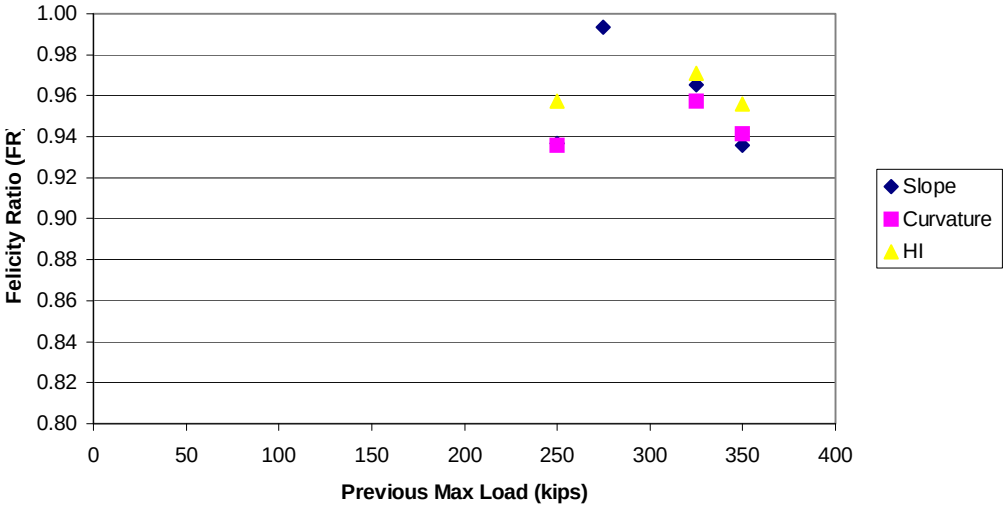

b) R15I

Figure 3.21 – Felicity Ratio vs Previous Maximum Load for Static Load to Failure

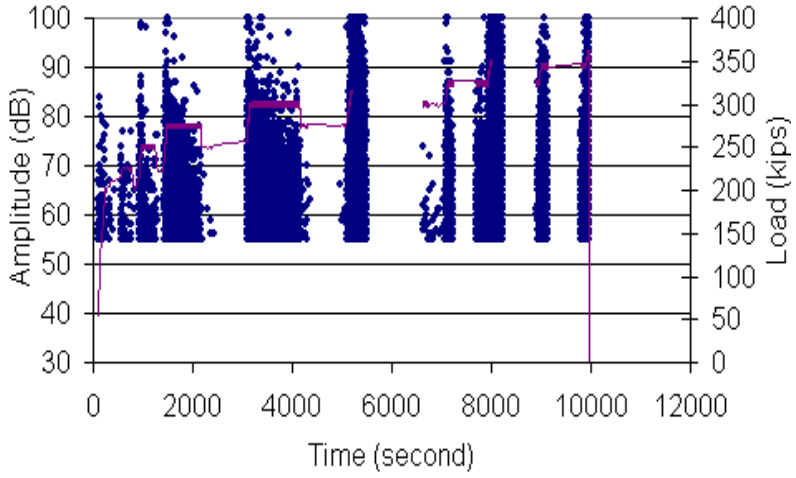

a) R6I

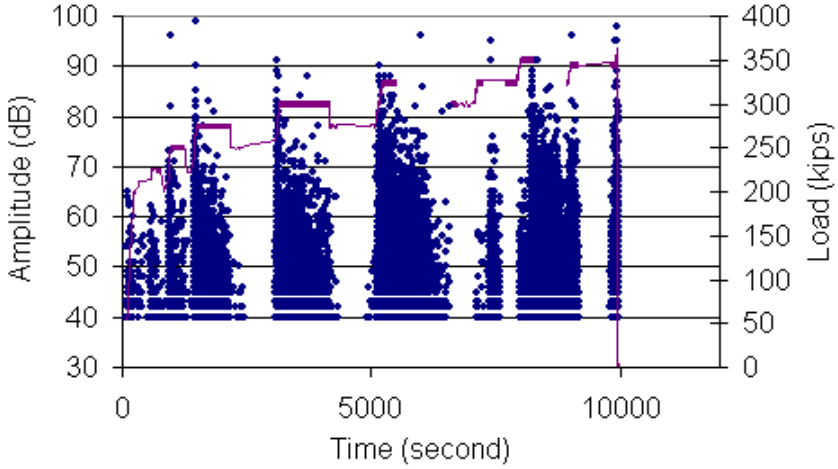

b) R15I

Figure 3.22 – Amplitude vs Time Graphs for Static Test Load to Failure of Fatigue Test B

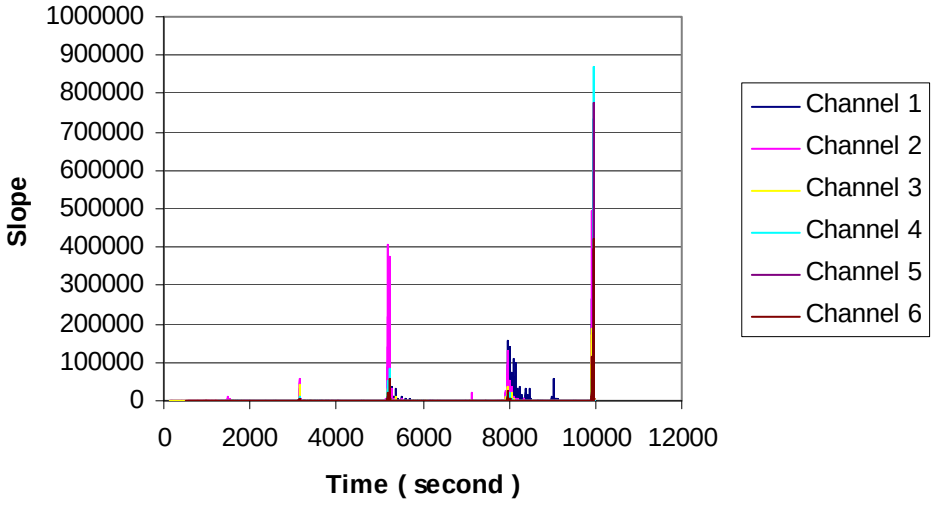

a) R6I

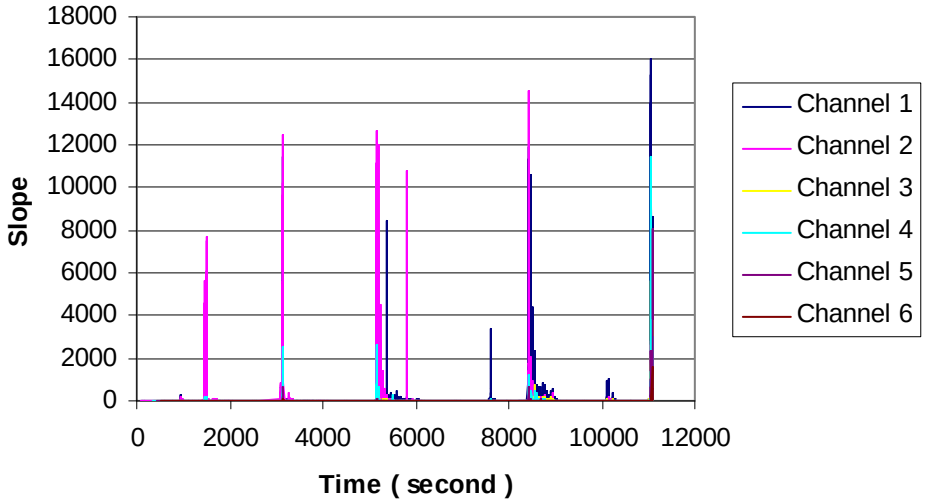

b) R15I

Figure 3.23 – Slope of Cumulative Signal Strength vs Time Curve for Static Load to Failure of Fatigue Test B

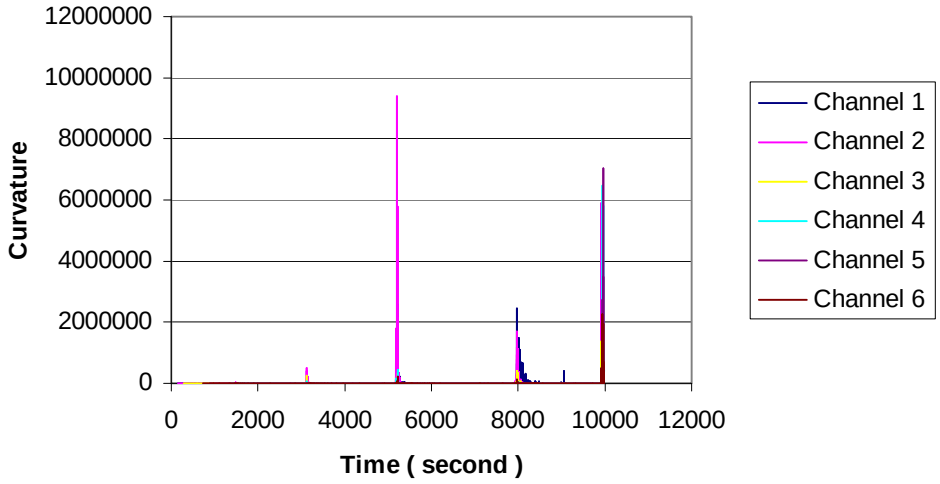

a) R6I

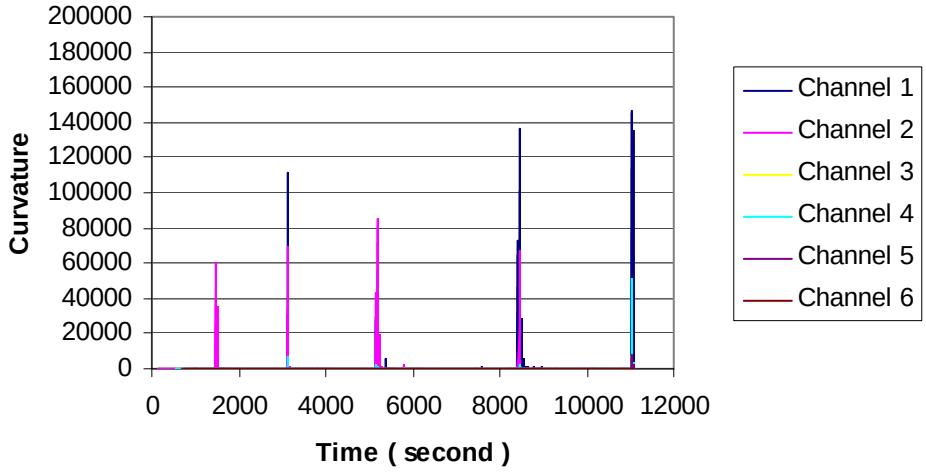

b) R15I

Figure 3.24 – Curvature of Cumulative Signal Strength vs Time Curve for Static Load to Failure of Fatigue Test B

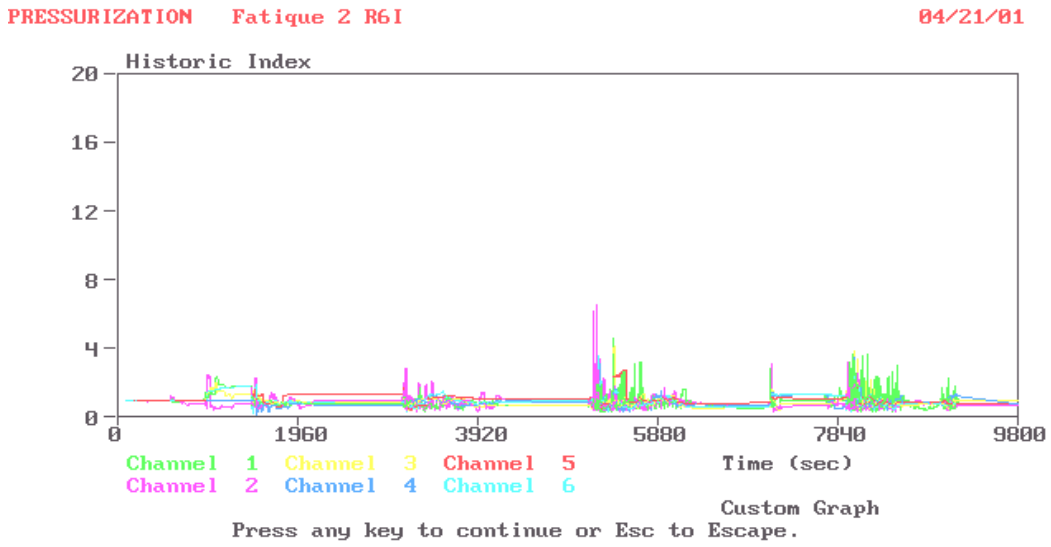

a) R6I

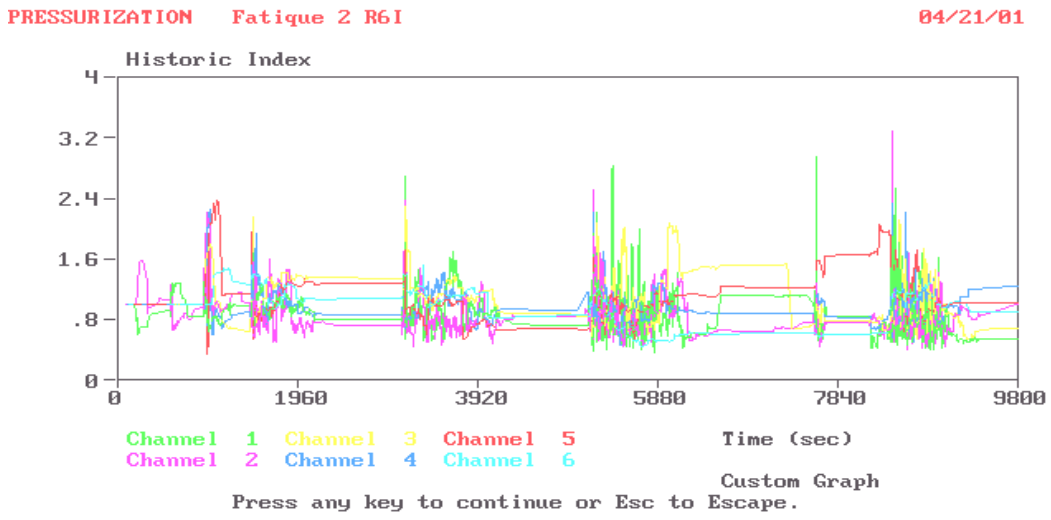

b) R15I

Figure 3.25 – Historic Index vs Time Curve for Static Load to Failure of Fatigue Test B

3.7 SUMMARY OF SHEAR-DOMINATED FATIGUE TESTS

The following summarizes the results of shear-dominated fatigue tests.

1. For Fatigue Test A, the Kaiser effect broke down after the first static load, and the Felicity ratio became an important parameter. This was because shear cracks were generated during the first static load and continued to develop throughout the test.
2. For Fatigue Test B specimen, no significant emission was detected and no significant damage propagated during cyclic load.
3. The Felicity ratio provided a good index of structural damage.
4. Curvature, slope and historic index criteria performed well in determining the onset of significant emission.
5. Severity, high signal strength hits and high amplitude hits were tried as criteria to detect the onset of significant emission. These methods did not perform well.
6. The number of hits during unloading appeared to be independent of the number of load cycles.
7. For the Fatigue B specimen, the signal strength recorded during cyclic loading was low after the first static load, but slowly increased after many cycles. No knee was seen in the curve of cumulative signal strength.
8. The R6I sensors are more sensitive to genuine data and to background noise than the R15I sensors.

9. Data recorded by both the R6I and R15I sensors showed the same trends.

Chapter 4 – Acoustic Emission Monitoring of Pull-out Tests

The most severely damaged region of a prestressed concrete girder with premature ASR/DEF concrete deterioration is typically at the end, where the prestressing force is transferred to the concrete. Premature deterioration cracking in such end regions raises concerns about the adequacy of the bond between the concrete and prestressing strand. To address these concerns, pull-out tests were performed on slices of a Type C girder and the prestressed box girders. The specimens were cut from girders with premature concrete deterioration. During the tests, the specimens were subjected to different levels of transverse confining load. The characteristics of the acoustic emission signals during strand pull out are of particular importance to the research reported in this thesis and are discussed in this chapter.

4.1 TEST SETUP

The Type C prestressed girder (G2) and the full-scale prestressed box girder (BG1S) were used to prepare the specimens for the pull-out tests. These two had premature concrete deterioration and were visually inspected by researchers Yong-Mook Kim and Brian Tinkey (Tinkey 2000).

Using hydro-blasting, slices were cut from the bottom flange at the middle span of the G2 girder, and 133.75 inches from south end of BG1. The hydro-blast method was used to cut the specimen and remove concrete cover from a portion

of the prestressing strands in order to allow the strands to be gripped and pulled by a hydraulic ram. The hydro-blast method can remove the concrete without causing additional cracks in the remaining concrete. Silicone was used to fill cracks at the surface before casting gypsum plaster (Hydrostone) on the cross-sections of the specimens. The purpose of the silicon was to prevent the plaster from filling the cracks. In addition, silicon was used to prevent gypsum plaster from bonding to the prestressing strands. Gypsum plaster was used in the test to make the surface of specimens smooth for the hydraulic ram to push against. Figure 4.1 shows cross sections and locations of monitored strands for both specimens.

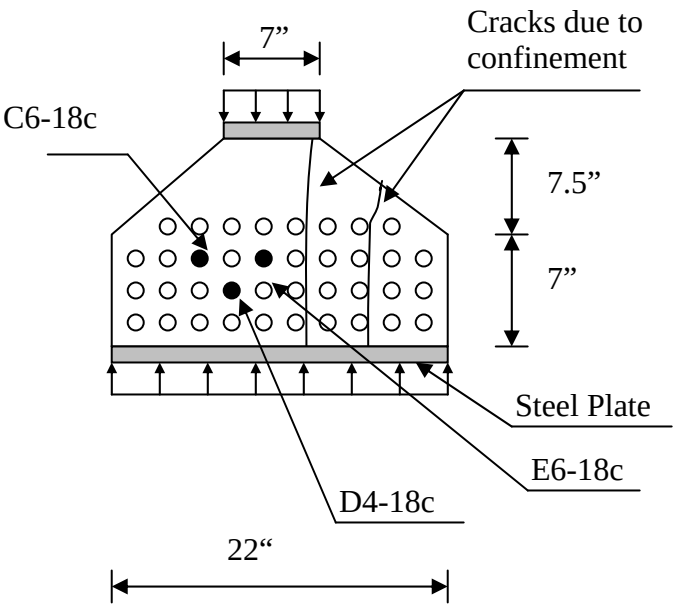

a) Specimen from G2

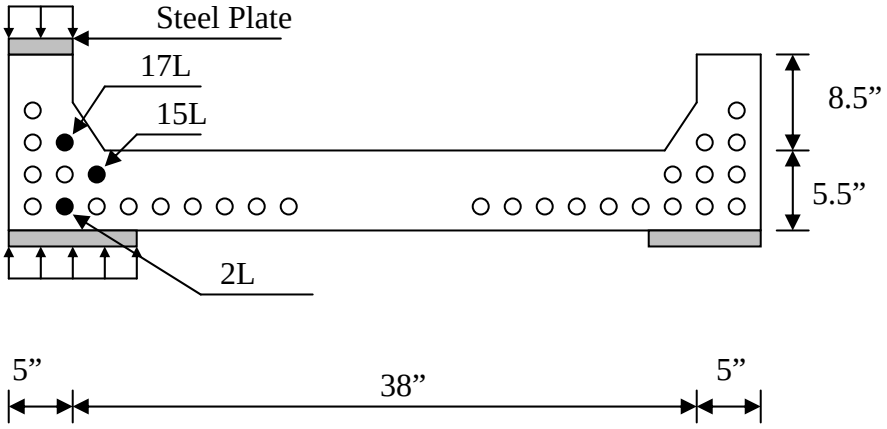

b) Specimen from BG1S

Figure 4.1 – Locations of Strands on Pull-out Specimens

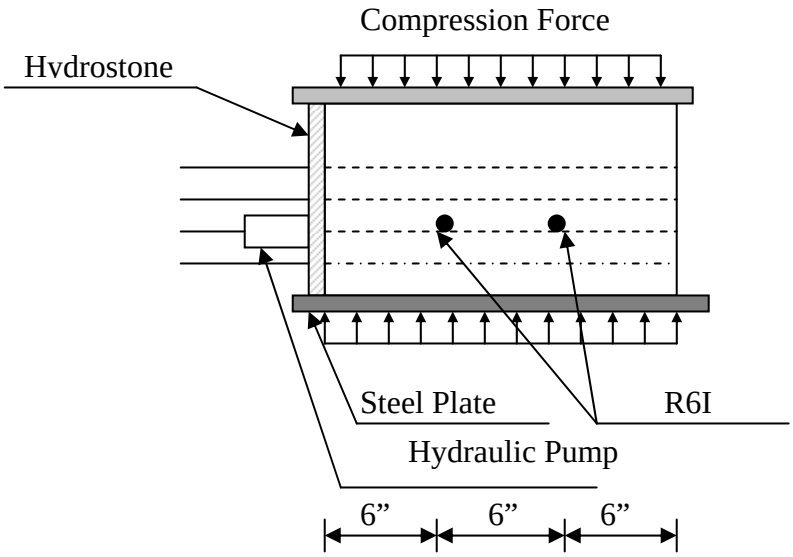

a) Specimen from G2

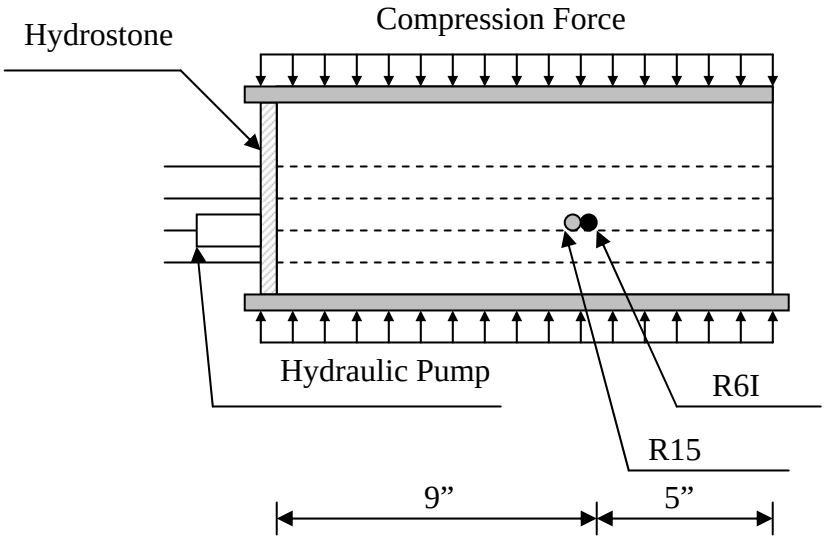

b) Specimen from BG1S

Figure 4.2 – Test Setup of Pull-Out Test

Acoustic emission monitoring was carried out with a six-channel MISTRAS 2001 instrument manufactured by PAC. R6I and R15I sensors were used. Two R6I sensors were mounted on the slice removed from the Type C girder (G2) and one R6I and one R15I sensors were mounted on the slice removed from box girder (BG1S). Sensor positions are shown in Figure 4.2. The test settings, except for threshold, were similar to those used for the fatigue tests and listed in Table 3.1. The threshold was set at 45 dB.

The loading schedule was designed so that the bond strength could be studied. To imitate field loading condition, the effect of transverse compression reactions was considered. To accomplish this, a transverse compression force was applied to the specimen, and the strand was pulled until it slipped. The transverse compression force was held for approximately 3 minutes to let emission die out. Additional compression force was applied to the specimen and held for 3 minutes before reapplying tension load to the same strand, to the next level necessary to cause to slip. The next strand was tested with the same pattern of loading but with different levels of compression force.

4.2 RESULTS OF PULL-OUT TESTS ON TYPE C SPECIMEN

Acoustic emission monitoring was performed on three strands of the slice removed from the Type C girder. During the pull-out tests, each strand was subjected to different levels of transverse compression forces. The tests were performed on strands C6-18c, D4-18c, and E6-18c, respectively (Figure 4.1).

Acoustic emission data were analyzed, and results are shown in Figures 4.3 through 4.6.

The results show the effect of transverse confinement on the pull-out strength. The more transverse load, the greater the pull-out strength. The initial pull-out strength of each strand was a combination of bond strength and friction between the strand and concrete, while the second and third pull-out loads depended only on the friction between the strand and concrete.

Hits with unique acoustic emission characteristics were detected during pull-out. Very long-duration hits were detected when the strands started to slip, especially for strand C6-18c. The longest durations were 82,561, 106,642, and 221,355 μsec for the first, second, and third pull-out loads, respectively. For D4-18c and E6-18c, the longest duration of hits were 106,607 and 81,570 μsec. These long-duration hits also had high amplitudes. Long-duration hits can be used in field testing as an indicator of strand slip. For the test done on strand C6-18c, the greater the applied transverse compression load, the longer the duration of the hits. Hits with high signal strength and high amplitude were detected when the strands started to slip.

Test data were also analyzed by amplitude distribution. The experimental data, however, show a variation in the b-value. This is shown in Table 4.1. Figure 4.7 shows the curve between cumulative hits and amplitude for strand C6-18c.

Unfortunately, the transverse compression loads applied to the specimen induced cracks, whose propagation could be identified from the acoustic emission

signals detected during the increase in the transverse compression load. For clarity, data acquired during increases in transverse compression load has been filtered out and is not shown in Figures 4.3 through 4.6.

From the tests, hits with amplitudes higher than 85 dB were first detected at 94%, 63%, and 50% of the first pull-out loads for strands C6-18c, D4-18c, and E6-18c respectively. High-amplitude hits tended to be detected at a lower percentage of pull-out load when there was more damage in the specimen.

Table 4.1 – b-Values of Strand Pull-out Tests for Specimen from G2 (R6I Sensors)

Strand	b-Value
C6-18c	1.54
D4-18c	1.45
E6-18c	1.48

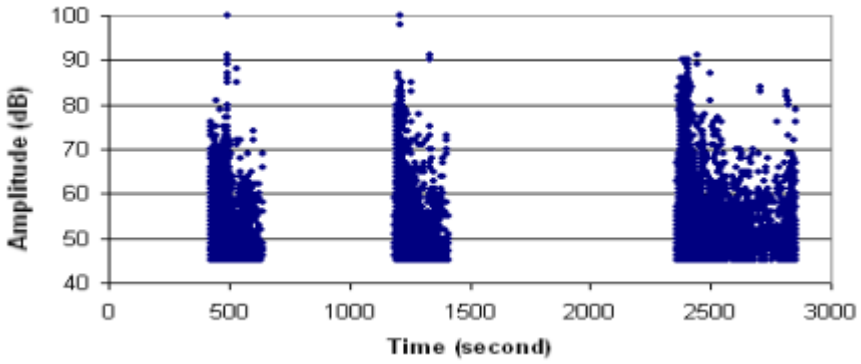

a) Amplitude vs Time

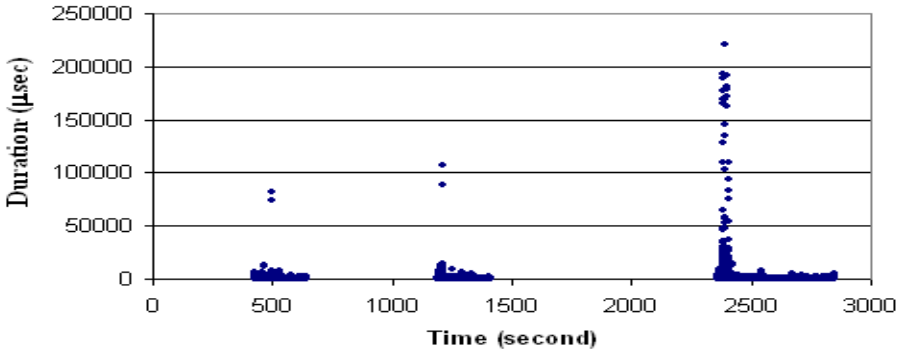

b) Duration vs Time

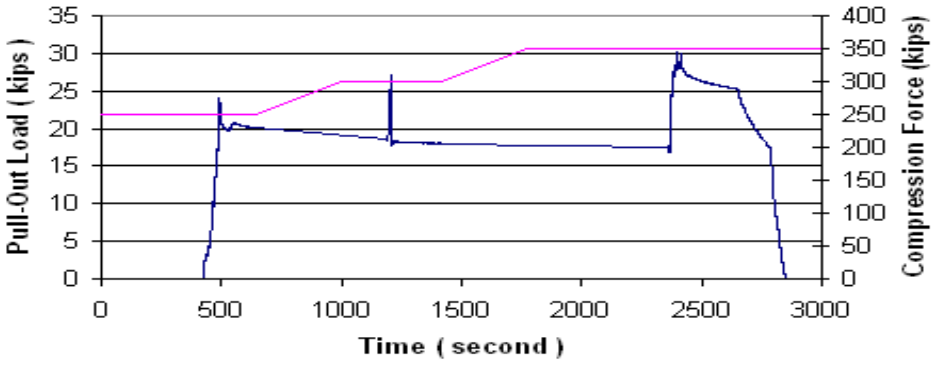

c) Load vs Time

Figure 4.3 – Time-Based Graphs for Strand C6-18c

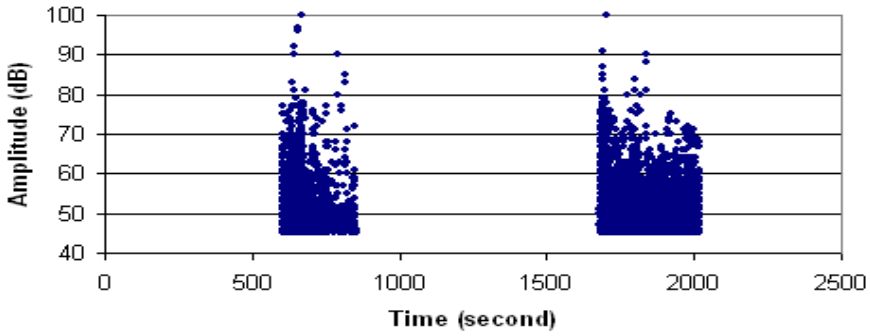

a) Amplitude vs Time

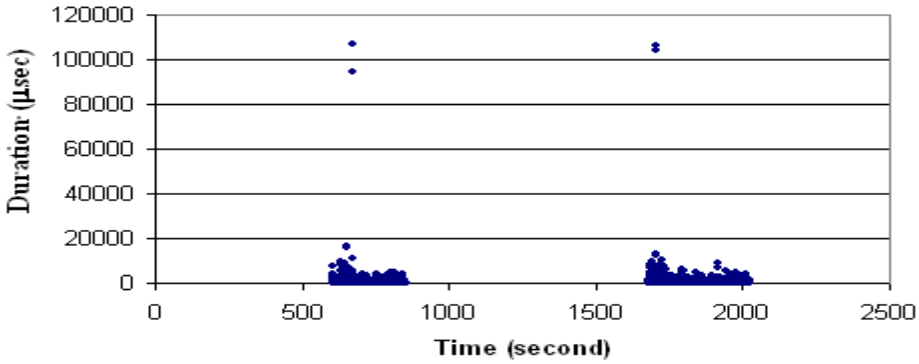

b) Duration vs Time

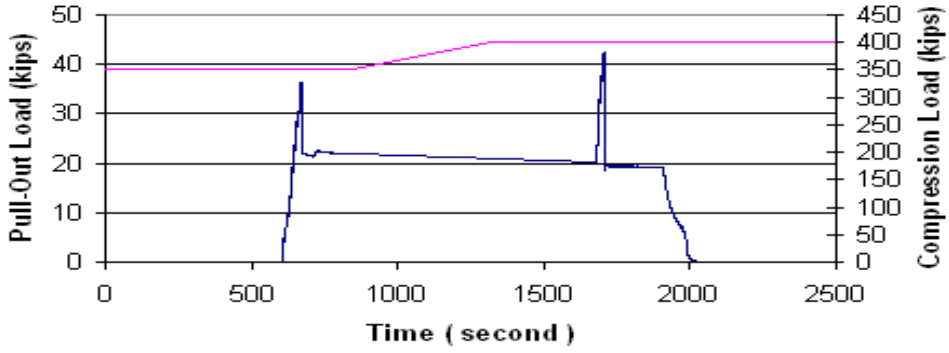

c) Load vs Time

Figure 4.4 – Time-Based Graphs for Strand D4-18c

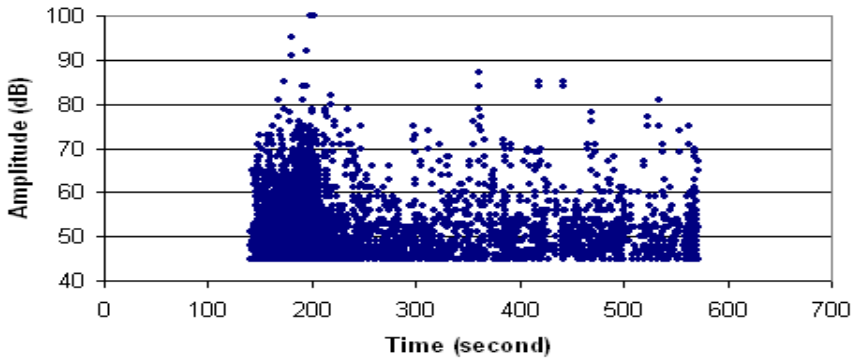

a) Amplitude vs Time

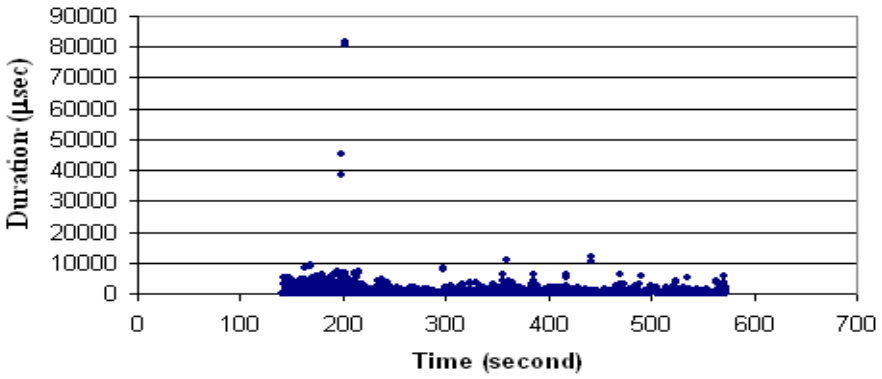

b) Duration vs Time

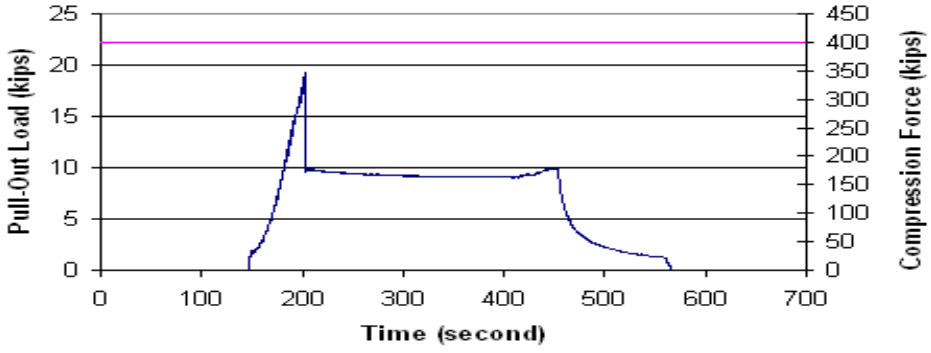

c) Load vs Time

Figure 4.5 – Time-Based Graphs for Strand E6-18c

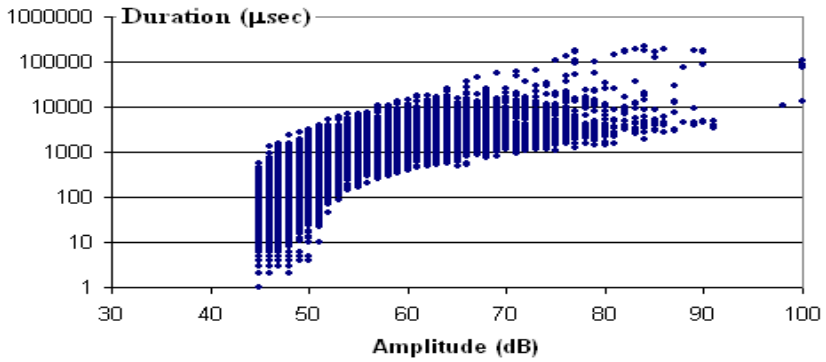

a) Strand C6-18c

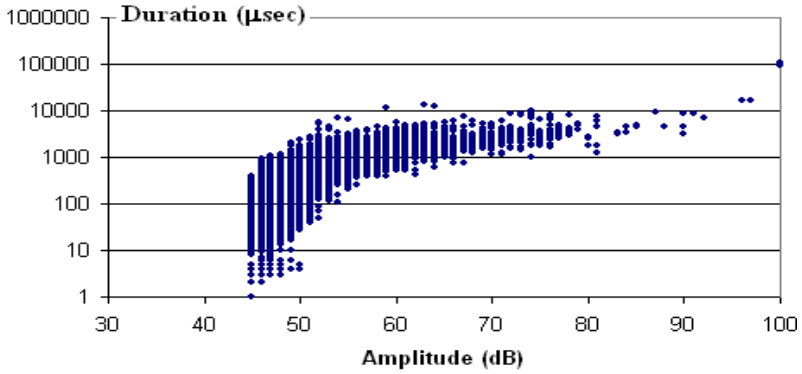

b) Strand D4-18c

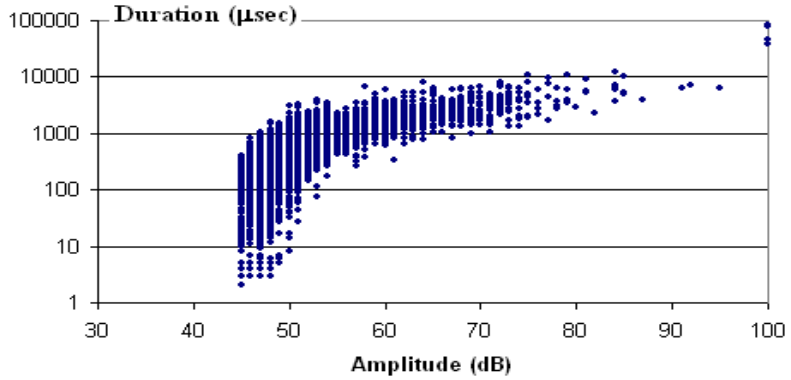

c) Strand E6-18c

Figure 4.6 – Duration vs Amplitude for Specimen from G2

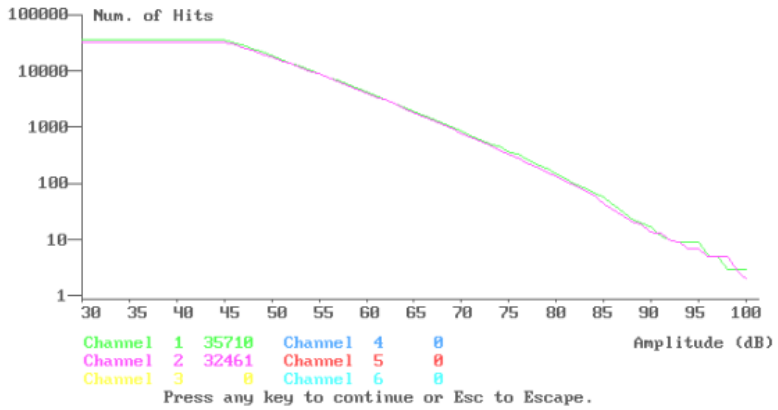

Figure 4.7 – Cumulative Hits vs Amplitude for Strand C6-18c

4.3 RESULTS OF PULL-OUT TESTS ON BOX GIRDER SPECIMEN

Acoustic emission monitoring was performed on three strands of one slice removed from the prestressed concrete box girder (BG1S). During the pull-out tests, each strand was subjected to different levels of compression forces. The tests were performed on strands 17L, 15L and 2L respectively and acoustic emission data were analyzed.

R6I and R15I sensors were used for these tests. The results from the two sensors are shown in Figures 4.8 to 4.11. Acoustic emission data from the R15I during the first pull-out load on strand 17L are not available because of an instrument error. Data from the other stepped loadings and other strands show the same unique characteristics as was reported for the slice removed from G2. Hits with very long duration and high amplitude were detected by both the R6I and R15I sensors when the strands started to slip. The longest durations detected by R6I were 171,119, 491,717, and 487,057 μsec for strands 17L, 15L, and 2L,

respectively. Corresponding durations from the R15I sensor were 24,139, 4,671, and 57,849 μsec. In general, the maximum duration of the long duration hits detected by the R6I was greater than detected by the R15I. High amplitude and high signal strength hits were also detected at the maximum pull-out load. As was expected, more hits were detected by the R6I than by the R15I. Amplitude-distribution analysis was applied to the data from the tests. As with the tests performed on the slice removed from G2, the experimental data show a variation in the b-value. This is shown in Table 4.2. Additional research using more carefully controlled tests is required in order to establish if the b-value variation is to be expected with strand slip, or is an effect of the test specimens and loading procedure used for these studies.

During the tests, the applied transverse compressive stresses were much less than the compressive strength of the specimen. Unlike the tests performed on the slice removed from G2, the applied transverse compression forces did not induce cracks in the specimen.

Table 4.2 – b-Values of Strand Pull-out Tests for Specimen from BG1S (R6I and R15I Sensors)

	b-Value	
Strand	R6I	R15I
17L	1.38	1.4
15L	1.64	1.59
2L	1.23	1.38

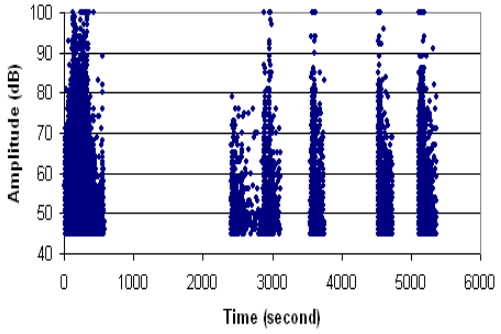

R6I

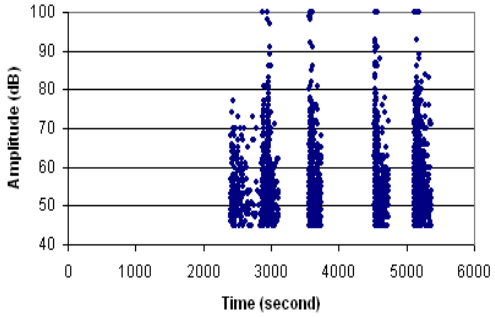

R15I

a) Amplitude vs Time

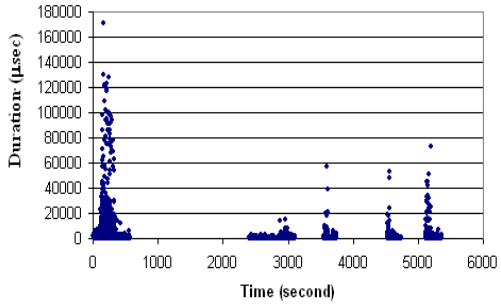

R6I

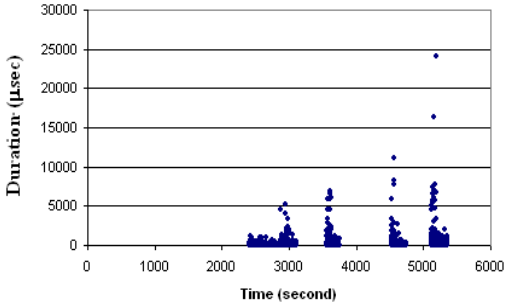

R15I

b) Duration vs Time

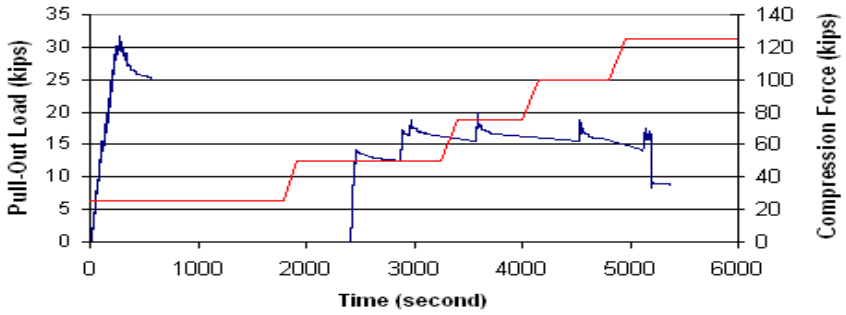

c) Load vs Time

Figure 4.8 – Time-Based Graphs for Strand 17L

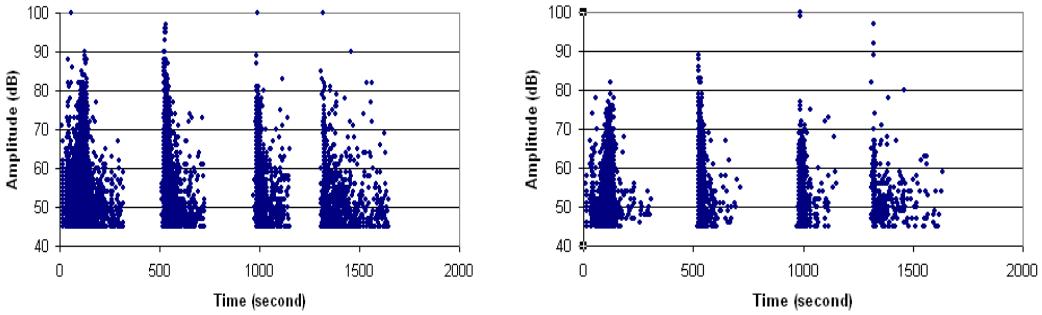

R6I R15I

a) Amplitude vs Time

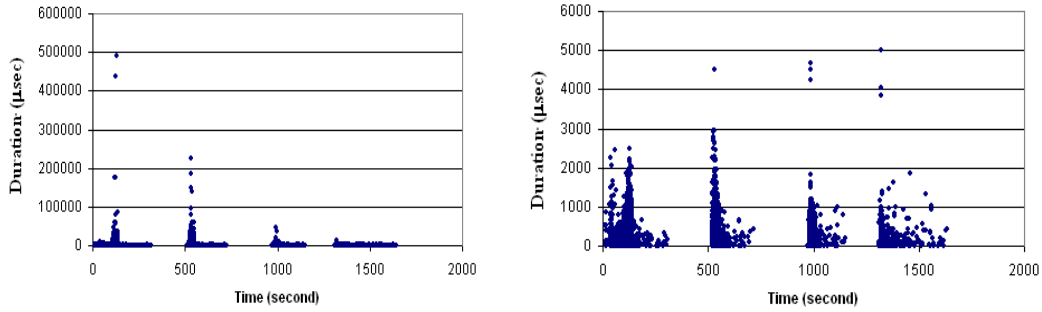

R6I R15I

b) Duration vs Time

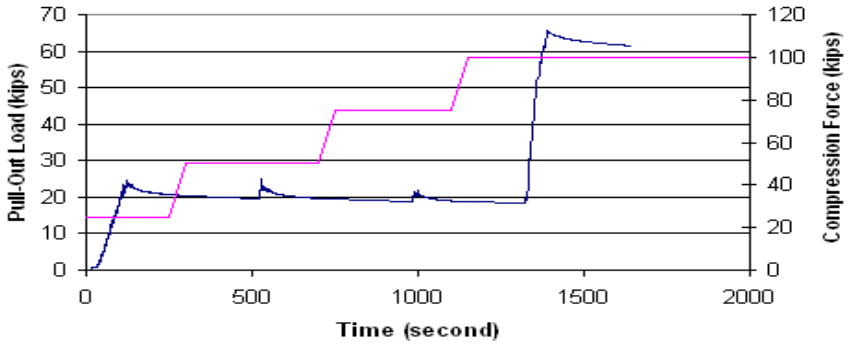

c) Load vs Time

Figure 4.9 – Time-Based Graphs for Strand 15L

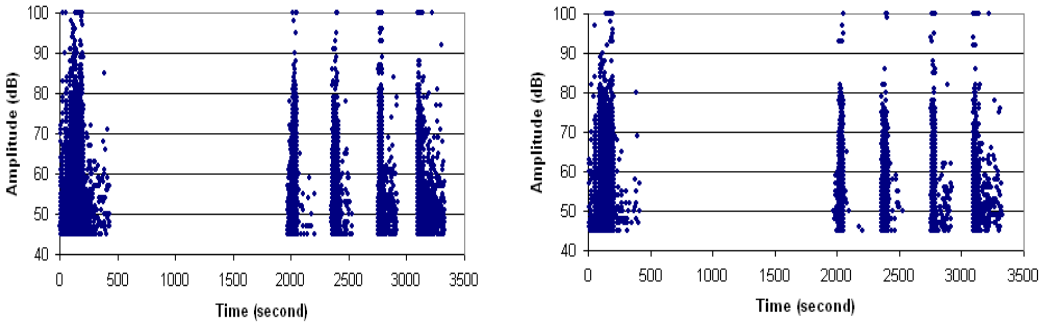

R6I R15I

a) Amplitude vs Time

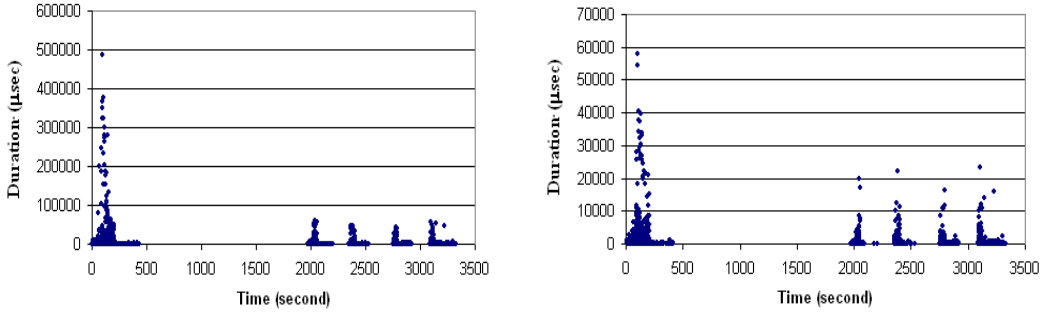

R6I R15I

b) Duration vs Time

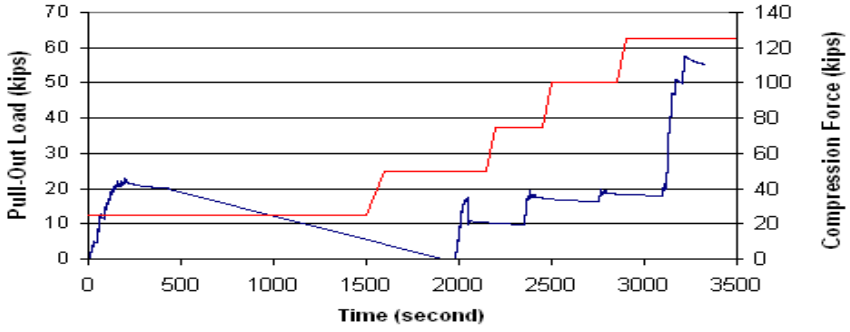

c) Load vs Time

Figure 4.10 – Time-Based Graphs for Strand 2L

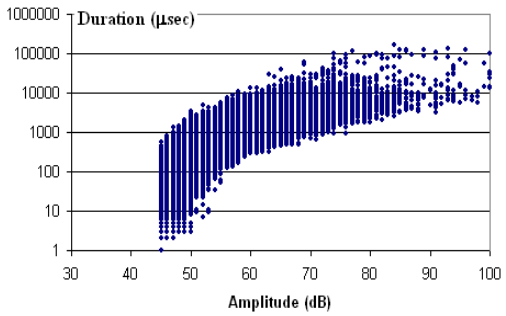

R6I

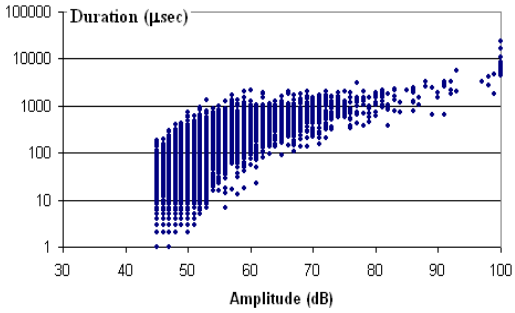

R15I

a) Strand 17L

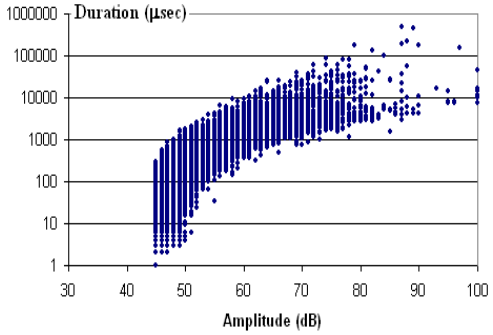

R6I

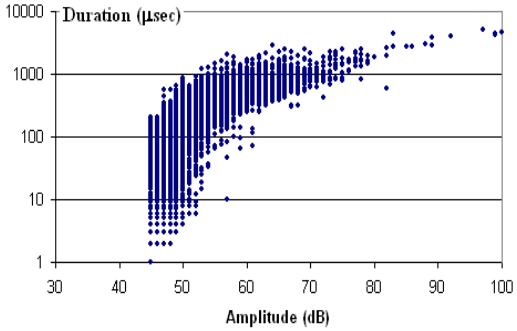

R15I

b) Strand 15L

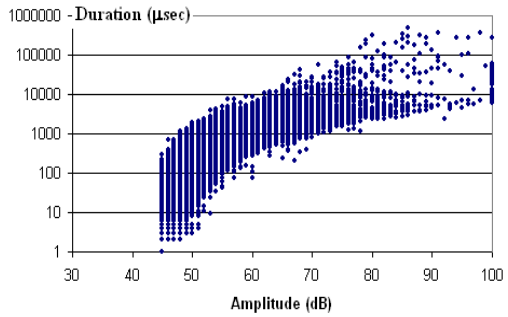

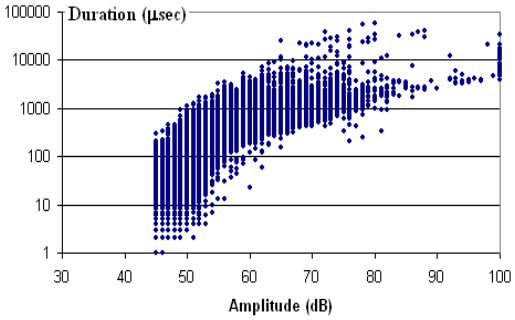

c) Strand 2L

Figure 4.11 – Duration vs Amplitude for Specimen from BG1S

4.4 DISCUSSION OF PULL-OUT TESTS

Acoustic emission monitoring of the pull-out tests revealed a unique signature associated with strand slip. Hits with very long duration are likely to be associated with slip between the prestressing strand and the concrete. Typically, hits with high amplitude and high signal strength will also be detected when slip occurs. From the tests, the R6I and the R15I sensors show the same trends. The R15I-detected hits are shorter in duration, however.

For specimens with severe premature concrete deterioration, high-amplitude hits tend to be detected at a lower percentage of the load causing strand slip. This finding confirms that acoustic emission gives an early warning of strand slip in ASR/DEF deteriorated members.

Chapter 5 – Acoustic Emission Monitoring in the Field

Over the last twenty years, acoustic emission inspection techniques have not developed as rapidly in the fields of civil engineering and geology as in the fields of mechanical engineering, petrochemical manufacturing, and other process industries. The typical goal of acoustic emission monitoring is to evaluate the structural integrity and condition of a structure. Acoustic emission is a global test method that can monitor the whole structure at one time. With this method, time and money can be saved compared to use of other nondestructive methods, such as ultrasonic or radiographic testing.

A number of prestressed concrete bridges around the State of Texas have a premature deterioration problem due to delayed ettringite formation (DEF) or alkali-silica reaction (ASR). Some of them show severe surface cracking raising questions regarding their current condition and probable service life. Acoustic emission is the only nondestructive method capable of detecting an actively growing crack. Two of the goals of this research program are to:

i) Define how acoustic emission can be applied to monitor and evaluate this kind of problem.

ii) Select an appropriate test method and instrumentation setup.

5.1 PROBLEMS ASSOCIATED WITH ACOUSTIC EMISSION MONITORING IN THE FIELD

As described in Chapter 2, acoustic emission monitoring works by detecting stress waves induced in a structure due to mechanisms such as crack propagation, dislocation, and mechanical rubbing. To analyze acoustic emission data, a genuine acoustic emission signal has to be recorded, and any nonrelevant signals (ASTM E1316), conventionally called " noise," must be filtered out. Noise sources can be impact, friction, or even the testing environment and electrical signals. For an in-service bridge, friction and impact sources caused by traffic provide most of the background noise.

5.1.1 Spectrum Analysis

An important technical aspect of an acoustic emission test is the selection of monitoring frequency. The many different types of available piezoelectric sensors can be categorized in two main groups: wide-band sensors and resonant sensors. Wide-band sensors respond to stress waves over a wide range of frequencies, while resonant sensors respond with greater sensitivity at specific frequencies. By collecting data at a particular frequency, resonant sensors can be made sensitive to relevant data but insensitive to background noise.

Resonant sensors available in the acoustic emission industry ranges from 20 kHz to 1 MHz. Background noise normally has a strong low-frequency signal. Selecting a higher frequency acoustic emission sensor can eliminate background noise while detecting genuine acoustic emission. On the

other hand, an acoustic emission stress wave is attenuated rapidly in the high-frequency range. Accordingly, the selected frequency range of the sensor must strike a balance between the advantage of reducing background noise and the disadvantage of attenuation of the stress wave as it travels away from the source.

Spectrum analysis is a frequency analysis of the acoustic emission signal to determine the different frequencies in the stress wave. It is helpful in optimizing the acoustic emission data and selecting sensor appropriate. In steel-bridge inspection, resonant sensors with frequency of 150 or 300 kHz are widely used. A lower range of frequency is required for monitoring concrete structures because of the high attenuation caused by the inhomogeneity and the various sizes of aggregate. In the following section, background noise experiments examining in-service bridges are reported. These tests provide guidance in selecting an appropriate frequency range for prestressed concrete bridge inspection.

5.1.2 Swansong Filter

An important method for eliminating background noise is the use of the Swansong filter, as described below. Normally, a bearing pad is used to support a prestressed concrete girder at abutment or column. The bearing pad also isolates the girder from noise that could be transmitted through the supports. When traffic passes over a bridge, mechanical rubbing at expansion joints and traffic impacts will generate noise that can be detected by acoustic

emission sensors. Acoustic emission hits associated with this noise will often have long durations and low amplitudes. One post-test filter used to remove mechanical rubbing noise is the Swansong II filter, which is recommended by the Association of American Railroads (AAR IM-101). The Swansong II filter is defined by:

If $(A_i - A_{th}) < 5$ and $D_i > 2$

or $(A_i - A_{th}) < 10$, $D_i > 3.5$…….……...…….(5.1)

or $(A_i - A_{th}) < 15$, $D_i > 4.5$

eliminate all hits during the period (secs)

$(T_i - 0.5)$ to $(T_i + 0.5)$…….....(5.2)

where for a given hit, i

A_i = Amplitude (dB)

A_{th} = Data Acquisition Threshold (dB)

D_i = Hit Duration (ms)

T_i = Arrival time (secs)

Equation 5.1 is used to define noisy hits and must be applied to all data from all channels.

5.1.3 Guard Sensor

Guard sensors are a powerful technique to eliminate background noise from acoustic emission data that originates from a local area. Guard sensors are not normally used when acoustic emission is being used as a global technique to monitor a large area of a structure.

An objective of this research is development of an acoustic emission instrument that can be used in the field to monitor an ASR/DEF deteriorated region of a prestressed concrete beam. The initial deterioration will be detected by visual inspection and the monitor will be used to determine the structural significance of the damage. In this situation, the monitor will not be used to evaluate the entire beam but only the regions of apparent severe damage in combination with high shear or flexural stress. Guard sensors are particularly suitable for this application.

The basic concept of the guard sensor is shown in Figure 5.1. If the primary sensor picks up an acoustic emission signal before one of the guard sensors, the source of the stress wave is located in the area of interest. With an effective arrangement of guard sensors, any sound coming from outside the area of interest will be detected by a guard sensor first, and can be separated from the acoustic emission data detected by the primary sensor. In Figure 5.1, the primary sensor defines the area of interest. In practice, emission can originate from within the material, and the area of interest is a three-dimensional region. Further, the region of interest can be defined by more than one sensor. The only requirement is that this region be bounded by guard sensors or by a physical boundary, such as the bottom of the beam.

The guard-sensor technique can be applied in two different ways. The first is through hardware circuitry having the ability to apply guard sensors in real time. In this case, if a guard sensor detects any acoustic emission signals before the primary sensors, the hits on the guard sensors are assumed to come

from outside the area of interest. The instrument therefore suppresses data acquisition on the primary sensors for a predetermined period of time. Any hit occurring during this time will be not recorded. Understandably, the shortest lockout time has to be at least the time needed for the noise to pass through the area of interest.

The second way is through post-test analysis. During the test, all hits detected by both primary sensors and guard sensors are recorded. Post-test software is used to identify which sensors were hit first by an event, and which acoustic emission originates in the region of interest and which comes from outside. This type of analysis is sometimes referred to as “first hit” analysis. The post-test analysis method retains all data and allows for manual inspection of the data. Accordingly, there is less chance of discarding genuine data. On the other hand, the post-test method does not permit a real-time assessment of the significance of the acoustic emission data, and requires the instrument to store several orders of magnitude more data.

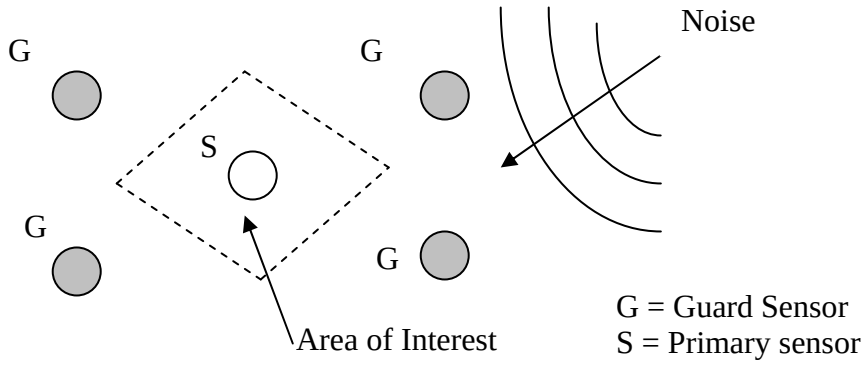

Figure 5.1 - Typical Guard Sensor Setup

5.2 BACKGROUND-NOISE TESTS

Acoustic emission monitoring was conducted at five different sites in order to record background noise. Acoustic emission data were used to evaluate different approaches for separating background noise from genuine acoustic emission data. Some of the tests were done at a mid-span of a beam (flexure-dominated region), while others were done near the support (shear-dominated region).

5.2.1 Instrumentation for Background-Noise Tests

Two types of the resonant sensors were used for the tests. Both sensor types were manufactured by Physical Acoustic Corporation (PAC). The sensors, designated R6I and R15I, have resonant frequencies at 60 kHz and 150 kHz.

Three acoustic emission instruments were used to acquire data. The first, shown in Figure 5.2, is a six-channel LOCAN AT instrument, manufactured by PAC. It is an analog instrument, with an Intel 8 MHz 8086 CPU.

Figure 5.2 – LOCAN AT Analog Acoustic Emission Instrument

A six-channel MISTRAS 2001, also manufactured by PAC, is the second instrument used in the tests. The MISTRAS, shown in Figure 5.3, is a digital instrument with an Intel Pentium 166 MHz processor. This instrument has the ability to record a signal wave form and operate guard sensors.

Figure 5.3 – MISTRAS 2001 Digital Acoustic Emission Instrument

The third instrument used for the background noise tests is a Local Area Monitor (LAM), shown in Figure 5.4, also manufactured by PAC. The LAM is a digital instrument with a PC-104 CPU board, and a PC-104 modem. The system was specifically designed under a Federal Highway Administration project for remote monitoring. Setting up the instrument, downloading the acoustic emission data and controlling the machine can be done remotely. An internal battery can run the instrument up to 12 hours without recharging. The LAM can capture and store digitized wave forms and operate guard sensors.

Figure 5.4 – LAM Digital Acoustic Emission Instrument

The instrument settings used for all three instruments are detailed in Table 5.1.

Table 5.1 - Instrument Setting during Background Noise Tests

Quantity	*Values*
Hit Definition time (HDT)	400 μs
Voltage Threshold	40 dB or 50dB
Sensor Preamplifier	40 dB
Peak Definition Time	200 μs
Hit Lockout time	200 μs

5.2.2 Southbound Mopac Railroad Overpass between Braker and Burnet, Austin, Texas

At this site, background noise due to traffic was monitored. Data were collected using the LOCAN 320 data acquisition instrument. 60 kHz and 150 kHz resonant sensors with integral preamplifiers were used to monitor the characteristics of the background noise. A threshold of 40 dB was set for all channels. The outside (west) and the third from outside I-shape prestressed concrete girders were monitored. The outside girder supported the exit lane, while the third girder supported the middle and inside lanes going in the southbound direction. Data were recorded on the top flange, at mid-depth, and on the bottom flange. Two similar sensors were attached on both sides of the girder for each test. Figure 5.5 shows a sensor attached to the top flange and connected to the instrument. Sensor holders are mounted at the mid-height and on the bottom flange. Sensors were attached on the girder one foot from

the end. Background noise on the top flange was recorded first for 15 minutes and then these two sensors were moved in turn to the mid-depth and the bottom flange. During monitoring, the traffic flow was recorded.

Figure 5.5 – Attached Sensor Location

Plots of amplitude versus time for each hit and traffic flow are shown in Figures 5.7 through 5.9. Lane 1 is the exit lane. Lane 2 and Lane 3 are the middle and inside lanes going the southbound direction.

Figure 5.6 – Southbound Mopac Railroad Overpass between Braker and Burnet, Austic, Tx

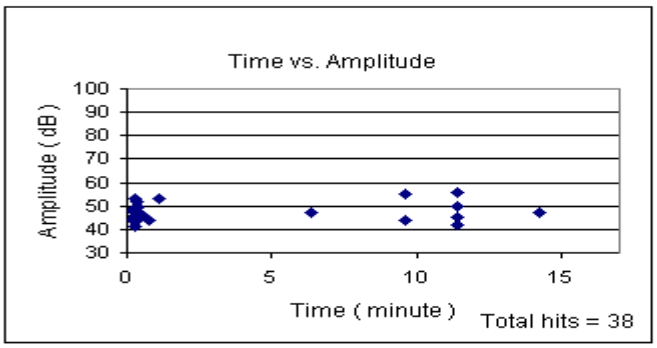

Lane	Number of heavy trucks
1	0
2	4
3	3

a) Top Flange

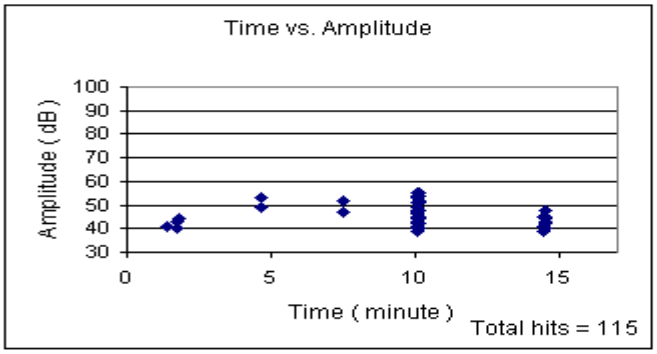

Lane	Number of heavy trucks
1	3
2	5
3	3

b) Mid-depth

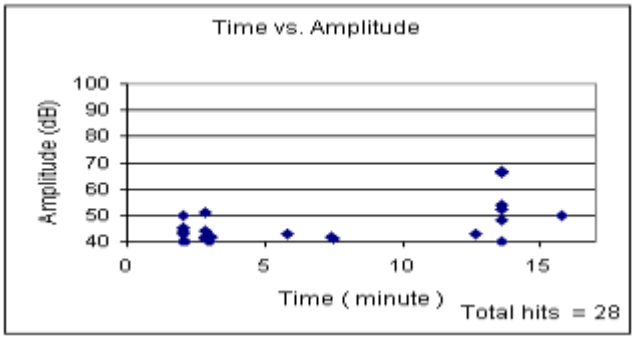

Lane	Number of heavy Trucks
1	2
2	2
3	5

c) Bottom Flange

Figure 5.7 - Background Noise Recorded with an R6I on the Outside Girder of Mopac during Background Noise Tests

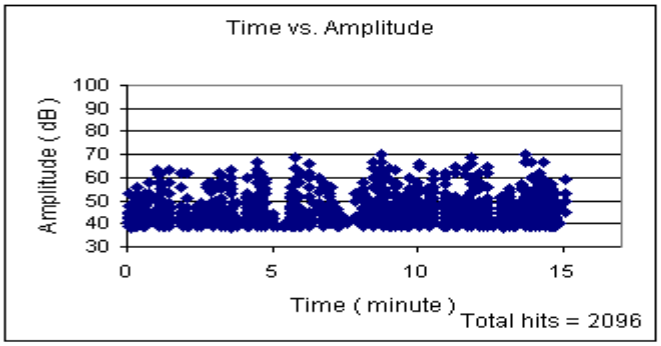

Lane	Number of heavy trucks
1	0
2	1
3	1

a) Top Flange

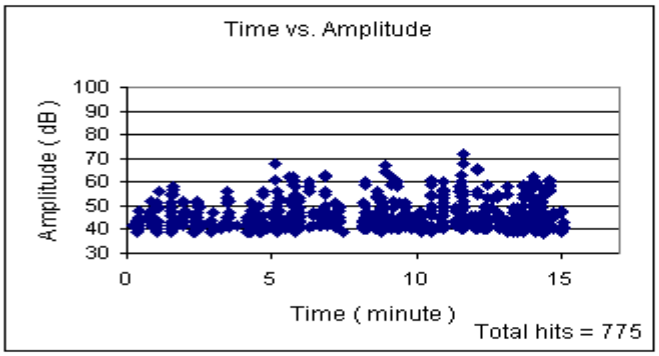

Lane	Number of heavy trucks
1	0
2	2
3	2

b) Mid-depth

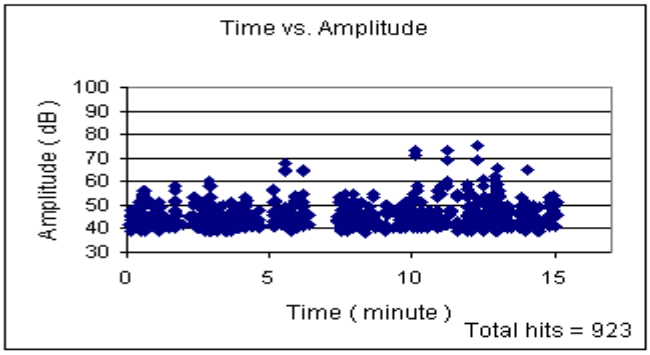

Lane	Number of heavy truck
1	0
2	2
3	3

c) Bottom Flange

Figure 5.8- Background Noise Recorded with an R6I on the Third Girder of Mopac during Background Noise Tests

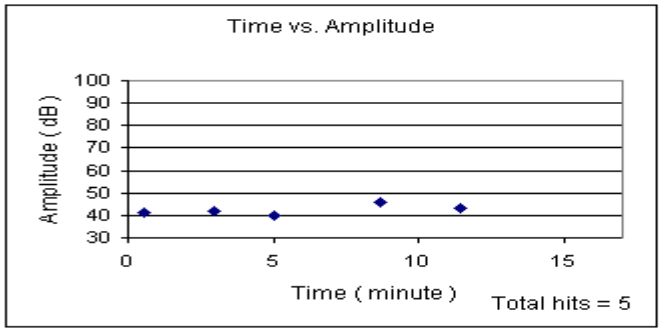

Lane	Number of heavy trucks
1	0
2	3
3	1

a) Top Flange

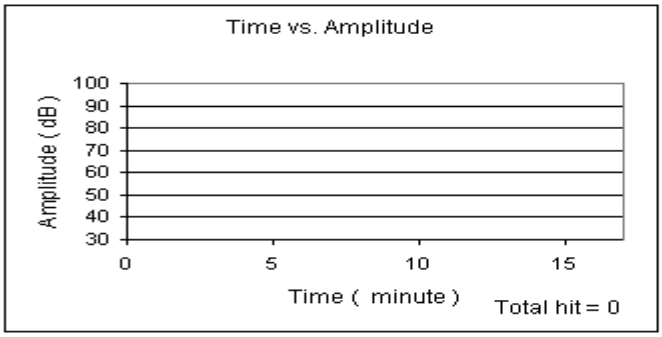

Lane	Number of heavy trucks
1	0
2	1
3	2

b) Mid-depth

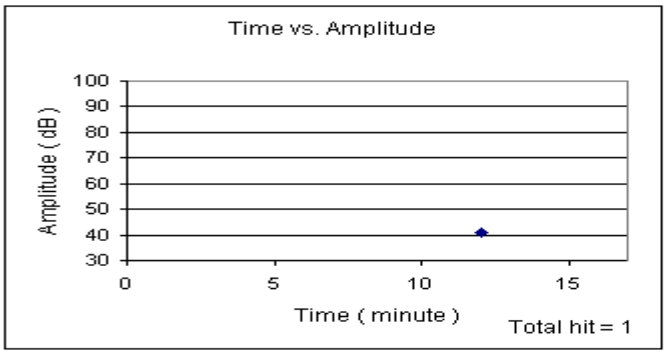

Lane	Number of heavy trucks
1	0
2	1
3	2

c) Bottom Flange

Figure 5.9 - Background Noise Recorded with an R15I on the Third Girder of Mopac during Background Noise Tests

From the plots, it can be seen that the girder supporting the main lane of Mopac has a greater amount of background noise than the girders supporting the exit lane. This is as expected. Background noise was reduced significantly by using a sensor with a higher resonant frequency. As can be seen, there are significantly fewer hits when the R15I sensor was used. Fewer than 10 hits were detected by the R15I during a 15-minute monitoring period of the third girder, and only 1 hit on the bottom flange.

It is concluded from these tests that background noise can be controlled by use of an R15I sensor. R6I sensors, in contrast, are very sensitive to background noise and are unsuitable for field application.

5.2.3 I-35 Overpass U-Turn Lane near 41st Street, Austin, Texas

The Mopac site discussed in Section 5.2.2 had a low amount of traffic passing over the bridge, and may not be typical. The site at the I-35 overpass U-turn lane near 41st Street was selected because it had heavy traffic passing over the bridge.

Figure 5.10 – I-35 Overpass of U-Turn Lane near 41st Street

The LOCAN 320 data acquisition instrument was used to record emission. As shown in Figure 5.10, a portable generator provided electricity to the instrument. The Mopac test showed that an R15I sensor reduces background noise compared to an R6I. In order to confirm this result, R6I and R15I sensors were used with two different levels of threshold setting. The outside girder supporting the exit lane (Exit 236B) and the third girder supporting the middle and inside lanes going in the southbound direction were selected to be monitored. Two sensors were attached on each side of the beam at the top flange, mid-depth, and bottom flange. The sensors were attached at mid-span of the I-shaped prestressed concrete girders. This is shown in Figure 5.11

Figure 5.11 – Arrangement of Acoustic Emission Sensors

The outside girder was monitored first. Thresholds equal to 50 and 40 dB were used for the R6I and R15I, respectively. The background noise was monitored for 15 minutes in each test. The plots of amplitude versus time are shown in Figures 5.13, 5.14 and 5.15. Lane 1 is the exit lane. Lane 2 and lane 3 are the middle and inside lanes going the southbound direction.

Figure 5.12 – I-35 Overpass U-Turn Lane near 41st Street, Austin, TX

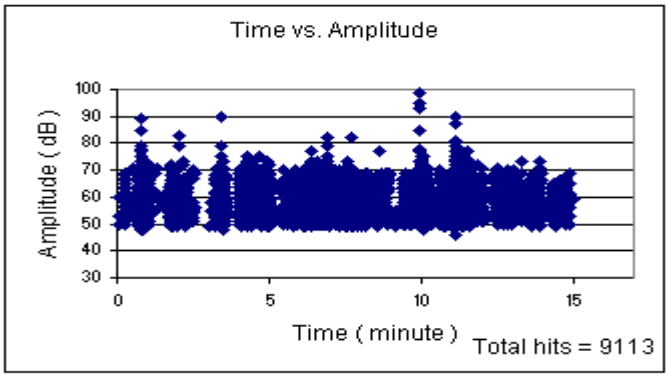

Lane	Number of Heavy Trucks
1	2
2	23
3	13

a) Top Flange

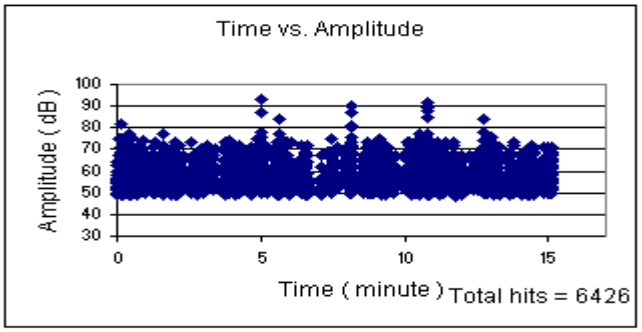

Lane	Number of Heavy Trucks
1	0
2	15
3	14

b) Mid-depth

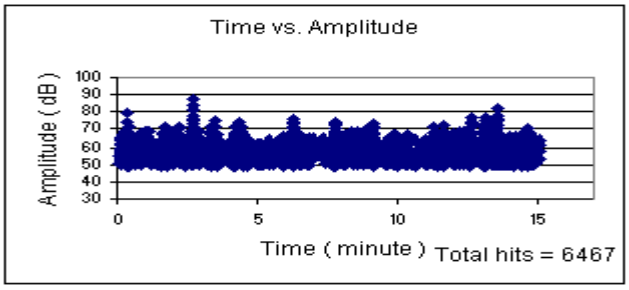

Lane	Number of Heavy Trucks
1	1
2	19
3	16

c) Bottom Flange

Figure 5.13 – Background Noise Recorded with an R6I on the Outside Girder of I-35 near 41st Street during Background Noise Tests

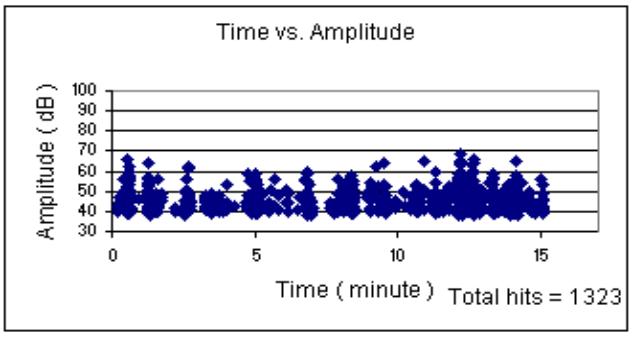

Lane	Number of Heavy Trucks
1	0
2	22
3	10

a) Top Flange

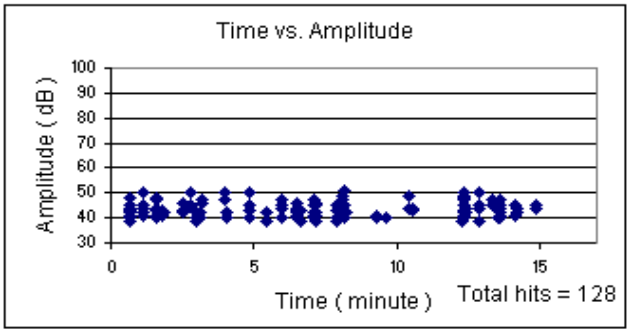

Lane	Number of Heavy Trucks
1	1
2	19
3	19

b) Mid-depth

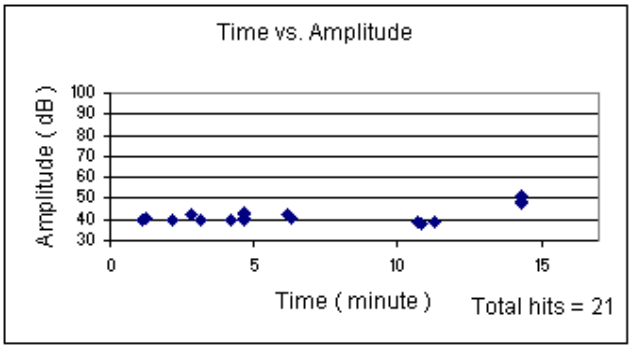

Lane	Number of Heavy Trucks
1	0
2	17
3	31

c) Bottom Flange

Figure 5.14 – Background Noise Recorded with an R15I on the Outside Girder of I-35 near 41st Street during Background Noise Tests

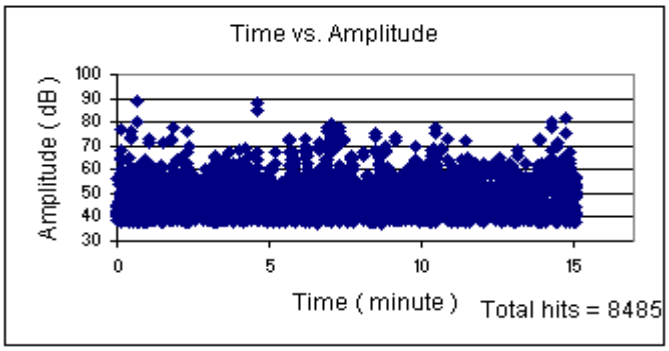

Lane	Number of Heavy Trucks
1	0
2	25
3	13

a) Top Flange

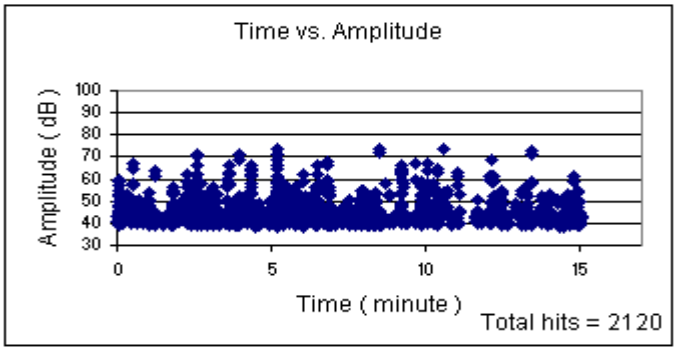

Lane	Number of Heavy Trucks
1	0
2	22
3	18

b) Mid-depth

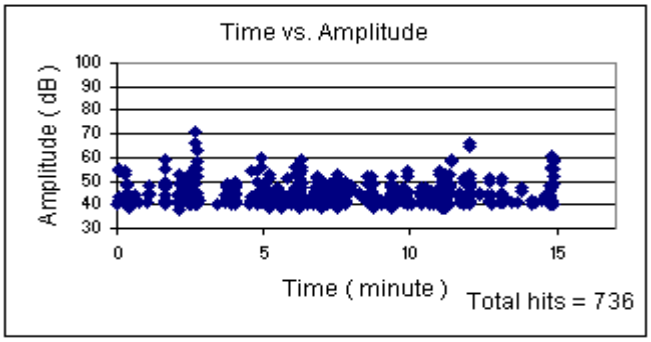

Lane	Number of Heavy Trucks
1	0
2	30
3	26

c) Bottom Flange

Figure 5.15 – Background Noise Recorded with an R15I on the Third Girder of I-35 near 41st Street during Background Noise Tests

Figure 5.13 shows a large number of hits detected by the R6I sensors on the outside girder, even though during the testing time only a few trucks passed over the exit lane. When sensors were changed from R6I to R15I, background noise was reduced dramatically. It remained as a problem at the top flange but was not significant at the bottom flange (Figure 5.14). The data collected on the outside girder indicate, as before that excessive background noise makes an R6I sensor undesirable for field use.

In these tests, two sensor thresholds were tried. The higher threshold reduces the sensitivity of the sensor. The results show that for an R15I sensor, a 50 dB threshold provides a good compromise between background noise and sensitivity. If hits with an amplitude lower than 50 dB are eliminated from the R15I data on the outside girder, only a few hits remain.

Unfortunately, setting a 50 dB threshold and using an R15I sensor did not solve the background noise problem on the inside girder. Accordingly, the data were reanalyzed using a post-test filtering technique. It was speculated that the background noise might be caused by mechanical rubbing at the expansion joint. To test this theory, the Swansong II filter was used to filter the acoustic emission data. A portion of the analyzed data is shown in Figures 5.16 to 5.18.

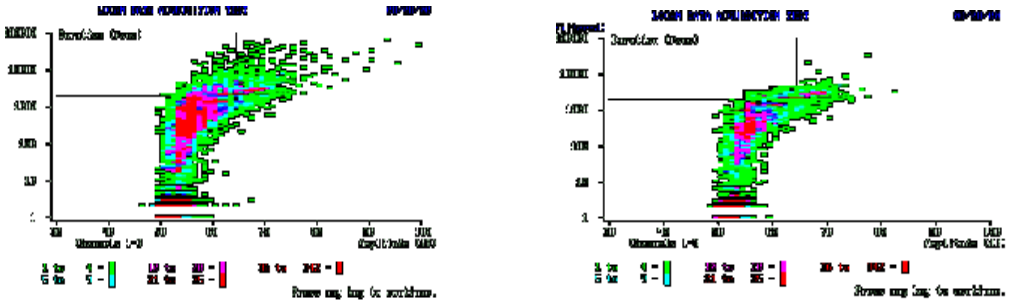

a) Before filtering b) After filtering

Figure 5.16 – R6I Data from Outside Girder at the Top Flange

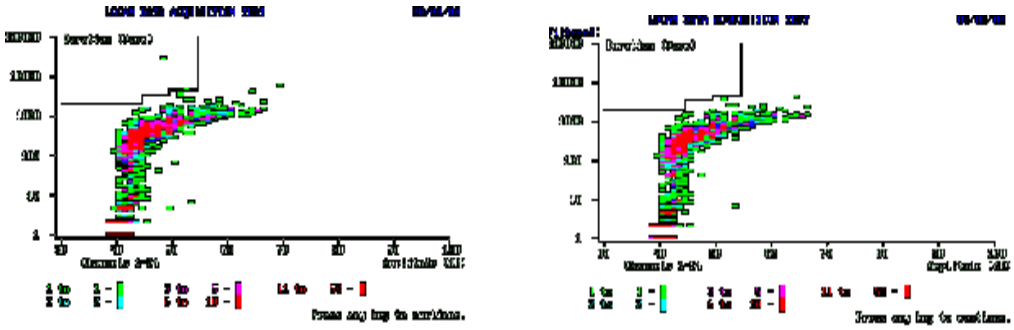

a) Before filtering b) After filtering

Figure 5.17 – R15I Data from Outside Girder at the Top Flange

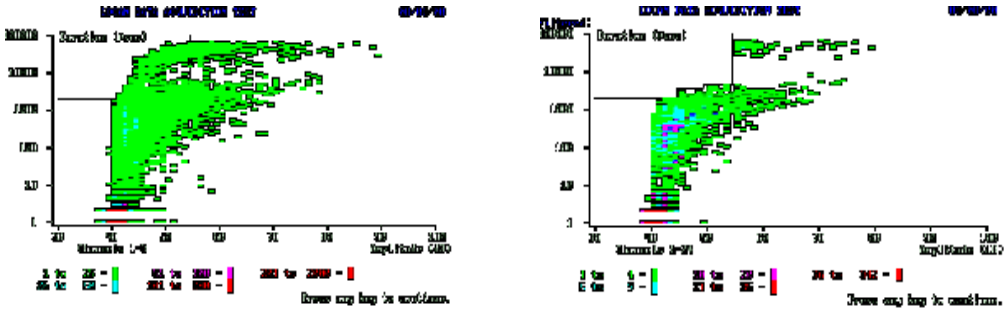

a) Before filtering b) After filtering

Figure 5.18 – R15I Data from the Third Girder at the Top Flange

The Swansong II filter did not perform well. While it eliminated some background noise in some tests, the filter did not work for the data detected by the R15I on the top flange of the outside girder.

The following conclusions are drawn from the I-35 near 41st Street tests:

i) R6I sensors are very susceptible to background noise and are not recommended for field monitoring applications.

ii) R15I sensors are much less susceptible to background noise than the R6I sensors, and are recommended.

iii) Background noise originates in the roadway and is sharply attenuated through the depth of the girder.

iv) Use of a 50 dB threshold with an R15I sensor eliminates a significant portion of the background noise.

v) The Swansong II filter is unsatisfactory for removing background noise.

5.2.4 Northbound I-35 Overpass at Airport Boulevard, Austin, Texas

Two phases of background noise monitoring were carried out at this site. The purpose of the first phase was to investigate the background noise from the northbound lanes at the support near an abutment. This area was expected to have the most severe background noise. In the second phase, guard sensors were set up in order to evaluate the guard technique. Tests were conducted using several different sensor arrangements.

In the first phase, R6I and R15I sensors were used. The outside girder supporting the exit lane and the fourth girder supporting the inside lane going in the northbound direction were chosen to be the representative of other girders (Figure 5.19). The top flange, mid-depth and bottom flange were examined. Two similar sensors were mounted on opposite sides of the girder at each test location. Sensors were attached to the girder one foot from the end. Background noise on the top flange was recorded first for 15 minutes and then these two sensors were moved in turn to the mid-depth and bottom flange. A LOCAN 320 data acquisition instrument was used. The threshold was set to 40 dB. Other setting details were as shown in Table 5.1. The plots of amplitude versus time are shown in Figures 5.20, 5.21, and 5.22. Lane 1 is the exit lane. Lanes 2 and 3 are the middle lanes and Lane 4 is the inside lane going the northbound direction.

Figure 5.19 – Northbound I-35 Overpass at Airport Blvd., Austin, TX

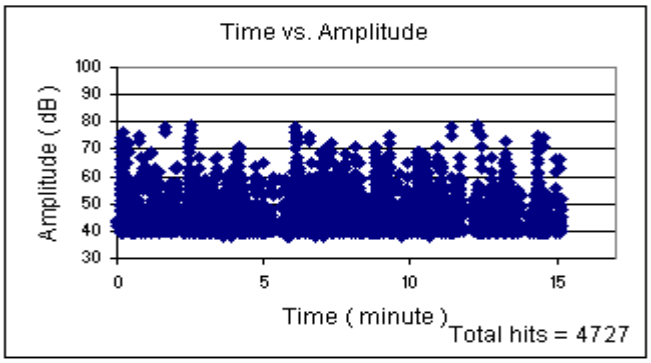

Lane	Number of heavy trucks
1	2
2	10
3	15
4	19

a) Top Flange

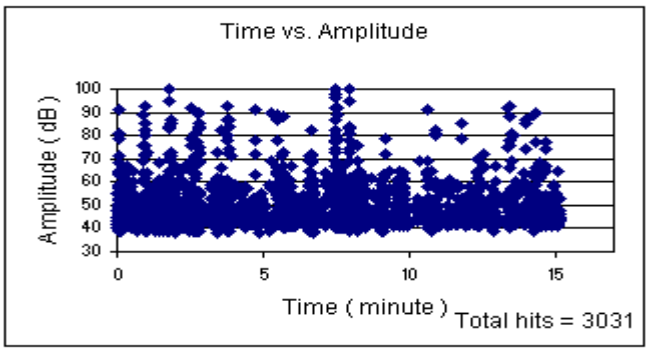

Lane	Number of heavy trucks
1	9
2	11
3	13
4	28

b) Mid-depth

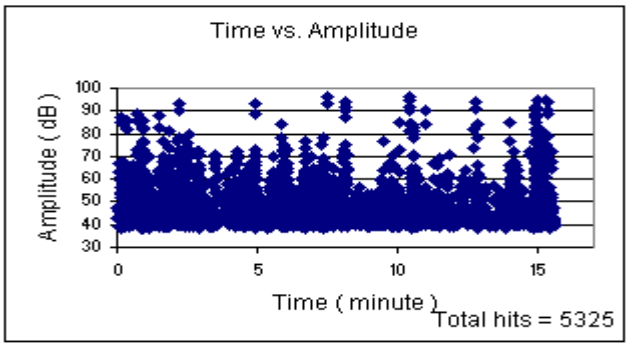

Lane	Number of heavy trucks
1	11
2	9
3	17
4	18

c) Bottom Flange

Figure 5.20 – Background Noise Recorded with an R6I on the Outside Girder of I-35 overpass at Airport Blvd. during Background Noise Tests

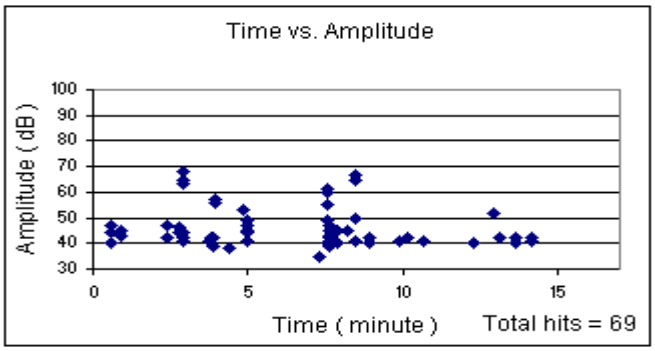

Lane	Number of heavy trucks
1	8
2	8
3	20
4	20

a) Top Flange

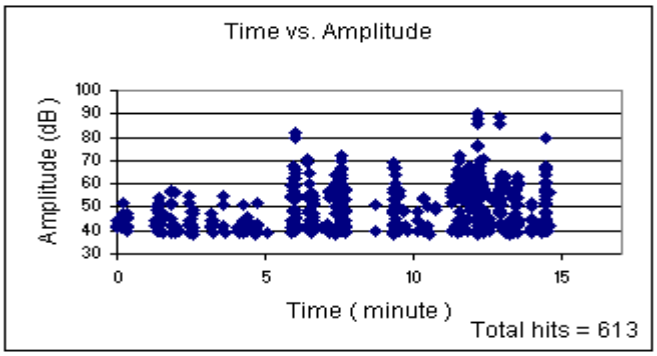

Lane	Number of heavy trucks
1	7
2	12
3	18
4	22

b) Mid-depth

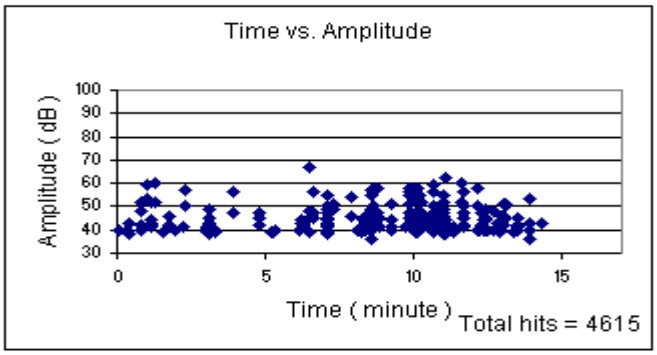

Lane	Number of heavy trucks
1	5
2	13
3	17
4	31

c) Bottom Flange

Figure 5.21 – Background Noise Recorded with an R15I on the Outside Girder of I-35 overpass at Airport Blvd. during Background Noise Tests

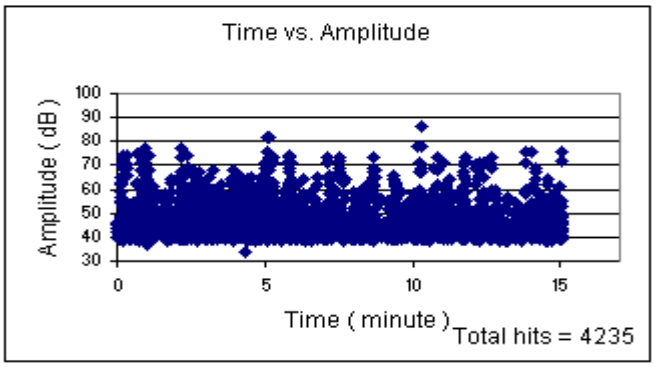

Lane	Number of heavy trucks
1	6
2	15
3	26
4	23

a) Top Flange

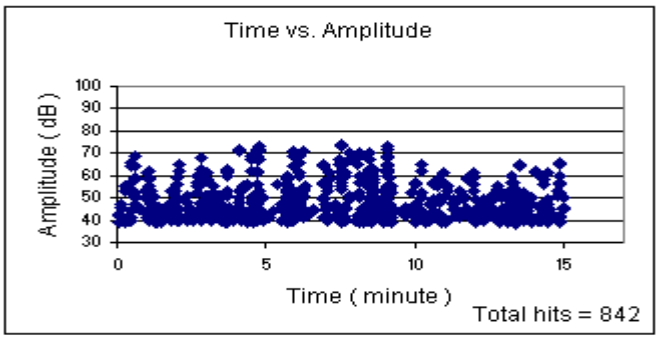

Lane	Number of heavy trucks
1	3
2	7
3	21
4	16

b) Mid-depth

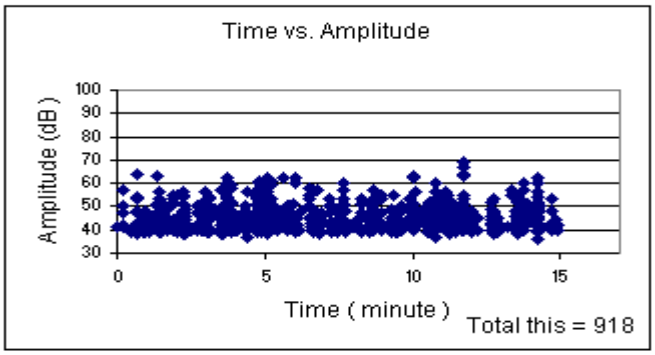

Lane	Number of heavy trucks
1	6
2	14
3	20
4	15

c) Bottom Flange

Figure 5.22 – Background Noise Recorded with an R15I on the Fourth Girder of I-35 overpass at Airport Blvd. during Background Noise Tests

Background noise was severe on the interior girder, and a significant numbers of high-amplitude hits were detected. At the top flange, a tremendous number of hits were detected. Even with the R15I and a 50 dB threshold, background noise was significant at all positions on the beam.

Data from this background noise test were also filtered by the Swansong II filter. The results are shown in Figures 5.23 through 5.25. It is clear that the Swansong II filter can eliminate some noise from acoustic emission data, but it is not the solution for field monitoring.

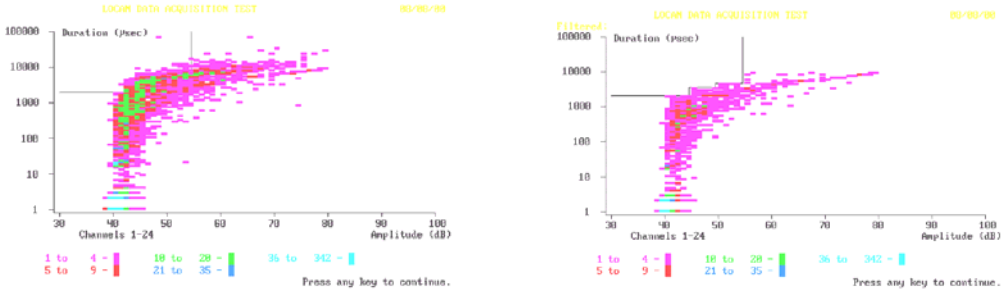

a) Before filtering b) After filtering

Figure 5.23 – R6I Data Recorded on the Outside Girder at the Top Flange

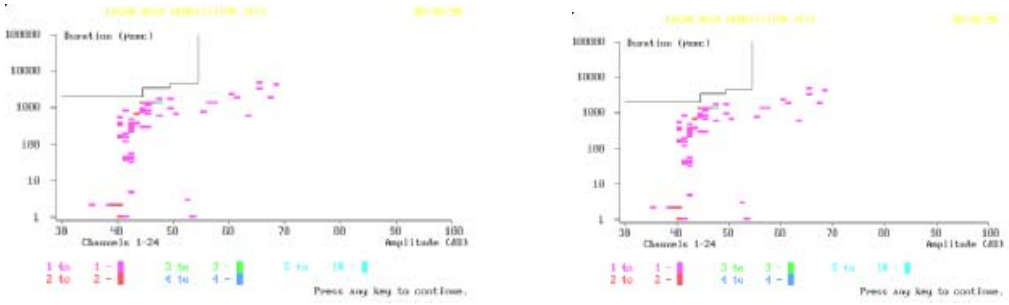

a) Before filtering b) After filtering

Figure 5.24 – R15I Data Recorded on the Outside Girder at the Top Flange

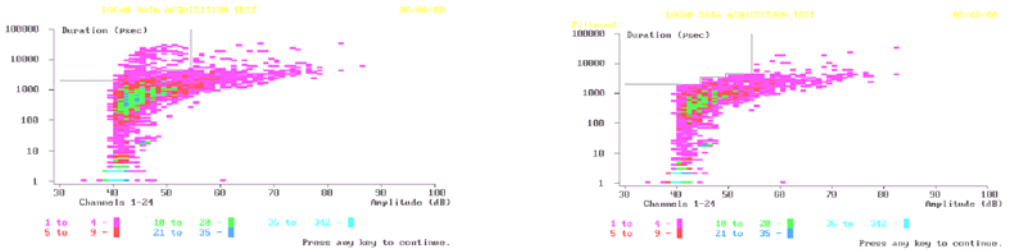

a) Before filtering b) After filtering

Figure 5.25 – R15I Data Recorded on the Fourth Girder at the Top Flange

The conclusions from the first phase of testing at the northbound I-35 overpass at Airport boulevard are the same as those set out at the end of Section 5.2.3 for the I-35 overpass near 41st Street.

In the second phase, the background noise from the southbound direction lanes was monitored using guard sensors. The LAM was used to record the data. Parameter settings were as shown in Table 5.1 with a 50 dB threshold. The R15I sensors were mounted on each side of the fourth

prestressed concrete girder, as shown in Figure 5.26. The odd and even numbers represent positions on the east and west sides of the girder, respectively. Different primary and guard sensors were selected for each test. Details are shown in Table 5.2.

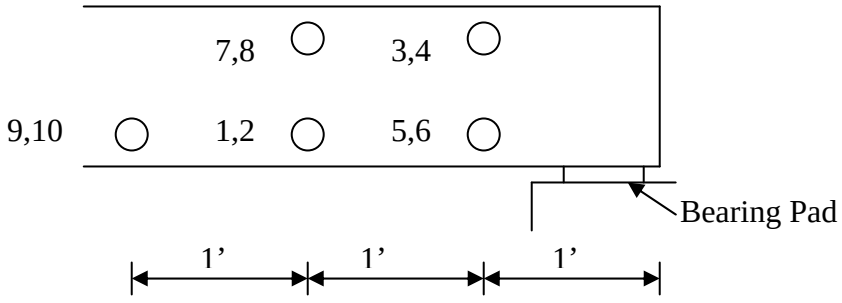

Figure 5.26 – Locations of Acoustic Emission Sensors

Five different tests were carried out. During each test, background noise was monitored for 10 minutes. Guard sensors were activated and only signals detected by first-hit sensors were recorded. The LAM instrument maintains a real time count of the number of hits striking the primary sensors, even if they are not recorded because the event strikes the guard sensor first. This total, which is not recorded in the data file, was noted and is shown in Table 5.2. The results for each test are shown in the table. The traffic condition was monitored and is reported in Table 5.3.

Table 5.2 - Results from Guard Test at I-35 Overpass at Airport Blvd.

Test	Primary Sensors	Guard Sensors	Number of hits striking primary sensors including hits which strike a guard sensor first	Number of first hits striking primary sensors
A	1,2	3,4	146	8
B	1,2	5,6	119	2
C	1,2	7,8	408	4
D	1,2	9,10	390	4
E	1,9	5,7	Not recorded	10

Table 5.3 - Number of Truck during Testing

Test	Lane1 (Exit Lane)	Lane2	Lane3*	Lane4*
A	2	8	8	3
B	3	7	19	2
C	1	12	19	3
D	3	15	14	5
E	2	16	12	1

*Lane supported by the monitored girder

The following conclusions are drawn from the guard sensor tests.

i) The guard sensors eliminated many hits from the data, leaving only a few hits to be detected by the primary channels.

ii) Traffic noise can come from all directions.

iii) To effectively eliminate background noise, a number of guard sensors are required, and need to be located on different sides of the primary sensors.

iii) Guard sensors can be used in conjunction with a 150 kHz resonant sensor and a 50 dB threshold to eliminate background noise.

5.2.5 Beltway 8 over State Highway 3, Houston, Texas

Beltway 8 over State Highway 3 is a bridge with premature concrete deterioration at the support and in the middle of the span. The first experiment was set up to monitor acoustic emission data around the cracked region at the middle of the span. Guard sensors were used. Unfortunately, the cracked beam was part of the frontage road and during the 10-minute monitoring period, no heavy trucks passed over this bridge. No hits were detected on either the primary or guard sensors.

For the second experiment, monitoring was performed on an interior girder supporting the main eastbound lanes. The girder was in good condition with no indication of premature deterioration. Traffic on this structure was heavy and continuous.

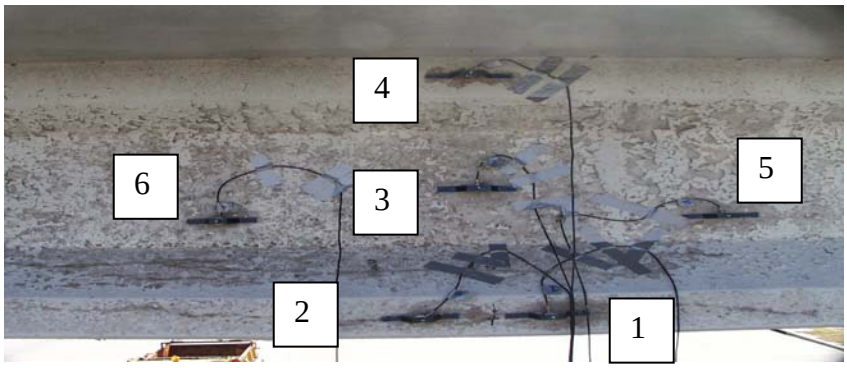

Figure 5.27 – Positions of Sensors at Middle of the Span of Exterior Girder

Figure 5.27 shows the exterior girder on the frontage road. In addition to showing the sensor positions, the cracks in the concrete can be seen running in the longitudinal direction along the bottom flange. An identical sensor arrangement was used to monitor the main eastbound lanes of Beltway 8. R15I sensors were used for the tests. A six-channel MISTRAS 2001 was used to record emission, and a 40 dB threshold was set for every channel.

Two testing programs were performed on this girder. For the first test, Channels 1, 2, and 3 were activated for 15 minutes. A total of 41 hits were detected on all channels. Data are shown in Figure 5.28.

For the second program, guard sensors were activated. Channels 1 and 2 served as the primary channels, while Channels 4, 5, and 6 acted as guard channels, and Channel 3 was not used. Other instrument settings were the same as for the previous program. After a 15-minute monitoring session, the guard sensors detected 23 hits. No hits were detected by the primary sensors.

These two testing programs show that the background noise due to traffic can be eliminated from acoustic emission data by the appropriate placement of guard sensors and selection of a suitable sensor frequency.

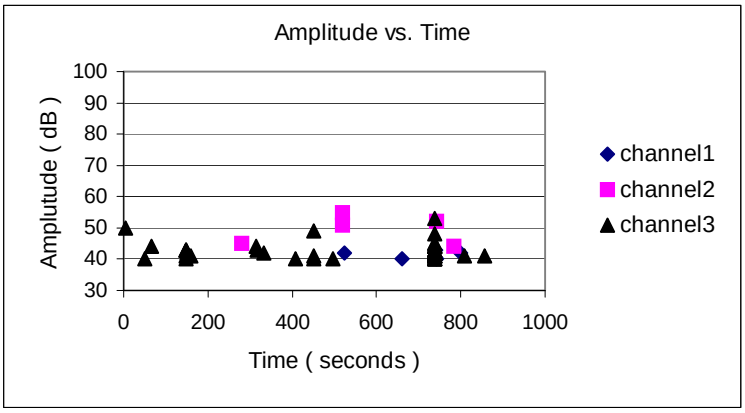

Figure 5.28 - Amplitude vs Time for the First Testing Program of Beltway 8 East Traffic Lane

Table 5.4 - Number of Trucks during Monitoring of Beltway 8 East Traffic Lanes

	Lane 1*	Lane 2	Lane 3
Without guard sensor	16	5	0
With guard sensors	15	10	0

* Lane supporting by the monitored girder

5.3 CONTINUOUS MONITORING, SAN ANTONIO, TEXAS

A continuous monitoring test was carried out on Pier D35C near the Fredericksburg Road exit of I-35 in San Antonio, Texas. This pier has premature concrete deterioration at the corner on the top. The maximum crack size is 0.020 inch. On the east side, an epoxy repair material has been put into the cracks to prevent moisture penetrating into the structure. Continuous

acoustic emission monitoring was performed during the period 11/15/2000 to 11/20/2000.

Figure 5.29 – Monitored Column in San Antonio, TX

5.3.1 Instrumentation Setup

The Local Area Monitor (LAM) was used to collect acoustic emission data at this site. 150 kHz resonant sensors with integral preamplifiers were used to monitor the background noise from traffic, and the acoustic emission from cracks. The cracks were far from the main bridge girders, and background traffic noise was not expected to be severe. Five sensors were mounted on the pier for the first 3 days of the testing program. Guard sensors were not used during this period. During the last three days of the testing program, three additional sensors were attached to the pier. These sensors

were set as guard sensors. The location of each sensor is shown in Figure 5.30. Guard sensors are denoted by the prefix G.

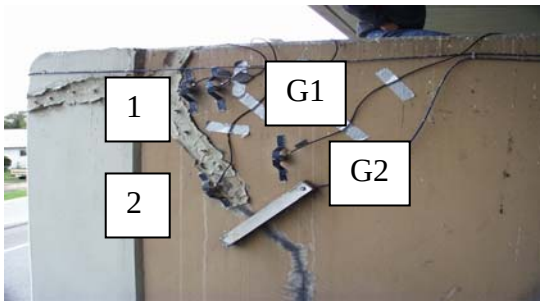

a) West Side

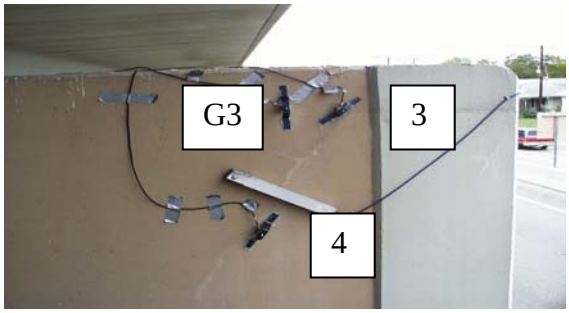

b) East Side

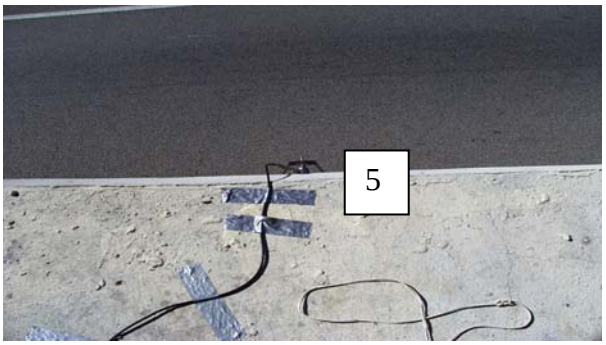

c) North Side

Figure 5.30 – Locations of Primary Sensors and Guard Sensors

The acoustic emission instrument and generator were placed on the top of the pier during the test period (Figure 5.31). The instrument settings used for the test are shown in Table 5.5.

Figure 5.31 – Location of LAM and Generator

Table 5.5 Test Parameters for Continuous Monitoring Test

Quantity	*Values*
Hit Definition time (HDT)	400 μs
Threshold	55 dB
Sensor Preamplifier	40 dB
Peak Definition Time	200 μs
Hit Lockout Time	200 μs

5.3.2 Result of Continuous Monitoring Test

Acoustic emission data were analyzed by using the criteria for onset of significant emission as defined in Chapter 3. Five acoustic emission sensors were mounted on the east, west and north sides of the pier. Channel 5 was located on the north side of the pier. This sensor did not have any cover and it rained every day during the test. A lot of background noise was detected by Channel 5. As it is believed that this was due to the rain, only data from channels 1, 2, 3, and 4 are analyzed and reported.

During the first three days of monitoring, 339 hits were detected by Channels 1, 2, 3,and 4. These data are shown in Figures 5.32 and 5.33. Only a few hits with high amplitude were detected. Curvature, slope and HI criteria were used to determine the onset of significant emission. The maximum values of slope and curvature are less than 1 and do not pass the criteria defined in Chapter 3. The maximum magnitude of the historic index is 1.6, which is less than the defined criterion. Based on these three criteria, the detected emission indicates that DEF does not have a significant effect on the structural integrity of the structure.

For the last three days of monitoring, guard sensors were activated. 467 hits were eliminated by the guard sensors, and 349 hits were detected by the primary sensors. Because of the limited number of available channels in the instrument, the guard sensor arrangement was not optimum. The guard sensors, however, worked well to eliminate background noise. Based on the evaluation criteria, the emission detected during the monitoring period is not

significant. Figures 5.32 and 5.34 show the results from the test with guard sensors.

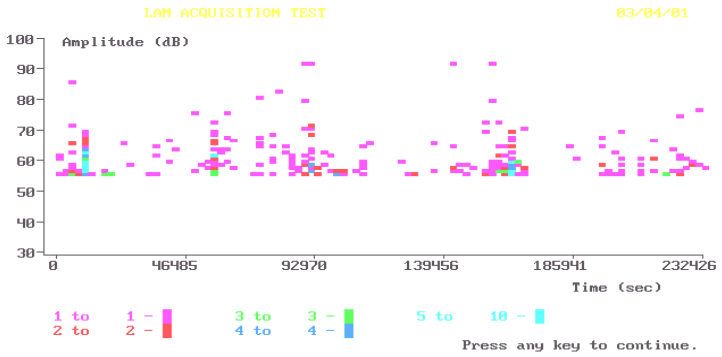

a) First Three Days without Guard Sensors

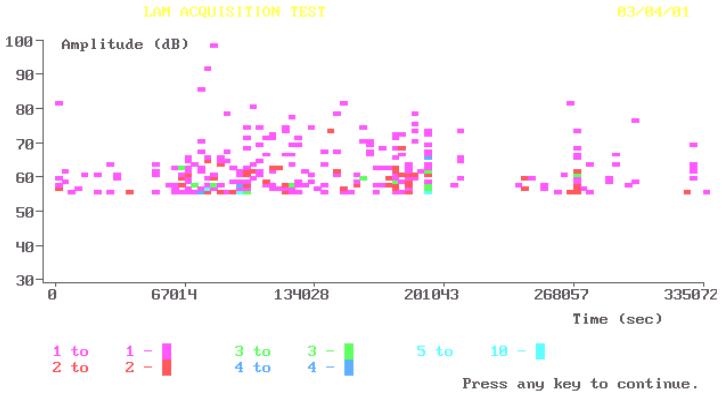

b) Last Three Days with Guard Sensors

Figure 5.32 – Amplitude vs Time Graphs of Continuous Monitoring

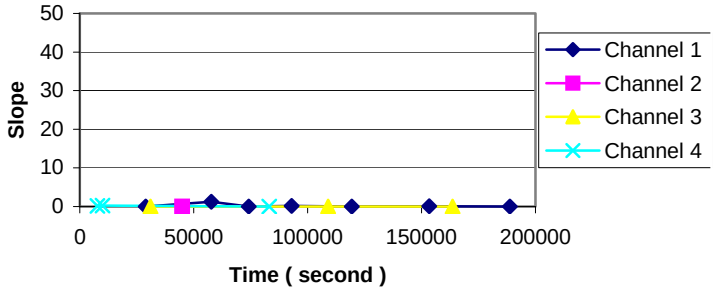

a) Slope of Cumulative Signal Strength vs Time Curve

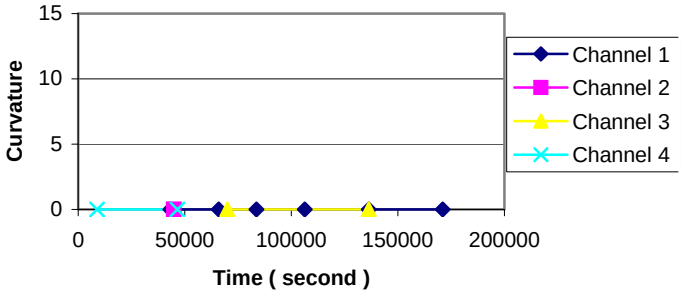

b) Curvature of Cumulative Signal Strength vs Time Curve

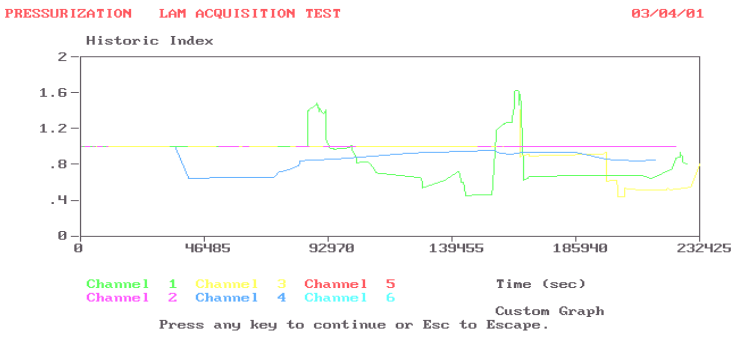

c) Historic Index vs Time

Figure 5.33 – Time-Based Curves for the First Three Days of Continuous Monitoring without Guard Sensors

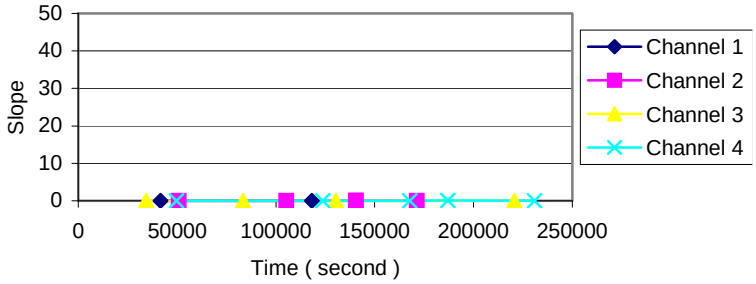

a) Slope of Cumulative Signal Strength vs Time Curve

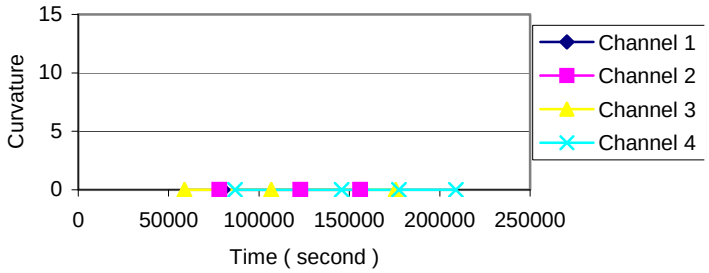

b) Curvature of Cumulative Signal Strength vs Time Curve

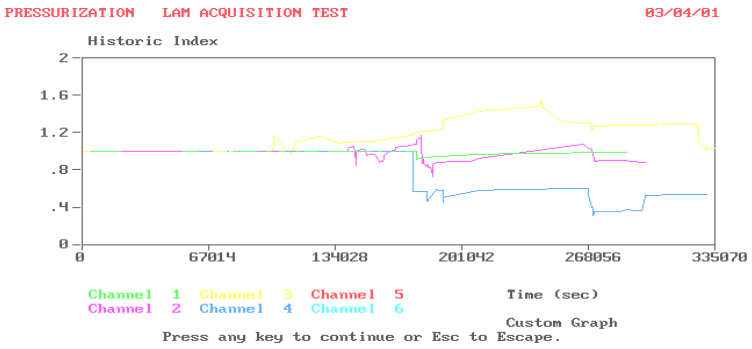

c) Historic Index

Figure 5.34 – Time-Based Curves for the Last Three Days of Continuous Monitoring with Guard Sensors

The following conclusions are drawn from the continuous monitoring tests conducted at San Antonio during six days of monitoring:

i) A commercially available instrument has been demonstrated for six days in a practical field monitoring application.

ii) Background noise was manageable through use of appropriate sensor frequencies, signal thresholds, and guard sensors.

iii) Even though the recorded data probably contained genuine emission, the data analysis criteria confirmed that the observed concrete deterioration had not seriously affected the structural integrity of that portion of the structure monitored during this test.

5.3.3 Discussion of Acoustic Emission Monitoring in the Field

Acoustic emission field tests were performed at six different sites. The structures that were monitored were mostly prestressed concrete girders. One reinforced concrete pier was monitored. Some of the structures were in a good condition. Others had premature concrete deterioration. Two different frequency sensors, different acoustic emission parameters, different signal thresholds, Swansong filtering, and guard sensors were evaluated as methods of managing background noise, which was primarily due to traffic. The results show that 150 kHz sensors with 50 to 55 dB threshold setting can reduce background noise in severe traffic noise conditions. The guard-sensor technique worked very well in this application. For local area monitoring, the

guard-sensor technique is effective. It is less suitable if a large area of the structure is to be monitored, because many sensors are likely to be required.

From the continuous monitoring test, background noise from sources such as wind and rain are a concern for field monitoring.

Chapter 6 - Additional Analysis of Previous Tests

In Chapter 3, acoustic emission tests performed on a prestressed concrete girder are described. The Felicity ratio was one acoustic emission parameter used to evaluate the condition of the specimens. Lower Felicity ratios are associated with a higher level of damage. To determine the Felicity ratio, the onset of significant emission must be defined. Curvature, slope, and historic index (HI) criteria were proposed in Chapter 3 and used to determine the onset of significant emission or the "knee" of curve. These three criteria will now be used to reanalyze the tests of Tinkey (2000).

The material in this chapter is intended to confirm the validity of the proposed criteria, and to provide additional information on which to base the proposed evaluation criteria for acoustic emission monitoring of prestressed concrete structures.

6.1 FLEXURE-DOMINATED BOX GIRDER TESTS

Flexure-dominated tests were performed on BG1, BG2, BG4 by Anna Boenig (Boenig 2000) and Brian Tinkey (Tinkey 2000). The girders had different levels of premature ASR/DEF concrete deterioration. The dimensional details of these girders were described in Chapter 3.

Flexure tests under four-point loading were performed on the girders. Acoustic emission monitoring was undertaken during loading to approximately

50% of the ultimate loads. A six-channel MISTRAS 2001 instrument and six 60 kHz resonant sensors were used to collect acoustic emission data. The sensors were arranged to cover an expected flexural crack area in the middle of the span, and their threshold was set to 45 dB.

The loading schedule was developed so that the Kaiser effect and the Felicity ratio could be determined. Load was increased in 10-kip increments, and held at the higher load until the rate of acoustic emission decreased to a minor level. Then, the load was decreased to 5 kips and held for approximately 4 minutes. This loading schedule was continued until failure (Figure 6.1).

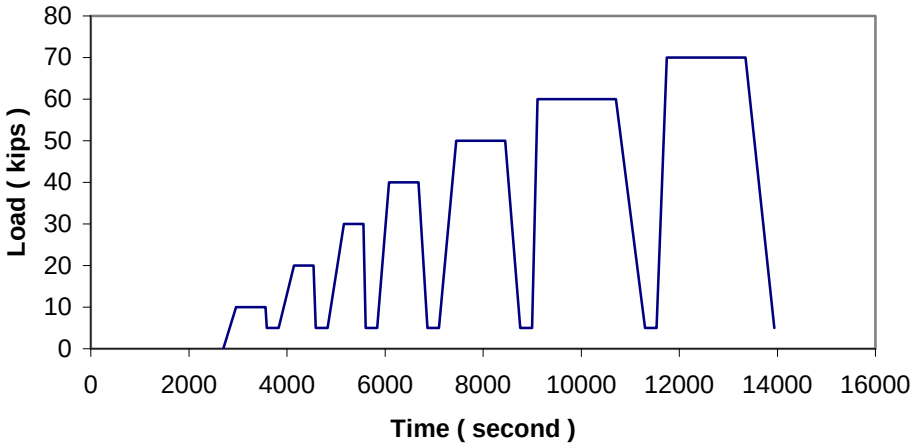

Figure 6.1 – Loading Schedule for Flexure-Dominated Test on Box Girders

6.1.1 Result of Additional Analysis of Flexure-Dominated Tests

Curvature, slope and HI criteria are used to determine loads at the onset of significant emission. The Felicity ratio and number of hits during unloading with an amplitude greater than or equal to 55 dB will be the parameters considered.

Tables 6.1, 6.2 and 6.3 and Figures 6.2 and 6.3 show the results from reanalyzing Tinkey's data for BG1, BG2, and BG4. The results show agreement between each of the criteria. The Felicity ratios calculated from curvature, slope and HI criteria were similar. The curvature and slope criteria tend to indicate a slightly lower load than the HI criterion when the previous maximum load is larger than 40% of the ultimate load. The curvature and slope criteria gave approximately the same load at the onset of significant emission. At low loads, the Kaiser effect held for all specimens. There was no significant emission during reloading and for a significant increase in load above the previous load for specimens BG1 and BG4 at the low loads (Tables 6.1 and 6.3). The Kaiser effect started to break down at 40% of the ultimate load, slightly before the first visual crack. The number of hits during unloading started to increase considerably after the load corresponding to the first visual crack loads.

The loads at the first visible crack and the ultimate loads were similar for all three specimens, even though the specimens had very different levels of premature deterioration. A possible explanation for this is that the rating of the amount of deterioration was based on visual inspection of the ends of the girder and the damage was less in the flexure-dominated region.

Table 6.1 - Load at Onset of Significant Emission, Felicity Ratio, and Number of Hits during Unloading for BG1

Previous Max Load (kips)	Percent of Ultimate Load	Slope		Curvature		HI		Emission during Unloading, Hits
		Load (kips)	FR	Load (kips)	FR	Load (kips)	FR	
9.8	8.26	18.93	1.93	NSE		19.46	1.99	1
20	16.86	28.96	1.45	NSE		27.69	1.38	0
30	25.30	35.53	1.18	39.18	1.31	39.68	1.32	0
39.4	33.22	43.20	1.10	44.38	1.13	45.67	1.16	1
50	42.16	39.37	0.79	38.82	0.78	47.16	0.94	51
60	50.59	36.99	0.62	36.72	0.61	52.39	0.87	2034
65	54.81	34.99	0.54	34.71	0.53	58.78	0.90	6178

Note: 1. NSE = No Significant Emission

2. The first crack was seen at 60 kips.

3. BG1 failed at 118.6 kips.

4. BG1 was in a good condition.

Table 6.2 - Load at Onset of Significant Emission, Felicity Ratio, and Number of Hits during Unloading for BG2

Previous Max Load (kips)	Percent of Ultimate Load	Slope		Curvature		HI		Emission during Unloading, Hits
		Load (kips)	FR	Load (kips)	FR	Load (kips)	FR	
10	8.60	11.31	1.13	11.97	1.20	11.02	1.10	6
20	17.20	22.07	1.10	23.59	1.18	22.90	1.15	16
30	25.80	32.19	1.07	32.91	1.10	34.20	1.14	20
40	34.39	39.92	1.00	40.85	1.02	44.16	1.10	39
50	42.99	43.00	0.86	43.17	0.86	46.91	0.94	125
60	51.59	46.66	0.78	43.63	0.73	52.27	0.87	1483

Note: 1. The first crack was seen at 60 kips. 2. BG2 failed at 116.3 kips. 3. BG2 was in an intermediate condition.

Table 6.3 - Load at Onset of Significant Emission, Felicity Ratio, and Number of Hits during Unloading for BG4

Previous Max Load (kips)	Percent of Ultimate Load	Slope		Curvature		HI		Emission during Unloading, Hits
		Load (kips)	Load (kips)	Load (kips)	FR	Load (kips)	FR	
10	8.41	16.26	16.26	NSE		19.07	1.91	0
20.1	16.90	24.87	24.87	27.76	1.38	24.68	1.23	1
30.7	25.82	33.47	33.47	34.96	1.14	38.89	1.27	1
40.4	33.98	40.95	40.95	40.57	1.00	44.50	1.10	2
50.5	42.47	47.87	47.87	47.49	0.94	48.11	0.95	23
62.5	52.57	49.51	49.51	48.50	0.78	52.93	0.85	623

Note: 1. NSE = No Significant Emission

2. The first crack was seen at 60 kips.

3. BG4 was in a severe condition.

4. BG4 failed at 118.9 kips.

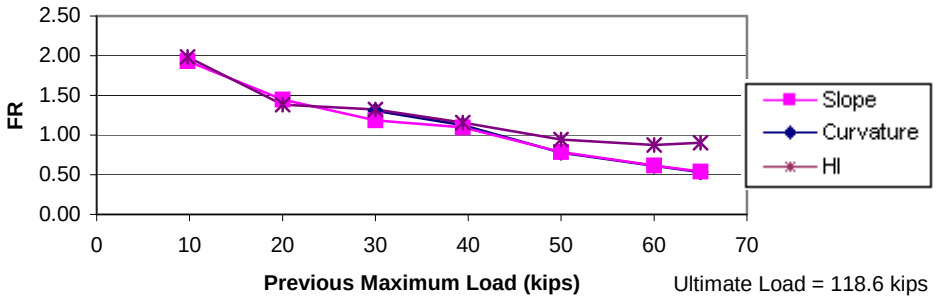

a) BG1

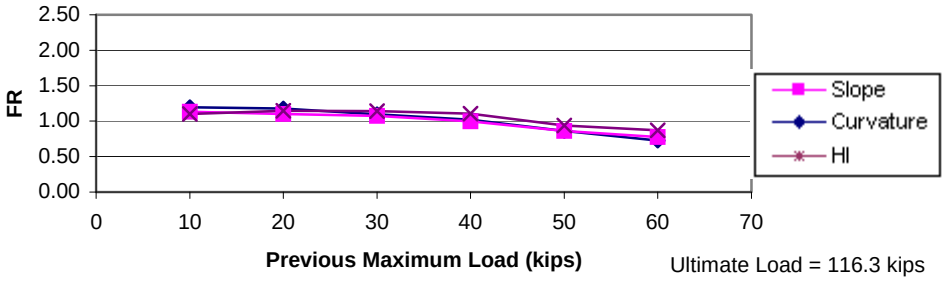

b) BG2

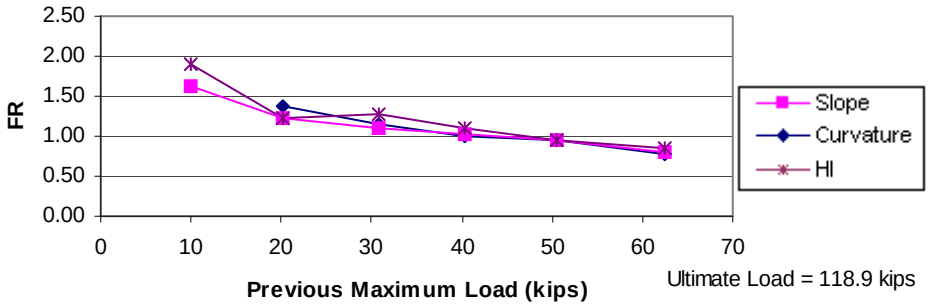

c) BG4

Figure 6.2 – Felicity Ratio vs Previous Maximum Load for Flexure-Dominated Tests

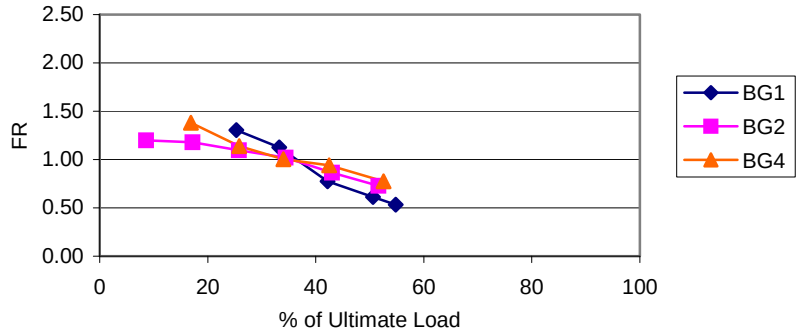

a) Curvature

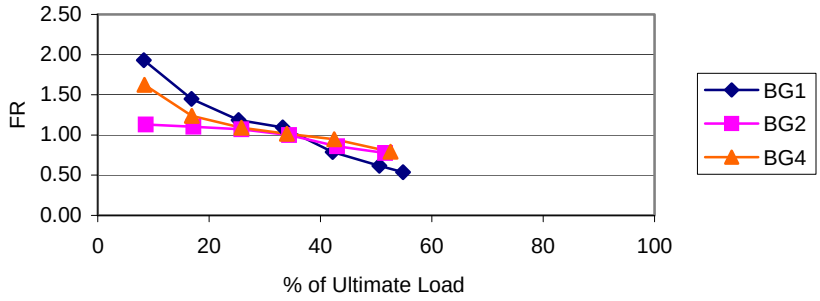

b) Slope

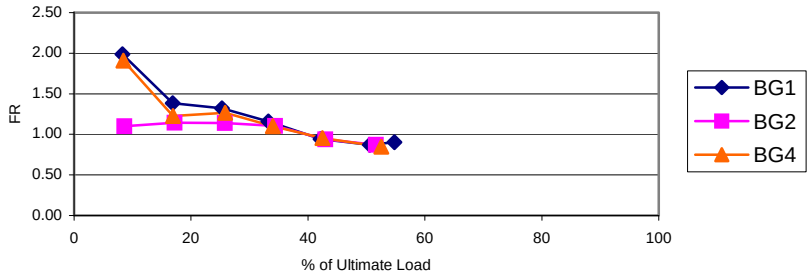

c) Historic Index

Figure 6.3 – Felicity Ratio vs % of Ultimate Load for Flexure-Dominated Tests

6.2 SHEAR-DOMINATED BOX GIRDER TESTS

Shear-dominated tests were performed on the ends of BG1, BG2 and BG4. A different nomenclature was developed in order to distinguish the shear test from the flexural test. The shear tests on BG1, BG2 and BG4 were called BG1S, BG2S, and BG4S respectively.

The testing setup of specimens BG1S and BG4S was designed to represent the real support position used in the field, while that of BG2S was intended to crush a compression strut. BG1S and BG4S were set up with a shear span of 2 times the distance from the top of the beam to the centroid of the prestessing strand. This distance is 46 inches. A shear span of 1.5 times the distance from the top of the beam to the centroid of the prestresssing strand was used for BG2S. This distance is 35.5 inches.

The loading schedule was designed so that the Kaiser effect and the Felicity ratio could be determined. It was similar to the loading schedule used for the flexure-dominated test, except that a 20-kip load increment was used in the shear-dominated test.

A six-channel MISTRAS 2001 instrument and six 60 kHz resonant sensors were used to collect acoustic emission data during the tests. These sensors were arranged to cover the expected cracking areas in the shear spans. The threshold was set to 45 dB. Acoustic emission monitoring was performed up to approximately 50% of the ultimate loads for BG1S and BG2S. BG4S was monitored up to 90% of its ultimate load.

6.2.1 Result of Additional Analysis of Shear-Dominated Tests

Using the three criteria proposed in Chapter 3, data are analyzed to determine the Felicity ratios. The number of hits during unloading with an amplitude equal or greater than 55 dB are also considered. The results of the analyses are shown in Tables 6.4, 6.5, and 6.6, and in Figures 6.4 and 6.5.

The curvature, slope and HI results are in general agreement. The loads at the onset of significant emission given by the HI criterion were slightly higher than the loads determined from the curvature and slope criteria. The Kaiser effect broke down and the Felicity ratio began to indicate the presence of structural damage at loads of about 30% of the ultimate load. These loads are below the load corresponding to the first visually observed crack, which was detected at 38%, 48%, and 73% of the ultimate load for BG1S, BG2S, and BG4S, respectively. The variation in the loads at the first visually detected crack is to be expected. The first crack is difficult to determine in the deteriorated girders because of the large amount of cracking already present. The Felicity ratio decreased when specimens were subjected to a higher load. At about 80% of the ultimate load, the Felicity ratio dropped to 0.6 in BG4S. The more damage in a specimen, the greater the number of hits during unloading.

It should be noted that BG1S and BG2S failed due to crushing in the compression strut, while BG4S failed because of a bearing failure. Stand slip occurred in both BG2S and BG4S.

Table 6.4 - Load at Onset of Significant Emission, Felicity Ratio, and Number of Hits during Unloading for BG1S

Previous Max Load (kips)	Percent of Ultimate Load	Slope		Curvature		HI		Emission during Unloading, Hits
		Load (kips)	FR	Load (kips)	FR	Load (kips)	FR	
20	4.73	28.44	1.42	NSE		32.90	1.65	0
41	9.69	43.79	1.07	45.67	1.11	51.97	1.27	1
61	14.42	64.95	1.06	58.58	0.96	64.30	1.05	2
80	18.91	78.80	0.99	81.43	1.02	88.23	1.10	9
101	23.88	99.78	0.99	102.11	1.01	112.16	1.11	20
122	28.84	115.87	0.95	118.96	0.98	131.60	1.08	55
142	33.57	132.91	0.94	135.81	0.96	136.09	0.96	57
162	38.30	131.23	0.81	135.91	0.84	148.80	0.92	159
182	43.03	143.20	0.79	139.09	0.76	154.03	0.85	383

Note: 1. NSE = No Significant Emission

2. The first crack was seen at 160 kips.

3. BG1S failed at 423 kips.

4. BG1S was in a good condition.

Table 6.5 - Load at Onset of Significant Emission, Felicity Ratio, and Number of Hits during Unloading for BG2S

Previous Max Load (kips)	Percent of Ultimate Load	Slope		Curvature		HI		Emission during Unloading, Hits
		Load (kips)	FR	Load (kips)	FR	Load (kips)	FR	
56	15.64	58.15	1.04	51.75	0.92	62.86	1.12	16
73	20.39	68.50	0.94	73.59	1.01	73.28	1.00	22
95	26.54	73.78	0.78	88.09	0.93	94.21	0.99	84
114	31.84	76.98	0.68	84.98	0.75	111.04	0.97	95
133	37.15	70.95	0.53	84.32	0.63	128.98	0.97	81
153	42.74	86.39	0.56	132.15	0.86	136.83	0.89	130
172	48.04	88.65	0.52	99.39	0.58	95.33	0.55	209
194	54.19	87.33	0.45	130.08	0.67	179.46	0.93	267

Note: 1. The first crack was seen at 170 kips. 2. BG2S failed at 358 kips.

3. BG2S was in an intermediate condition.

Table 6.6 - Load at Onset of Significant Emission, Felicity Ratio, and Number of Hits during Unloading for BG4S

Previous Max Load (kips)	Percent of Ultimate Load	Slope		Curvature		HI		Emission during Unloading, Hits
		Load (kips)	FR	Load (kips)	FR	Load (kips)	FR	
40.7	11.27	NSE		NSE		NSE		0
60	16.62	NSE		NSE		NSE		0
82.3	22.80	90.50	1.10	NSE		90.13	1.10	3
99.8	27.65	115.56	1.16	NSE		105.46	1.06	8
121	33.52	127.20	1.05	NSE		122.29	1.01	16
140.2	38.84	120.98	0.86	136.22	0.97	131.64	0.94	18
161.6	44.76	151.50	0.94	151.84	0.94	135.76	0.84	32
181.8	50.36	170.90	0.94	182.97	1.01	158.94	0.87	41
201.6	55.84	177.64	0.88	200.55	0.99	166.79	0.83	47
223.3	61.86	198.03	0.89	201.30	0.90	186.62	0.84	85
242	67.04	192.79	0.80	204.39	0.84	234.49	0.97	344
262.2	72.63	163.43	0.62	193.35	0.74	194.84	0.74	589
281.62	78.01	181.20	0.64	176.24	0.63	194.46	0.69	781
301.06	83.40	153.89	0.51	146.98	0.49	179.83	0.60	899
322.3	89.28	126.03	0.39	153.71	0.48	181.87	0.56	1721

Note: 1. NSE = No Significant Emission 2. The first crack was seen at 260 kips.

3. BG4S failed at 361 kips. 4. BG4S was in a severe condition.

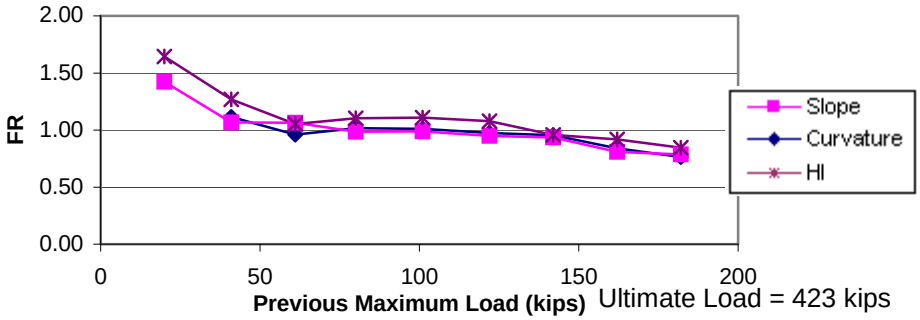

a) BG1S

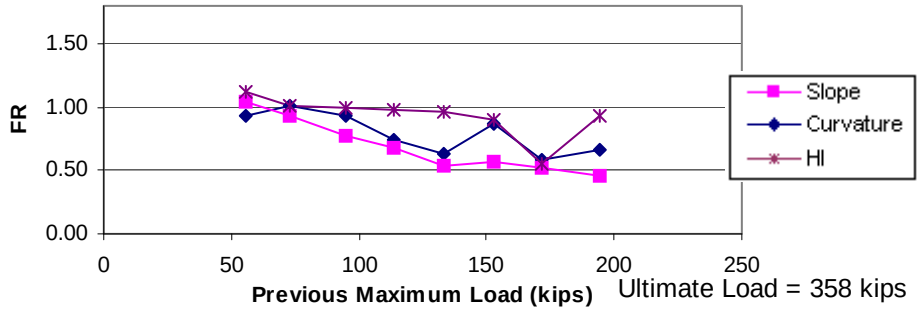

b) BG2S

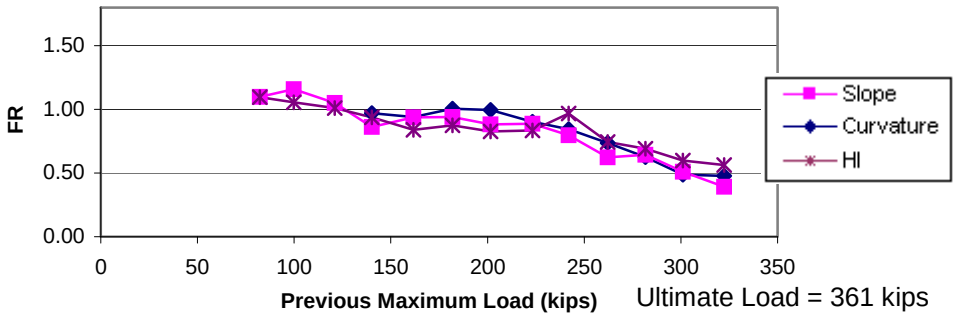

c) BG4S

Figure 6.4 – Felicity Ratio vs Previous Maximum Load for Shear-Dominated Tests on Box Girders

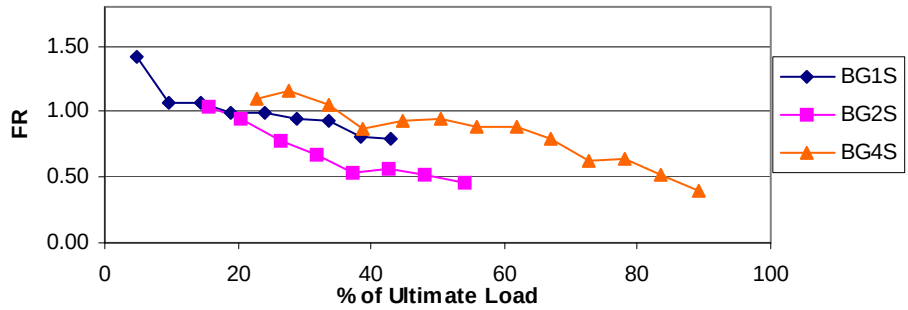

a) Slope

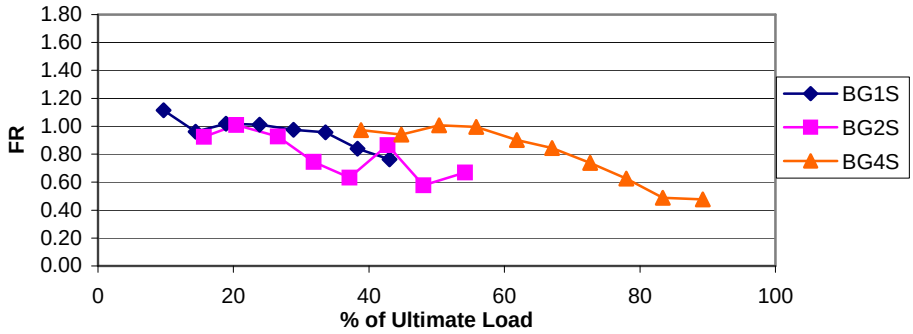

b) Curvature

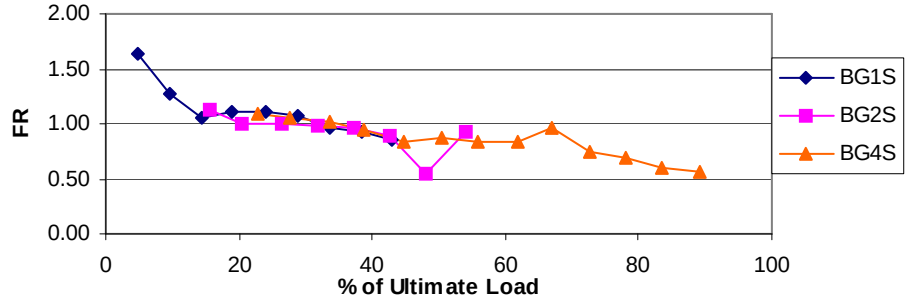

c) Historic Index

Figure 6.5 – Felicity Ratio vs % of Ultimate Load for Shear-Dominated Tests on Box Girders

6.3 SHEAR-DOMINATED TESTS ON TYPE C GIRDER SECTIONS

Four shear-dominated tests: G1ES, G1WS, G2ES, and G2WS, were performed on two Type C girders by Kim and Tinkey (Tinkey 2000). The two girders had premature ASR/DEF concrete deterioration. The cracks were concentrated at the ends of the girders. Cracks away from the ends were oriented horizontally. Both girders had been in service prior to removal for laboratory testing.

The loading schedule of G1ES, G1WS, and G2ES was designed so that the Kaiser effect and the Felicity ratio could be studied. Load was increased in 30-kip increments, and held at the higher load until the rate of acoustic emission decreased substantially. The load was then decreased to 5 kips and help until emissions died out. This loading schedule was continued until failure. The loading schedule of G2WS was not suitable for determination of the Felicity ratio. Accordingly, the data from this specimen is not analyzed.

Acoustic emission was monitored to approximately 70% of the ultimate loads. A six-channel MISTRAS 2001 instrument and six 60 kHz sensors were used to collect the acoustic emission data. The sensors were arranged to cover the expected cracking areas at the ends of the girders, and a 45 dB threshold was used.

6.3.1 Result of Additional Analysis of Shear-Dominated Tests on Type C Girders.

The curvature, slope and historic index criteria proposed in Chapter 3 are used to determine the onset of significant emission. The Felicity ratio and number

of hits during unloading with amplitude equal to or greater than 55 dB are determined. The results of the analyses are shown in Tables 6.7, 6.8, and 6.9 and Figure 6.6 and 6.7.

As can be seen in Figure 6.6, the three criteria are in agreement in determining the load at the onset of significant emission. Like the previous results from the box section girders, the historic index criterion gave the load at the onset of significant emission slightly higher than that determined by the curvature and slope criteria. At low loads, no significant emission was detected and the Kaiser effect held. The Kaiser effect begins to break down at approximately 40-50% of the ultimate loads, while the first major visually detected crack occurs at 80%, 71%, and 57% of the ultimate loads for G1ES, G2ES, and G1WS, respectively. The greater the load applied to the specimens, the lower the values of the Felicity ratios. The Felicity ratio decreased significantly at 70% of the ultimate load for G2ES. The value decreased from 0.90 to 0.44 for the last 40-kip load increment.

The number of hits during unloading started to increase dramatically after the first major crack was detected.

Table 6.7 - Load at Onset of Significant Emission, Felicity Ratio, and Number of Hits during Unloading for G1ES

Previous Max Load (kips)	Percent of Ultimate Load	Slope		Curvature		HI		Emission during Unloading, Hits
		Load (kips)	FR	Load (kips)	FR	Load (kips)	FR	
40	6.44	35.50	0.89	40.38	1.01	45.00	1.13	11
70	11.27	68.00	0.97	69.13	0.99	91.50	1.31	4
102.5	16.51	100.25	0.98	98.00	0.96	119.00	1.16	22
123	19.81	121.00	0.98	141.88	1.15	149.50	1.22	51
154.5	24.88	164.25	1.06	165.87	1.07	168.00	1.09	60
193	31.08	187.50	0.97	183.25	0.95	189.50	0.98	124
212	34.14	208.25	0.98	212.13	1.00	211.50	1.00	59
256.5	41.30	236.00	0.92	243.88	0.95	255.00	0.99	328
272.5	43.88	243.75	0.89	259.38	0.95	290.00	1.06	132
308	49.60	271.25	0.88	292.38	0.95	220.50	0.72	460
333	53.62	303.00	0.91	323.63	0.97	319.50	0.96	448
361	58.13	291.00	0.81	322.25	0.89	364.00	1.01	510
398	64.09	349.75	0.88	359.13	0.90	374.50	0.94	964
429	69.08	300.25	0.70	371.75	0.87	387.50	0.90	779
460	74.07	334.50	0.73	384.50	0.84	393.00	0.85	1159

Note: 1. The first major crack was seen at 500 kips 2. G1ES failed at 621 kips

Table 6.8 - Load at Onset of Significant Emission, Felicity Ratio, and Number of Hits during Unloading for G2ES

Previous Max Load (kips)	Percent of Ultimate Load	Slope		Curvature		HI		Emission during Unloading, Hits
		Load (kips)	FR	Load (kips)	FR	Load (kips)	FR	
40	6.44	63.00	1.58	NSE		60.00	1.50	1
83	13.36	106.50	1.28	104.50	1.26	120.00	1.45	3
121	19.48	138.50	1.14	138.50	1.14	138.00	1.14	9
141	22.70	157.50	1.12	159.25	1.13	159.00	1.13	27
162	26.08	171.50	1.06	177.00	1.09	177.00	1.09	42
182	29.30	190.00	1.04	192.00	1.05	196.00	1.08	36
199	32.04	215.50	1.08	214.50	1.08	218.00	1.10	24
220	35.42	233.50	1.06	231.50	1.05	239.00	1.09	45
241	38.80	253.00	1.05	261.00	1.08	274.00	1.14	54
279	44.92	283.50	1.02	281.50	1.01	288.00	1.03	121
319	51.36	311.00	0.97	307.50	0.96	333.00	1.04	146
360	57.96	331.50	0.92	320.00	0.89	354.00	0.98	225
399	64.24	350.00	0.88	348.00	0.87	359.00	0.90	582
440	70.84	157.00	0.36	168.25	0.38	194.00	0.44	10154

Note: 1. NSE = No Significant Emission 2. The first major crack was seen at 440 kips.

3. G2ES failed at 621 kips.

Table 6.9 - Load at Onset of Significant Emission, Felicity Ratio, and Number of Hits during Unloading for G1WS

Previous Max Load (kips)	Percent of Ultimate Load	Slope		Curvature		HI		Emission during Unloading, Hits
		Load (kips)	FR	Load (kips)	FR	Load (kips)	FR	
63	9.86	NSE		NSE		62.04	0.98	1
63	9.86	66.71	1.06	68.60	1.09	NSE		4
91	14.24	96.25	1.06	118.53	1.30	NSE		19
121	18.93	130.99	1.08	147.38	1.22	NSE		26
151	23.62	156.56	1.04	166.41	1.10	154.35	1.02	29
182	28.47	198.56	1.09	201.89	1.11	211.60	1.16	50
214	33.48	216.46	1.01	227.89	1.06	221.52	1.04	87
242	37.86	239.85	0.99	237.92	0.98	251.64	1.04	71
271	42.40	263.08	0.97	268.16	0.99	267.27	0.99	166
304	47.56	267.12	0.88	270.26	0.89	275.82	0.91	256
339	53.04	272.34	0.80	295.07	0.87	273.92	0.81	538
366	57.26	290.71	0.79	289.29	0.79	291.01	0.80	2090
399	62.42	264.26	0.66	262.90	0.66	257.69	0.65	3987

Note: 1. NSE = No Significant Emission 2. The first major crack was seen at 365 kips.

3. G1WS failed at 639.2 kips.

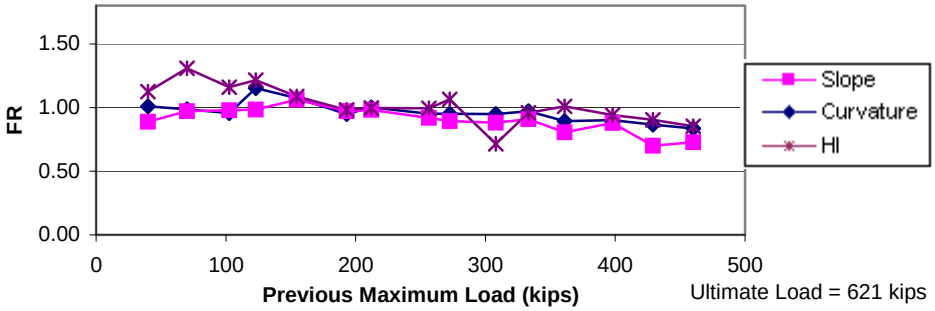

a) G1ES

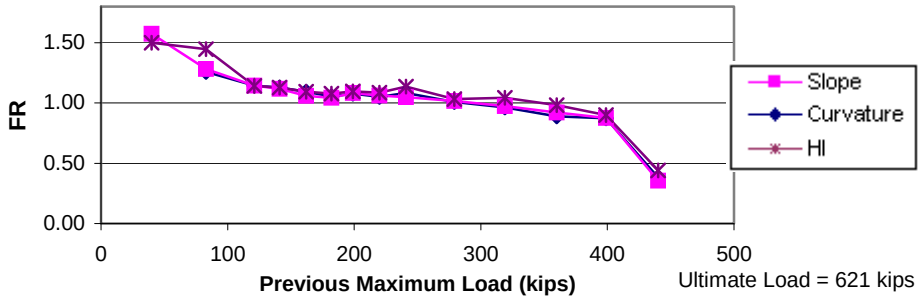

b) G2ES

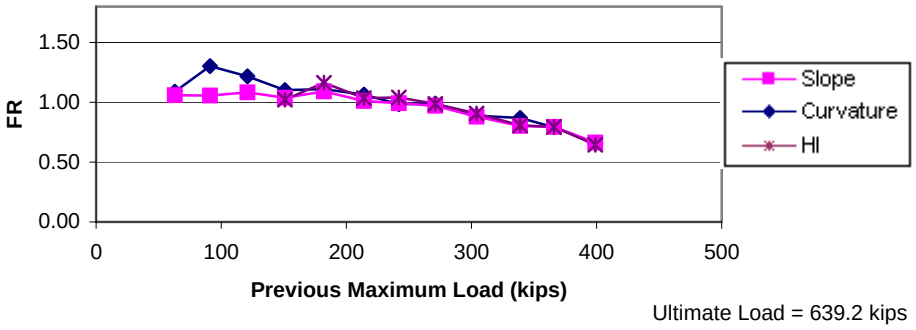

c) G1WS

Figure 6.6 – Felicity Ratio vs Previous Maximum Load for Shear-Dominated Tests on Type C Girders

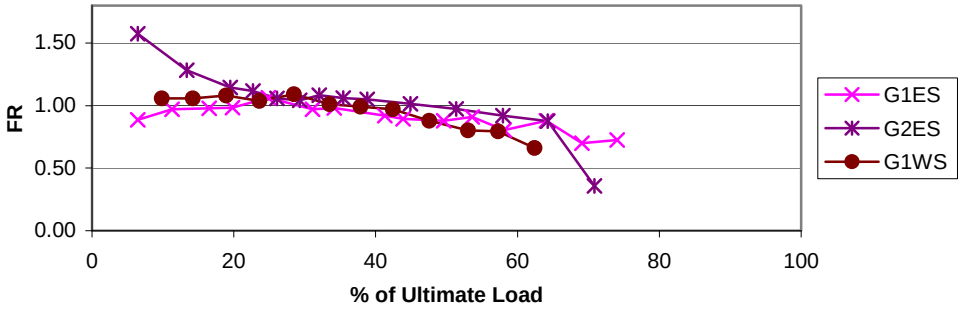

a) Slope

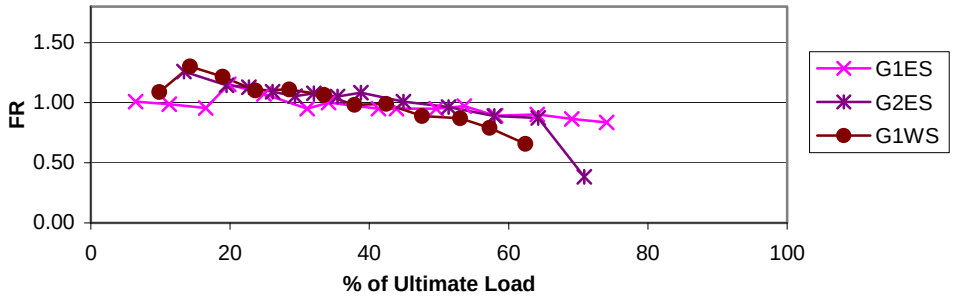

b) Curvature

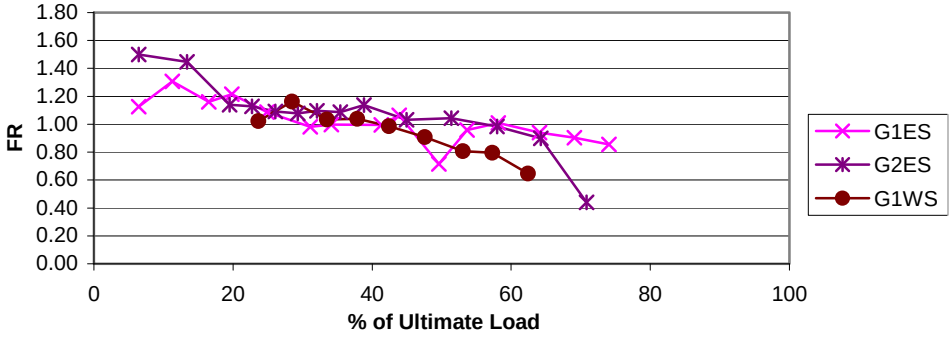

c) Historic Index

Figure 6.7 - Felicity Ratio vs % of Ultimate Load for Shear-Dominated Tests on Type C Girders

6.4 DISCUSSION OF ADDITIONAL ANALYSIS OF PREVIOUS TEST

In this chapter, data from previous tests were reanalyzed. The results confirmed the validity of the criteria proposed in Chapter 3. The Felicity ratios determined from the curvature, slope and historic index criteria were generally similar. The historic index criterion tended to give a slightly higher value of load for the onset of significant emission.

In all tests, the Felicity ratio indicated a developing structural problem before the first visually detected crack. The greater the damage in a specimen, the lower the Felicity ratio, and the higher number of hits during unloading.

In the flexure-dominated tests, the first cracking loads were about 50% of the ultimate loads. The number of hits started to increase considerably after this load level. This is in agreement with the tests done by Yepez (Yepez 1997). The onset of emission in a flexure-dominated test is in a range of 40-50% of the ultimate load.

In the shear-dominated tests on box girders, the Kaiser effect started to break down at a lower percentage of the ultimate load than in the flexure-dominated tests.

Chapter 7 – Test Procedure

The experimental results from 3 flexure tests, 6 shear tests, and 2 shear fatigue tests carried out at the Ferguson Structural Engineering Laboratory and from 6 background noise field tests of in-service bridges show that acoustic emission monitoring is a practical method for evaluating the structural condition of a prestressed concrete girder. Based on these results, a standard procedure for acoustic emission field monitoring of a prestressed concrete girder is proposed.

7.1 STANDARDIZED TESTING PROCEDURE

A field test procedure for acoustic emission testing of prestressed concrete girders subjected to premature ASR/DEF concrete deterioration is included as an appendix. The procedure has been developed by the author and Dr. Timothy Fowler and is based on research reported in this thesis and by Yepez (1997) and Tinkey (2000). The procedure includes evaluation criteria that provide a warning of structural deterioration or overload.

Evaluation is on a per-channel basis and is based on the Felicity ratio and amplitude of hits during loading. The Felicity ratio, which is the ratio between the load at the onset of significant emission and the previous maximum load, and large amplitude hit criteria must both be exceeded to trigger the “warning” and/or “serious” condition alert.

Various techniques were evaluated in the laboratory for determining the "onset of significant emission," including slope, curvature, and historic index. The slope and curvature methods are based on the rate of signal strength and the change in rate of signal strength, both time dependent phenomena. In the laboratory, rates of loading can be controlled and these are valid parameters for evaluating acoustic emission research data. In the field, however, the rate of loading of a girder cannot be controlled and even though the slope and curvature techniques can be used on a qualitative basis they are not suitable as a definition of onset of emission for the Felicity ratio. Accordingly, the procedure requires the Felicity ratio to be based on the historic index.

The laboratory experiments utilized R6I and R15I sensors. Field testing showed that use of R6I sensors is not practical due to traffic noise. Accordingly, the procedure specifies use of 150 kHz resonant sensors. Integral sensors, with the preamplifier integral with the sensor are specified. This type of sensor is used to minimize interference from electromagnetic sources.

An underlying assumption of the procedure is that the ASR/DEF damage will be detected visually, and that the acoustic emission monitoring system will be used to monitor local areas of concern. Accordingly, the system operates as a local inspection technique rather than a global technique. Guard sensors are required to ensure that traffic noise is eliminated from the data. The guard sensors must protect all acoustic emission channels from all possible sources of the traffic noise.

It is important to ensure that background noise from rain does not trigger the warning or severe condition alert. Methods for controlling environmentally generated background noise are being addressed as part of two United States Department of Transportation SBIR programs and will be available for implementation in a field monitoring program.

A relative measure of the load imposed on the structure by the traffic is a required part of the procedure. This information is required in order to relate the stress history to the acoustic emission data for the Felicity ratio calculations. In order to achieve this, a measurement of deflection, strain, or acceleration is required. In addition, it is necessary that the monitor store a record of recent maximum loads imposed on the structure.

The genuine acoustic emission data are compared with the evaluation criteria given in Tables 7.1 and 7.2 to define the onset of significant emission. The load at onset of significant emission is used to calculate the Felicity ratio. The test threshold is set at 55 dB.

If the evaluation criteria are exceeded, the procedure includes two rating levels. The first is called a “warning condition.” If the warning condition is triggered, follow-up inspection should be undertaken. This inspection could include a detailed review of the acoustic emission data, a more through follow-up acoustic emission test using a controlled load. If the severe condition is detected, the structure must be shut down and follow-up investigations performed

Table 7.1 Evaluation Criteria for Flexure-Dominated Region

Criterion	*Warning*	*Severe*
Felicity Ratio	≤ 0.95	≤ 0.60
Amplitude during Loading, dB	≥ 75	≥ 75

Table 7.2 Evaluation Criteria for Shear-Dominated Region

Criterion	*Warning*	*Severe*
Felicity Ratio	≤ 0.90	≤ 0.60
Amplitude during Loading, dB	≥ 75	≥ 75

Instrument settings and calibration, surface preparation, and sensor mounting are also included in the procedure.

7.2 TxDOT Application

The proposed procedure can be used to evaluate the condition of TxDOT's in-service prestressed concrete girders that have experienced premature deterioration due to alkali-silica reaction (ASR) and delayed ettringite formation (DEF). It is likely that further research will permit the procedure to be used for structures such as column and abutment caps.

Chapter 8 – Summary and Conclusions

8.1 SUMMARY

The experimental program carried out at the Ferguson Structural Engineering Laboratory and on six different in-service structures shows that acoustic emission can be used as a tool to evaluate the structural integrity of an in-service prestressed concrete girder that has experienced premature concrete deterioration.

Acoustic emission experiments were performed on a full-scale prestressed concrete box girder under the shear-dominated fatigue loading. The laboratory results show that the progressive deterioration in the specimens can be identified by acoustic emission. Signal strength (MARSE), emission during loading, historic index (HI), and the Felicity ratio, which is the ratio between the load at onset of significant emission and the previous maximum load, correlate to the degree of damage in a specimen. Felicity ratio is the most powerful acoustic emission parameter for evaluating the damage level in a prestressed concrete girder. A decrease in the Felicity ratio indicates an increased damage level.

In order to calculate the Felicity ratio, the onset of significant emission must be determined. The curvature, slope, and historic index (HI) criteria proposed in this thesis can be used as tools to determine the onset of significant damage. 60 kHz and 150 kHz resonant sensors were used in the experiments.

The results show that with an appropriate arrangement and instrument settings, both types of sensors can detect the onset of significant emission in concrete.

Strand pull-out tests were performed on two slices removed from the prestressed concrete girders. The two girders were a Type C I-shaped girder and a box girder. The tests show that acoustic emission can be used as a tool to identify strand slip. At the maximum pull-out load, as the strand starts to slip, hits with long duration are detected. This characteristic can be used during in-service tests of prestressed concrete girders to identify strand slip. This is particularly important for girders with ASR/DEF damage, which is often concentrated at the ends. If an acoustic emission sensor mounted on this end region can detect the slip between prestressing strands and concrete, it will provide the engineer with important information about the condition of the structure.

Field tests carried out on six different in-service structures show that acoustic emission can be used effectively in a noisy traffic environment. The appropriate type of sensor, instrument settings, and analysis techniques have been defined. A 150 kHz resonant sensor is recommended for field testing. It provides a balance between the need to detect genuine emission and the need to eliminate background noise. In field monitoring, a higher-frequency instrument is used than in the laboratory. This is because the laboratory provides an ideal environment for acoustic emission monitoring, without background noise. Traffic noise can be filtered from genuine acoustic emission data by using the guard sensor technique. This technique can be applied real time by the instrument hardware, or post-test with appropriate software. In an environment with severe

background noise and a large area of beam to be monitored, many guard sensors are required.

The laboratory experiments and the fields tests have led to development of a draft test procedure for evaluating the damage of a prestressed concrete girder with premature concrete deterioration. It is anticipated that maintenance personnel will determine appropriate repair and operating procedures for such a damaged structure.

8.2 CONCLUSIONS AND RECOMMENDATIONS

The following are the major conclusions and recommendations that result from this study and the earlier studies on which this is based (Yepez 1997, Tinkey 2000).

- Premature ASR/DEF deterioration in concrete structure can be detected by visual inspection. This technique is the best method for detecting the presence of this type of damage and providing a qualitative assessment of its significance.
- Ultrasonic testing, impact-echo examination, and short-pulse radar inspection are not suitable for qualitative evaluation of ASR/DEF damage.
- Acoustic emission inspection can be used on prestressed concrete girders to provide a warning of overload or significant structural degradation.

- Felicity ratio is the most important acoustic emission measure of structural deterioration in a prestressed concrete girder. For Felicity ratio calculation, the onset of significant emission should be based on the historic index.
- Background traffic noise can contaminate genuine acoustic emission data and make it difficult to interpret. The effect of the background noise can be mitigated by use of a 55 dB data-acquisition threshold, 150 kHz sensors, and guard sensors.
- A field test instrument has been successfully demonstrated for a six-day monitoring period on an Interstate highway structure. Data was acquired, background noise eliminated, and an assessment made of the condition of the structure.
- Strand slip can be identified by acoustic emission. Telltale long-duration hits associated with high amplitude are indications of strand slip.
- A draft procedure has been developed for field test monitoring of ASR/DEF-affected girders.
- It is recommended that an acoustic emission monitor be installed on one or more highway structures with ASR/DEF-damaged girders on a test basis. This initial implementation will be used to refine test procedure and resolve practical issues prior to introduction of a wider program of field monitoring.

- It is recommended that technology to identify and filter out environmental acoustic emission background noise be implemented into this program. The technology is already being developed under complementary Department of Transportation SBIR program.

References

AAR Casualty Prevention Circular No. CPC-1043: Procedure for Acoustic Emission Evaluation of Tank Cars and IM-101 Tanks, Association of American Railroads, Washington, DC.

ASME Section V, Article 12, Boiler and Pressure Vessel Code: Acoustic Emission Examination of Metallic Vessels During Pressure Testing, American Society of Mechanical Engineers, New York, NY.

ASME Section V, Article 11, Boiler and Pressure Vessel Code: Acoustic Emission Examination of Fiber Reinforced Plastic Vessels, American Society of Mechanical Engineers, New York, NY.

ASNT: Recommended Practice for Acoustic Emission Testing of Pressurized Highway Tankers Made of Fiberglass Reinforced Plastic with Balsa Cores, American Society for Nondestructive Testing, Columbus, OH.

ASTM F914: Standard Test Method for Acoustic Emission for Insulated Aerial Personal Devices, American Society for Testing Materials, Philadelphia, PA.

ASTM E569: Standard Practice for Acoustic Emission Monitoring of Structures During Controlled Stimulation, American Society for Testing and Materials

ASTM E1316: Standard Terminology of Nondestructive Examinations, American Society for Testing and Materials

Boenig (2000): Boenig, A., "Bridges with Premature Concrete Deterioration: Field Observations and Large-Scale Structural Testing," *M.S. Thesis*, University of Texas at Austin, May 2000.

Bungey (1990): Bungey, J., "Ultrasonic Testing to Identify Alkali-Silica Reaction in Concrete," *The 29th Annual British Conference on NDT*, Manchester, September 1990.

Fowler *et al*.: Fowler, T. J., Blessing, J. A., Conlisk, P. J., and Swansong, T. L., "The Monpac System," *Journal of Acoustic Emission*, Volume 8, Number 3.

Fowler (1979): Fowler, T. J., "Acoustic Emission of Fiber Reinforced Plastics," *Journal of the Technical Councils of ASCE*, Vol. 105, December 1979, ASCE, NY.

Heiple and Carpenter (1987): Heiple and Carpenter, "Acoustic Emission Produced by Deformation of Metals and Alloys - A Review: Part I," *Journal of Acoustic Emission*, Vol. 6, No. 4, 1987.

Heiple and Carpenter (1987): Heiple and Carpenter, "Acoustic Emission Produced by Deformation of Metals and Alloys – Part II," *Journal of Acoustic Emission*, Vol. 6, No. 3, 1987.

Hick *et al*. (1992): Hick, H., Willer, H., Winter, E., and Simacek, F., " Acoustic Emission Measurements on Bridges," *Journal of AE*, 1992, Vol. 10.

Hillger (1994): Hillger, W., "Inspection of Concrete by Ultrasonic Pulse-Echo-Technique," *6th European Conference on Nondestructive Testing*, Nice (France), Oct. 1994, Vol. 2, pp. 1159-1163.

Karabinis and Fowler (1983): Karabinis, A. H., and Fowler, T. J., "Experiences with Two Reinforced Concrete Aeration Basins," *the 1983 Fall Convention*, American Concrete Institute, Kansas City, Missouri, September 25-30, 1983.

Krause *et al*. (1993): Krause, M., Wiggenhauser, H., and Wilsch, G., "Advanced Pulse Echo Method for Ultrasonic Testing of Concrete," *Nondestructive Testing in Civil Engineering*, Liverpool (United Kingdom), Vol. 2, April 1993 pp. 821-827.

Klingner and Fowler (1998): Klingner, R. E., and Fowler, T. J., "Structural Assessment of In-Service Bridges with Premature Concrete Deterioration," *Project Proposal for TxDOT Project 0-1857*, Submitted 1998.

Nesvijski (1999): Nesvijski, E. G., "On the Necessity of a New Standard for the Acoustic Emission Characterization of Concrete and Reinforced Concrete Structures," *Acoustic Emission: Standards and Technology Update*, ASTM STP 1353, S.J. Vahaviolos, Ed., American Society of Testing and Materials, West Conshohocken, PA, 1999.

Ohtsu (1990): Ohtsu, M., "Current Research and Future Trend of AE Applications to Civil Engineering and Geological Technology," *The International Joint Meeting*, Japan, Oct. 1990.

Ohtsu (1988): Ohtsu, M., "Source Inversion Procedure for Acoustic Emission," *Progress in Acoustic Emission IV*, The Japanese Society of NDI, 1988.

Olson (1992): Olson, L. D., "Sonic NDE of Structural Concrete," *Nondestructive Testing of Concrete Elements and Structured*, San Antonio Texas (United States), April 1992.

Pollock (1978): Pollock, A. A., "Physical Interpretation of AE/ME Signal Processing," *the Second Conference on Acoustic Emission*, November 1978.

Pollock (1981): Pollock, A. A., "Acoustic Emission Amplitude Distributions," *International Advances in Nondestructive Testing*, Vol. 7, 1981, pp. 215-239.

Popovics and Rose (1990): Popovics, S., and Rose, J. L., "The Behavior of Ultrasonic Pulses in Concrete," *Cement and Concrete Research 20*, 1990, pp. 259-270.

Roche (2001): Roche, J. M., "Bridges with Premature Concrete Deterioration: Fatique Testing of Full-Scale, Prestressed Concrete Box Girders Failing in Shear," *Thesis Presented to The University of Texas at Austin*, May 2001.

Scarpellini *et al*. (1983): Scarpellini, R. S., Swanson, T. L., and Fowler, T. J., "Acoustic Emission Signatures of RP Defects," *International Symposium on Acoustic Emission From Reinforced Composites*, The Society of the Plastics Industry, Inc., July 1983.

Sri Ravindrarajah (1992): Sri Ravindrarajah, R., "Evaluation of Compressive Strength for High-Strength Concrete by Pulse Velocity Method," *Nondestructive Testing of Concrete Elements and Structures*, San Antonio Texas (United States), April 1992, pp. 115-126.

Swamy and Al-Hamed (1982): Swamy, R. N., Al-Hamed, A. H., "The Use of Pulse Velocity Measurements to Estimate Strength of Air-Dried cubes and Hence In-Situ Strength of Concrete," *Non-destructive Testing of Concrete*, ACI, September 1982, pp. 247-276.

Tinkey (2000): Tinkey, B. V., "Nondestructive Testing of Prestressed Bridge Girders with Distributed Damage," *Thesis Presented to The University of Texas at Austin*, May 2000.

Uomoto (1987): Uomoto, T., "Application of Acoustic Emission to the Field of Concrete Engineering," *Journal of Acoustic Emission*, Vol. 6, No. 3, 1987.

Wood (1999): Wood, B. R. A., Harris, R. W., and Porter, E. L., "Structural Integrity and Remant Life Evaluation Using Acoustic Emission Techniques," *Journal of Acoustic Emission*, Vol. 17, No. 3, 1999, pp. 121-126.

Yepez (1997): Yepez Roca, L. O., "Acoustic Emission Examination of High Strength Prestressed Concrete Girders," *Thesis Presented to The University of Texas at Austin*, August 1997.

Yuyama *et al*. (1994): Yuyama, S., Okamoto, T., and Nagataki, S., "Acoustic Emission Evaluation of Structural Integrity in Repaired Reinforced Concrete Beams," *Materials Evaluation*, January 1994, pp. 86-90.

Yuyama *et al*. (1995): Yuyama, S., Okamoto, T., and Shigeiski, M., "Acoustic Emission Generated in Corners of Reinforced Concrete Rigid Frame Under Cyclic Loading," *Materials Evaluation*, March 1995, pp. 409-412.

Yuyama *et al*. (1999): Yuyama, S., Okamoto, T., Shigeishi, M., Ohtsu, M., and Kishi, T., "A Proposed Standard For Evaluating Structural Integrity of Reinforced Concrete Beams by Acoustic Emission," *Acoustic Emission*: *Standards and Technology Update*, ASTM STP 1353, S.J. Vahaviolos, ED., American Society of Testing and Materials, West Conshohocken, PA, 1999.